A SCALE BY SCALE BUDGET IN WALL TURBULENCE

Nicoletta Marati

Universita' di Roma "La Sapienza"

Dipartimento di Meccanica e Aeronautica

Tutore: Prof. R. Piva, Dip. di Meccanica e Aeronautica, Università "La Sapienza"

Docente guida: Prof. C.M. Casciola, Dip. di Meccanica e Aeronautica, Università "La Sapienza"

Docenti Esaminatori: Prof. V. Ciampi, Dip. di Ingegneria Strutturale e Geotecnica, Università "La Sapienza",
Prof. B. Favini, Dip. di Meccanica e Aeronautica, Università "La Sapienza",
Ricercatore A. Fregolent, Dip. di Meccanica e Aeronautica, Università "La Sapienza"

The present work is devoted to the study of scale by scale dynamics of velocity and passive scalar fields which takes place in a turbulent channel flow. Starting from generalized forms of the classical Kolmogorov and Yaglom equations, a scale by scale balance for velocity and scalar fluctuations is evaluated by examing how the energy associated with a specific scale of motion is transfered through scales, and, simultaneously, how at the same scale the energy is exchanged with a properly defined spatial flux. The analysis is applied to a data set taken from a direct numerical simulation (DNS), exploiting spectral methods (Fourier in wall parallel planes, Chebyshev in the wall normal direction) for spatial discretization of normal velocity and normal vorticity equations and a mixed Crank-Nicholson/Runge-Kutta scheme for time advancement. The main findings concern the analyses of the different scale by scale behaviors displayed by the scalar and velocity fields, and the influence of boundary conditions on the mechanism of mixing.

Index

Chapter 1

Introduction

The present work is devoted to the study of scale by scale dynamics of velocity and passive scalar fields which takes place in a turbulent channel flow.

The first important characteristic of this kind of flow is the anisotropy induced by the mean gradient, which selects a privileged direction in the system. This anisotropy is reflected by the presence of a production term in the turbulent kinetic energy balance. Moreover the wall normal inhomogeneity, inherently present in wall bounded turbulence, induces a spatial redistribution of the turbulent kinetic energy. In this context the classical view of wall bounded flows is based on the division of the flow domain into well characterized regions where the different contributions to the balance of turbulent kinetic energy play different roles [76], [61], [18]. In particular, the buffer layer where production of turbulent kinetic energy exceeds dissipation and the logarithmic layer where production and dissipation are almost in balance. In this layer the mean profile is expected to be self-similar with respect to the wall normal distance [30], and should thus obey a logarithmic law.

In this framework recent Direct Numerical Simulations (DNS) have pointed out the role of inhomogeneity in connection with the self-sustaining capability of wall bounded flows [31]. However the description in physical space alone is insufficient to capture the complete dynamics of wall bounded turbulence. It is necessary to consider a parallel view based on the decomposition of the field into a hierarchy of scales of motion.

A correct understanding of the dynamics of the velocity field at different scales is of fundamental importance (see for instance the comprehensive review [70]) for the correct parametrization of the small scales in turbulence models. Particularly, the most relevant feature which characterize Large Eddy Simulation (LES) models is the capability to properly account for the flux of energy from the resolved to the sub grid scales. This flux is traditionally associated with two-point statistics, namely to the third order structure function, which appears in the Kolmogorov equation [53].

In the framework of Kolmogorov phenomenology [40] the small scales of any flow at sufficiently large Reynolds number are believed to approach a universal state, characterized by the constant flux of energy through the inertial scales. The inertial range is believed to manifest universality, in the sense that scaling laws appear with universal exponents, which are not dependent on the details of the flow at large scales. Above the inertial range shear dominated flow exhibit the so called production range, where the dynamics is dominated by the direct effects of the shear.

Recent results [21] may suggest that the production range of shear dominated flows has some universal features. We could anticipate that the dynamics in the logarithmic layer, where the local production of turbulent kinetic energy balances the local dissipation, could be similar to the dynamics of the homogeneous shear flow. Actually the scaling laws for the longitudinal velocity increments for the homogeneous shear [21], are reproduced in the logarithmic region of a zero pressure gradient boundary layer [7]. In the production range the entire turbulent statistics are strongly affected by the shear, e.g. the intermittency is enhanced as shown by both numerical [7], [74] and experimental [28], [65] results.

For inhomogeneous flows in addition to production, cascade and dissipation of energy it is necessary to consider spatial fluxes induced by the inhomogeneity. The classical cascade of energy through eddies of different size interacts with the spatial transfer of energy. This phenomenology is schematically represented in the following figure,

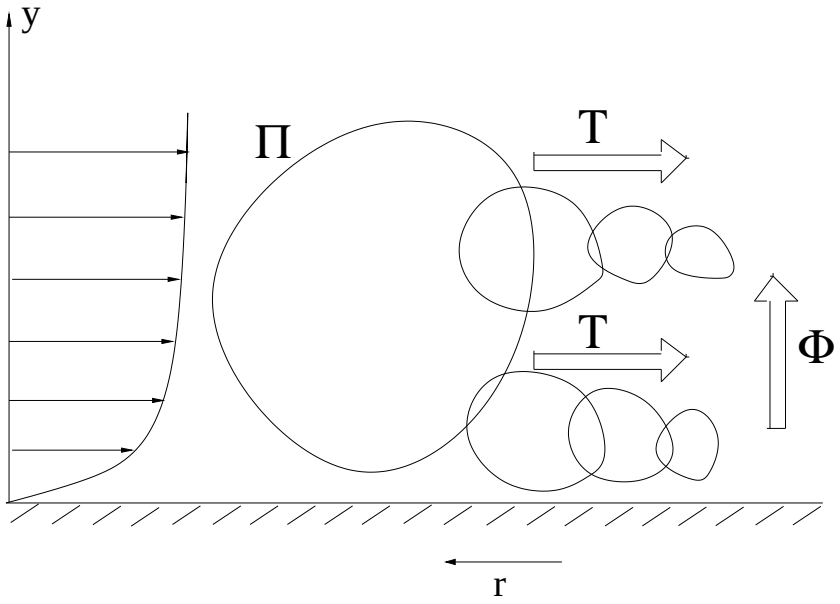

which shows the existence of a double transfer of energy. The first takes place in the wall normal direction and the second through eddies of different sizes. A certain scale at a given wall normal distance receives turbulent energy by different mechanisms: there can be a local production of energy Π due to the interaction between the largest structures and the mean shear, or the energy can be intercepted from the spatial flux Φ induced by the wall normal inhomogeneity. These two contributions initialize the cascade T through scales towards the dissipative range where the scale-energy is dissipated.

In this scenario it is necessary to consider a general approach, able to analyze the scale-dependent dynamics in inhomogeneous conditions. The appropriate tool is the generalized form of the Kolmogorov equation, which has been recently derived in [26] (see also [79] for a different approach, and the work [50]).

The procedure used to obtain this equation is sufficiently general to be extended to the derivation of the dynamical equations for higher order moments [25]. The resulting hierarchy of equations is not closed [42]. Any attempt to close the system writing the dynamical equations for the higher order structure functions would lead to an infinite set of equations. Hence to describe some general features of the statistical properties of the flow it is necessary to introduce some closure hypothesis. Given the impossibility to solve the exact system of the dynamical equations, the approach followed is to establish the relative importance of the different terms on the basis of DNS data. The main purpose is to describe the dynamics of the turbulent fluctuations at a specific scale as a function of the wall normal distance, see [11], [12] [13] and [45] for strictly related topics.

The proper quantity to consider to simultaneously describe the picture in the space of scales and in physical space is the second order structure function $\delta u^2 = \delta u_{\rm i} \delta u_{\rm i}$, where $\delta u_{\rm i} = u_i(x_{\rm s} + r_{\rm s}) - u_i(x_{\rm s})$, s=1,3 and i=1,3, denotes the fluctuating velocities increment between points $x_{\rm i}$ and $x'_{\rm i}$. Loosely speaking $\langle \delta u^2 \rangle$, where the angular brackets denote an ensemble average, is associated with the energy content of a given scale $r = \sqrt{r_{\rm s} r_{\rm s}}$, and depends both on the separation vector $r_{\rm i} = x'_{\rm i} - x_{\rm i}$ and the spatial position of the mid-point $X_{\rm ci} = (x'_{\rm i} - x_{\rm i})/2$ between $x_{\rm i}$ and $x'_{\rm i}$. The generalized form of the Kolmogorov equation (whose derivation is reported in appendix A) for an incompressible Newtonian fluid reads,

$$\frac{\partial\langle\delta u^2\rangle}{\partial t} + \frac{\partial\langle\delta u^2\delta u_{\rm j}\rangle}{\partial r_{\rm j}} + \frac{\partial\langle\delta u^2 u^*_{\rm j}\rangle}{\partial X_{\rm c_j}} + \frac{\partial\langle\delta u^2\rangle\delta U_{\rm j}}{\partial r_{\rm j}} + \frac{\partial\langle\delta u^2\rangle U^*_{\rm j}}{\partial X_{\rm c_j}} + 2\langle\delta u_{\rm j}\delta u_{\rm i}\rangle\frac{\partial\delta U_{\rm i}}{\partial r_{\rm j}} + 2\langle\delta u_{\rm i}u^*_{\rm j}\rangle\frac{\partial\delta U_{\rm i}}{\partial X_{\rm c_j}} = -\frac{2}{\rho}\frac{\partial\langle\delta p\delta u_{\rm i}\rangle}{\partial X_{\rm c_i}} + 2\nu\frac{\partial^2\langle\delta u^2\rangle}{\partial r_{\rm j}\partial r_{\rm j}} + \frac{\nu}{2}\frac{\partial^2\langle\delta u^2\rangle}{\partial X_{\rm c_j}\partial X_{\rm c_j}} - 4\langle\epsilon\rangle \tag{1.1}$$

where $u^*_{\rm i} = (u'_{\rm i} + u_{\rm i})/2$, $U_{\rm i}$ denotes the mean velocity, p is the pressure and $\langle\epsilon\rangle$ is the mean dissipation [1]. This evolution equation for the second order structure function allows to identify all the processes which characterize the dynamics of inhomogeneous flows both in the space of scales and in physical space. The $X_{\rm ci}$ dependence is associated with inhomogeneity, since the terms containing derivatives with respect to the mid-point vanish as homogeneous conditions are approached, and the generalized Kolmogorov equation 1.1 reproduces the equation used in the scale by scale budget for the homogeneous shear flow [9] (see also [59] for the derivation of closely related equations). If the flow is also isotropic the generalized Kolmogorov equation 1.1 reduces to the classical Kolmogorov equation 2.21.

We anticipate here that the breakdown of the generalized Kolmogorov equation 1.1 allows us to characterize the different regions of the channel in term of scale by scale dynamics (as discussed in chapter 5). In particular the buffer layer is the region where the scale-energy production exceeds the scale-energy dissipation, and this excess of scale-energy feeds the spatial flux in the wall normal direction. The logarithmic layer is characterized by a local balance between scale-energy production and dissipation, and the scale-energy is not released to and not received from the inhomogeneous spatial flux. In the space of scales, typically in the logarithmic layer, the large-scale production range is followed by a range dominated by the inertial transfer of scale-energy, which is closed by dissipation at local dissipative scales. In the buffer layer, instead, our results reveals the existence of a direct scale-energy cascade at small scales and an inverse cascade at large scales (i.e. an inertial transfer from small scales towards large scales).

In this work we will also focus on the problem of mixing, which is of great practical relevance in many technical applications. For instance in combustion processes it is desirable to enhance mixing in order to facilitate the close contact of fuel and oxidizer. The enhancement of mixing, due to chaotic advection associated with the turbulent

[1] Properly $\langle\epsilon\rangle$ is the pseudo-dissipation as described in appendix A

fluctuations, is one of the main features which characterize turbulence. The knowledge of turbulent mixing largely relies on the case of homogeneous isotropic flows, and the statistical characteristics of the scalar are described in a scale by scale context. At sufficiently large Reynolds and Péclét numbers $\mathrm{Pe} = \mathrm{Re}\,\mathrm{Pr}$ (where $\mathrm{Pr} = \nu/\chi$ is the Prandtl number, ν is the kinematic viscosity of the fluid and χ its thermal diffusivity) the small scales of the scalar field are believed to approach a universal state. This behavior is fully described by the Yaglom equation 4.4, which shows that in the inertial convective-subrange the flux of variance through scales is constant.

Recent studies (see among others [69], [10] and [77]) revealed that the scalar field presents some distinctive aspects with respect to the classical paradigm of the velocity field. In particular, these anomalies are thought to be associated with the spatial organization of the scalar field into ramp-cliffs structures, i.e. into well defined regions where large temperature gradients are localized, separated by others where the scalar is well mixed. These structures are supposed to be responsible for the permanence of the anisotropy at small scales for a scalar field subjected to an anisotropic large scales forcing, such as an externally imposed mean scalar gradient.

In many applications the presence of walls is of primary importance for mixing processes. For this purpose we address the problem of the passive scalar transport in a turbulent channel flow, as the simplest wall-bounded flow. The classical subdivision of the channel into different regions maintains a well defined meaning also for the scalar case. Indeed we can identify a diffusive sublayer, a buffer layer and a logarithmic layer according to the dominant contribution in the global variance budget. However the extent of these regions, which does not necessarily coincide with the respective counterparts of the velocity field, is strongly dependent on the value of the Prandtl number.

Recently a great deal of numerical and experimental studies, see for instance [34], [33] and [73], have shown that not only different molecular Prandtl numbers but also different wall boundary conditions profoundly affect the mechanism of heat transfer.

In this scenario, the temperature variance budget alone is insufficient to completely characterize the dynamics of the scalar field at different Pr numbers and wall boundary conditions. In order to evaluate how these conditions influence the scale by scale dynamics in an inhomogeneous context the appropriate tool is, in our opinion, a generalized form of the Yaglom equation, which can capture the scale dependent dynamics in presence of spatial fluxes induced by inhomogeneity. The generalized Yaglom equation (see par. 4.1), first derived in [27], explicitly reads

$$\frac{\partial\langle\delta\theta^2\rangle}{\partial t} + \frac{\partial\langle\delta\theta^2\delta u_{\mathrm{j}}\rangle}{\partial r_{\mathrm{j}}} + \frac{\partial\langle\delta\theta^2 u^*_{\mathrm{j}}\rangle}{\partial X_{\mathrm{c_j}}} + \frac{\partial\langle\delta\theta^2\rangle\delta U_{\mathrm{j}}}{\partial r_{\mathrm{j}}} + \frac{\partial\langle\delta\theta^2\rangle U^*_{\mathrm{j}}}{\partial X_{\mathrm{c_j}}} \tag{1.2}$$
$$+ 2\langle\delta u_{\mathrm{j}}\delta\theta\rangle\frac{\partial\delta\Theta}{\partial r_{\mathrm{j}}} + 2\langle\delta\theta u^*_{\mathrm{j}}\rangle\frac{\partial\delta\Theta}{\partial X_{\mathrm{c_j}}} = 2\chi\frac{\partial^2\langle\delta\theta^2\rangle}{\partial r_{\mathrm{j}}\partial r_{\mathrm{j}}} + \frac{\chi}{2}\frac{\partial^2\langle\delta\theta^2\rangle}{\partial X_{\mathrm{c_j}}\partial X_{\mathrm{c_j}}} - 4\langle\epsilon_\theta\rangle,$$

where $\delta\Theta = \Theta' - \Theta$ denotes the increment of the mean temperature, θ is the fluctuating temperature, and $\langle\epsilon_\theta\rangle$ is the mean scalar dissipation rate. This equation, like the generalized Kolmogorov equation for the velocity field, allows to identify all the processes which characterize the dynamics at a given scale for inhomogeneous flows.

Our findings show that the scale dependent dynamics of the scalar field in the core region is profoundly affected by the wall boundary conditions (as discussed in chapter 4). In particular if each wall is kept at a constant temperature, in order to obtain an antisymmetric mean temperature profile with respect to the centerline, the mean scalar gradient in the core region is almost constant. Here the local production of scale-variance balances the local dissipation and the spatial flux of scale variance is negligible. This flux, instead, is the source of scalar fluctuations in the bulk region where the mean scalar gradient vanishes for boundary conditions symmetric with respect to the centerline.

The present work is organized as follow: we give in chapter 2 a brief description of the main characteristics of homogeneous isotropic turbulence, focusing on the dynamics described by the energy balance equation both in physical and spectral spaces. After the description of the Kolmogorov phenomenology, we recall the exact result consisting of the Kolmogorov equation. Chapter 3 will deal with the specialization of the generalized Kolmogorov equation for different turbulent fields. Chapter 4 will introduce the problem of the transport of a passive scalar and it is mainly devoted to the derivation of the generalized Yaglom equation and its specialization for different scalar fields. In chapter 5 we will discuss the results obtained for the velocity field, based on a dataset taken from a direct numerical simulation of a low Reynolds number turbulent channel flow. Chapter 6 contains the analysis of one-point and two-point observables of the scalar field for different wall boundary conditions and Pr numbers. Finally in the last chapter a summary of the main findings and some final remarks are made. An appendix is also devoted to the derivation of the generalized Kolmogorov equation.

Chapter 2

Homogeneous isotropic conditions

The concept of homogeneous isotropic turbulence was introduced by Taylor (1935) and since then it has played a major role in the analysis of the structure of the turbulent flows. Let us recall that statistical homogeneity means that all the multidimensional probability densities of the velocities components are invariant with respect to translations and statistical isotropy means that the statistical characteristics of the field are invariant under rotations and reflections with respect to the coordinate axis.

The concept of homogeneous isotropic turbulence is a mathematical idealization, since this hypothesis could be fulfilled only if the fluid occupies an infinite space. However we can suppose that these hypothesis could be partially satisfied in small regions away from the boundaries of the flow. In this case we can refer to ergodicity [53] (to ensure the convergence in mean square of the spatial average to the probability mean) if the dimensions of this region are sufficiently large to ensure a substantial decorrelation of the velocity field with itself.

The statistical method used in the description of globally isotropic field can be used in a more general context according to the Kolmogorov hypothesis of local homogeneity and isotropy of the small scales of any turbulent flow, to be discussed in par. 2.4. My aim in this section is to present a concise description of the problem both in spectral space and in physical space.

2.1 Statistical properties

The main statistical features of the homogeneous and isotropic random velocity field are characterized by the second order two-point correlation tensor,

$$R_{\mathrm{ij}}\left(\ \boldsymbol{X}_{\mathbf{c}},\ \boldsymbol{r}, t\right) = \left\langle u_i\left(\boldsymbol{x}, t\right) u_j\left(\ \boldsymbol{x}\ \ +\ \ \boldsymbol{r}\ , t\right)\right\rangle , \tag{2.1}$$

where for homogeneity R_{ij} does not vary with the absolute position and must depend only on the separation vector $\boldsymbol{r}$. Recurring to isotropy R_{ij} should be independent of the direction of the separation vector and must be a function of the modulus r of the separation vector. R_{ij} is directly connected to the turbulent kinetic energy K per unit mass of the fluid,

$$K = \frac{1}{2}\langle u_i(\boldsymbol{x}) u_i(\boldsymbol{x})\rangle = \frac{R_{ii}(0)}{2} \tag{2.2}$$

Here and henceforth the dependence on t is not shown explicitly. It is useful to recur to the Fourier transform of R_{ij} [1] since spectral analyses gives a simple picture of the mechanisms involved in the cascade of energy. Let us introduce the *spectral tensor*

$$\Phi_{ij}(\boldsymbol{k}) = \left(\frac{1}{2\pi}\right)^3 \int R_{ij}(\boldsymbol{r}) e^{-i\,\boldsymbol{k}\cdot\boldsymbol{r}} d^3r\,, \tag{2.3}$$

and the inverse Fourier transform

$$R_{ij}(\boldsymbol{r}) = \int \Phi_{ij}(\boldsymbol{k}) e^{i\,\boldsymbol{k}\cdot\boldsymbol{r}} d^3k\,. \tag{2.4}$$

Φ_{ij} can also be viewed as the velocity correlation tensor in Fourier space [51], since it is easy to show:

$$\Phi_{ij}(\boldsymbol{k})\delta_{k+k'} = \langle \widehat{u}_i(\boldsymbol{k})\, \widehat{u}_j^*(\boldsymbol{k})\rangle \tag{2.5}$$

where $\delta_{k+k'}$ is the Kronecker symbol, and the hat denotes the Fourier coefficient of the variable. Hence

$$K = \frac{1}{2}\langle u_i(\boldsymbol{x})\, u_j(\boldsymbol{x})\rangle = \frac{1}{2}\int \Phi_{ii}(\boldsymbol{k})\, d^3k. \tag{2.6}$$

where Φ_{ij} represents the spectral density of the Reynolds stress tensor $\langle u_i(\boldsymbol{x})\, u_j(\boldsymbol{x})\rangle$. Now we can also relate the trace of Φ_{ij} (which in isotropic condition depends only on the modulus k of the wave vector) to the energy per unit mass of fluid K,

[1] Let us observe that R_{ij} is supposed to fall to zero sufficiently rapidly as the separation goes to infinity

$$K = \frac{1}{2} R_{\mathrm{ii}}(0) = \frac{1}{2} \int_{\mathbb{R}^3_{\boldsymbol{k}}} \Phi_{\mathrm{ij}}(\boldsymbol{k})\, d^3\, \boldsymbol{k} = \int_0^\infty 2\pi k^2 \Phi_{\mathrm{ii}}(k)\, dk = \int_0^\infty E(k)\, dk$$

Where in the last passage we used spherical coordinates. $E(k)$ is the wavenumber spectrum, and $E(k)\,dk$ represents the contribution to the kinetic energy from harmonic components whose wavenumber modulus lays between k and $k + dk$.

Let us now observe that in homogeneous isotropic conditions $\langle u_1^2 \rangle = \langle u_2^2 \rangle = \langle u_3^2 \rangle$ the root mean square velocities are equal and the turbulent kinetic energy is given by $K = 3\langle u_1^2 \rangle / 2$.

2.2 Dynamic equation for the tensor R_{ij}

Let us now show that it is possible to derive some "exact" results stemming from the Navier Stokes equation in homogeneous isotropic conditions [53], in particular we will derive the evolution equation for the correlation tensor. This equation is the starting point to derive the Kolmogorov equation and the energy balance equation both in physical and in spectral space.

Since isotropic turbulence is not self-sustained (meaning that a source that replenishes the energy dissipated by viscosity is not present) we are dealing with a problem of freely decaying turbulence. An evolution equation for R_{ij} can be derived if we write the system of Navier Stokes equation (see appendix A.1) for u_{i} at point x_{i} and for u'_{i} at point x'_{i}, then we multiply the first equation by u'_{j} and the second equation by u_{j}. After adding the two equations and averaging we obtain,

$$\frac{\partial \langle u_{\mathrm{i}} u'_{\mathrm{j}} \rangle}{\partial t} = \frac{\partial \left(\langle u_{\mathrm{i}} u_{\mathrm{k}} u'_{\mathrm{j}} \rangle - \langle u_{\mathrm{i}} u'_{\mathrm{j}} u'_{\mathrm{k}} \rangle \right)}{\partial r_{\mathrm{k}}} + \frac{1}{\rho} \left[\frac{\partial \langle p u'_{\mathrm{j}} \rangle}{\partial r_{\mathrm{i}}} + \frac{\partial \langle p' u_{\mathrm{i}} \rangle}{\partial r_{\mathrm{j}}} \right] + 2\,\nu \frac{\partial^2 \langle u_{\mathrm{i}} u'_{\mathrm{j}} \rangle}{\partial r_{\mathrm{k}} \partial r_{\mathrm{k}}} \qquad (2.7)$$

which is valid for an homogeneous field, not necessarily isotropic. Now let us introduce the third order two-point correlation tensor (triple velocity correlation),

$$S_{\mathrm{ij,k}} = \langle u_{\mathrm{i}}(\boldsymbol{x})\, u_{\mathrm{j}}(\boldsymbol{x})\, u_{\mathrm{k}}(\boldsymbol{x} + \boldsymbol{r}) \rangle$$

where the subscript after the comma denotes the variables evaluated at point x'_i. Substituting in equation 2.7,

$$\frac{\partial R_{\mathrm{i,j}}}{\partial t} = \frac{\partial \left(S_{\mathrm{ik,j}} - S_{\mathrm{i,jk}}\right)}{\partial r_{\mathrm{k}}} + \frac{1}{\rho}\left[\frac{\partial \langle p u'_{\mathrm{j}}\rangle}{\partial r_{\mathrm{i}}} + \frac{\partial \langle p' u_{\mathrm{i}}\rangle}{\partial r_{\mathrm{j}}}\right] + 2\,\nu \frac{\partial^2 R_{\mathrm{i,j}}}{\partial r_{\mathrm{k}} \partial r_{\mathrm{k}}}. \tag{2.8}$$

This is the dynamic equation which relates the second and third order correlation tensors for homogeneous, not necessarily isotropic turbulence. It can not be used to evaluate $R_{\mathrm{i,j}}$ if its value is known at some initial time, because of the presence of new unknowns, such as the triple velocity correlation [2], which is due to the non-linearity of the Navier-Stokes equation. If we try to close the system writing the dynamical equation for $S_{\mathrm{ij,k}}$ it would contain the fourth order correlation tensor, which is unknown. A continuation of this procedure would lead to an unclosed system characterized by a number of unknowns grater than the number of equations. Necessarily to close the system some closure hypothesis are needed.

2.2.1 Energy balance equation in physical space

The evolution equation for the turbulent kinetic energy $K = 1/2\langle u_{\mathrm{i}} u_{\mathrm{i}}\rangle$ can be easily obtained from equation 2.7 taking $r = 0$ and identifying $\mathrm{i} = \mathrm{j}$,

$$\frac{\partial K}{\partial t} = \frac{\partial \langle u_{\mathrm{i}}\, u_{\mathrm{i}}\, u_{\mathrm{k}}\rangle/2}{\partial x_{\mathrm{k}}} - \frac{1}{\rho}\frac{\langle \partial p u_{\mathrm{i}}\rangle}{\partial x_{\mathrm{i}}} + \nu \left\langle u_{\mathrm{i}} \frac{\partial^2 u_{\mathrm{i}}}{\partial x_{\mathrm{j}} \partial x_{\mathrm{j}}}\right\rangle \tag{2.9}$$

in homogeneous conditions the derivatives with respect to $\boldsymbol{x}$ vanish and the viscous term can be expressed in a simple form, so that the equation reads

$$\frac{\partial K}{\partial t} = -\nu \left\langle \frac{\partial u_{\mathrm{i}}}{\partial x_{\mathrm{j}}} \frac{\partial u_{\mathrm{i}}}{\partial x_{\mathrm{j}}}\right\rangle = -\langle \epsilon \rangle \tag{2.10}$$

where $\langle \epsilon \rangle$ is the mean viscous energy dissipation of the fluctuating motion into heat. Equation 2.10 is the energy balance equation in physical space, and essentially it describes the decrease of turbulent kinetic energy due to the action of the dissipation.

[2] The two points pressure-velocity correlation can be expressed in terms of $S_{\mathrm{ij,k}}$ using the solution of the Poisson equation

2.2.2 Kármán-Howarth equation

We outline here the principal steps followed in the derivation of the Kármán-Howarth equation (KH), more details can be found in [53], [4]. If we compute the trace of equation 2.8

$$\frac{\partial R_{\mathrm{i,i}}}{\partial t} \;=\; \frac{\partial \left(S_{\mathrm{ik,i}} - S_{\mathrm{i,ik}}\right)}{\partial r_{\mathrm{k}}} \;+\; 2\,\nu \frac{\partial^2 R_{\mathrm{i,i}}}{\partial r_{\mathrm{k}} \partial r_{\mathrm{k}}}\,, \tag{2.11}$$

where the term containing pressure disappears for homogeneity, while for isotropy $S_{\mathrm{i,ik}} = -S_{\mathrm{ik,i}}$

$$\frac{\partial R_{\mathrm{i,i}}}{\partial t} \;=\; 2\frac{\partial S_{\mathrm{ik,i}}}{\partial r_{\mathrm{k}}} \;+\; 2\,\nu \frac{\partial^2 R_{\mathrm{i,i}}}{\partial r_{\mathrm{k}} \partial r_{\mathrm{k}}}\,. \tag{2.12}$$

For a globally isotropic field the tensors $R_{\mathrm{i,i}}, S_{\mathrm{ik,i}}$ can be expressed in terms of two scalar functions:

$$R_{\mathrm{i,i}} \;=\; \langle u^2 \rangle \left[3 \;+\; r\frac{d}{dr}\right] \langle u_{\parallel} u'_{\parallel} \rangle \qquad\qquad S_{\mathrm{i\,k,i}} \;=\; \langle u^3 \rangle \;\frac{r_{\mathrm{k}}}{2} \;\left[\frac{4}{r} \;+\; \frac{d}{d\,r}\right] \langle u_{\parallel} \; u_{\parallel} \; u'_{\parallel} \rangle,$$

where $\boldsymbol{u}_{\parallel} = (u_{\mathrm{i}}\, r_{\mathrm{i}}/r^2)\, \boldsymbol{r}$, $\langle u^2 \rangle$ and $\langle u^3 \rangle$ are the variance and the skewness of the velocity field, respectively. Substituting these expressions in equation 2.12 we obtain

$$\left[3 \;+\; r\,\frac{d}{d\,r}\right] \frac{\partial \langle u_{\parallel} u'_{\parallel} \rangle}{\partial t} \;=\; \left[3 + r\,\frac{d}{d\,r}\right] \left(\frac{4}{r} + \frac{d}{d\,r}\right) \langle u_{\parallel} u_{\parallel} u'_{\parallel} \rangle$$

$$+ \;2\,\nu \left[3 \;+\; r\,\frac{d}{d\,r}\right] \left(\frac{d^2}{dr^2} \;+\; \frac{4}{r}\frac{d}{d\,r}\right) \langle u_{\parallel} u'_{\parallel} \rangle.$$

Since the equation $3\,h\,(r) + r\,h'\,(r)$, where $h\,(r)$ is a generic function of r, admits only the zero solution which is not singular at the origin, we have

$$\frac{\partial \langle u_{\parallel} u'_{\parallel} \rangle}{\partial t} = \left(\frac{4}{r} + \frac{d}{d\,r}\right) \langle u_{\parallel} u_{\parallel} u'_{\parallel} \rangle \;+\; 2\,\nu \left(\frac{d^2}{dr^2} \;+\; \frac{4}{r}\frac{d}{d\,r}\right) \langle u_{\parallel} u'_{\parallel} \rangle. \tag{2.13}$$

This is the Kármán-Howarth equation (1938) which leads to important relations among statistical properties.

2.3 Spectral energy balance

In order to give a simple picture of the energy transfer through different scales of motions or different wave-numbers we consider the evolution equation for the energy spectrum E (see par. 2.1, and [51]). It is sufficient to Fourier transform the trace of the evolution equation 2.7

$$\begin{aligned} \frac{\partial R_{\mathrm{i,i}}}{\partial t} &= T_{\mathrm{i,i}}(r,t) + P_{\mathrm{i,i}}(r,t) + 2\,\nu \frac{\partial^2 R_{\mathrm{i,i}}(r,t)}{\partial r_{\mathrm{k}} \partial r_{\mathrm{k}}} \\ \frac{\partial \Phi_{\mathrm{i,i}}}{\partial t} &= T'_{\mathrm{i,i}}(k,t) + P'_{\mathrm{i,i}}(k,t) - 2\,\nu k^2 \Phi_{\mathrm{i,i}}(k,t) \end{aligned} \tag{2.14}$$

where $P_{\mathrm{i,i}}$ is the pressure contribution, $T_{\mathrm{i,i}}$ the non linear contribution and $P'_{\mathrm{i,i}}$ and $T'_{\mathrm{i,i}}$ are the corresponding Fourier transforms. As a consequence the evolution equation for the energy spectrum $E(k,t) = 2\pi k^2 \Phi_{\mathrm{i,i}}$ easily follows:

$$\left(\frac{d}{dt} + 2\,\nu k^2\right) E(k,t) = TS(k,t) + PS(k,t)\ , \tag{2.15}$$

where clearly $TS(k,t) = 2\pi k^2 T'_{\mathrm{i,i}}(k,t) = 2\pi k^2 \int T_{\mathrm{i,i}}(r,t)\, e^{ik\vec{r}} d^3 r$, and similar relations hold for the other terms of the equation. $P_{\mathrm{i,i}}$ vanishes for homogeneity and incompressibility, so that $PS(k,t)$ is null for all k. As a consequence the effect of the pressure is to transfer energy between different velocity components leaving unchanged the energy content of a given wavenumber. Hence the effect of the pressure can be interpreted as a trend to equalize the energy content associated with different directions, i.e. a sort of trend towards an isotropic state. $TS(k,t)$ is the rate of change of the energy at a given wavenumber, stemming from the nonlinear term of the Navier-Stokes equations. Since $T_{\mathrm{i,i}}(0,t) = 0$, it follows that

$$\int_0^\infty TS\,(k,t)\,dk \;=\; 0\,. \tag{2.16}$$

Hence the nonlinear term can only change the energy distribution in the wavenumber space, without affecting the total amount of turbulent kinetic energy. If we integrate equation 2.15 with respect to k, we have

$$\frac{d\,K}{dt} \;=\; -\int_0^\infty 2\nu k^2 E\,(k,t)\,dk = -\langle\epsilon\rangle\,, \tag{2.17}$$

where in the last passage we used equation 2.10, which shows that the rate of decay of the turbulent kinetic energy is the dissipation rate. If we – incorrectly – neglect the non linear contribution, the solution of equation 2.15 takes the simple form $E\,(k,t) = E\,(k,t_0)\,exp\,[-2\nu k^2\,(t\,-\,t_0)]$, which shows that the energy decreases more rapidly for large k. In this case each harmonic component evolves independently from the others. The nonlinear term, however, couples the different components and redistributes the energy in Fourier space. Consequently we can suppose that the effect of the nonlinearity is to transfer energy from where there is a net production (typically at small $k's$) towards the region where the viscous dissipation is very rapid (typically at large $k's$).

The upper panel of figure 2.1 shows schematically the different terms in equation 2.15. The fact that the spectral transfer is negative at small wave numbers, in the so-called energy containing range, and positive at large wave numbers, in the dissipation range, shows that the energy is transferred or cascades from large to small scales.

To characterize the spectral behavior in the different ranges of scales (see for instance [43]), let us now consider the spectral energy balance 2.15 integrated from 0 to k or from k up to ∞

$$\frac{\partial}{\partial t}\int_0^k E\,(k',t)\,dk' \;=\; -\,W\,(k,t)\;-\;2\nu\int_0^k k'^2 E\,(k',t)\,dk' \tag{2.18}$$

$$\frac{\partial}{\partial t}\int_k^\infty E\,(k',t)\,dk' \;=\; W\,(k,t)\;-\;2\nu\int_k^\infty k'^2 E\,(k',t)\,dk', \tag{2.19}$$

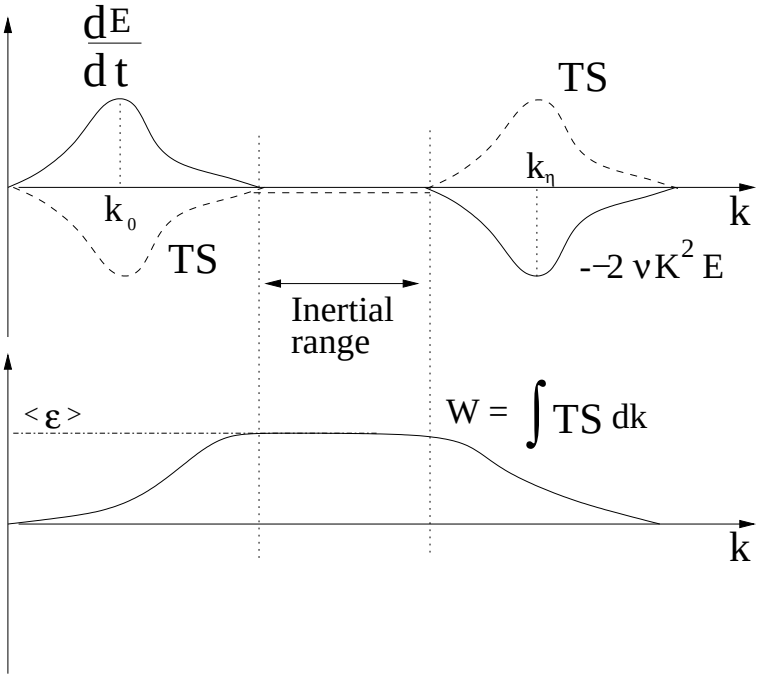

Figure 2.1: Upper panel: schematic illustration of the spectral energy budget 2.15. Lower figure: integral W of the transfer through scales term TS.

where $TS = -dW\left(k,t\right)/dk$, as shown in the lower panel of figure 2.1.

The first integral in equation 2.18 corresponds to the energy content of small k, W is the kinetic energy flux through the wavenumber under consideration and the second term on the right hand side is the direct viscous dissipation in this range. Similar comments apply for the second equation 2.19. At large Reynolds numbers the direct viscous dissipation is negligible at small wavenumber, and hence the decay of turbulent kinetic energy is balanced by the energy flux in this range. At large Re numbers, instead, (equation 2.19) the turbulent kinetic energy content is negligible and the flux of energy balances the dissipation. In an intermediate range of scales both production and dissipation are negligible and the spectral transfer TS presents a plateau at zero value and consequently the flux W is constant. These results are the main ingredients of the Kolmogorov phenomenology.

2.4 Locally isotropic turbulence (Kolmogorov phenomenology)

In this section we try to describe the phenomenology of the turbulence in the framework of Kolmogorov theory [53]. According to Richardson intuition (1920) the turbulent mo-

tion can be considered to be composed of a superposition of eddies with different sizes and different characteristic velocity and time scales. The eddy is a loose phenomenological concept, but it can be intended as a structure or a turbulent motion localized within a region of defined size. The larger eddies have a length scale l_0 which is of the same order of magnitude of the length of the domain embedding the fluid (this is a typical scale associated with the production of turbulent kinetic energy, such as the integral scale L) and their characteristic velocity is of the order of the root mean square velocity $u = \sqrt{u_1^2}$ [3]. Consequently the Reynolds number of these eddies $\mathrm{Re} = \mathrm{u}\,\mathrm{l}_0/\nu$ is large so that the effect of viscosity are negligibly small. These eddies are unstable and break down, and their energy is transferred by nonlinear interactions towards smaller eddies. These smaller eddies undergo a similar break down process and transfer their energy towards much smaller eddies. This process continues until the length scales involved are associated with velocity gradients sufficiently large to give an appreciable viscous dissipation of kinetic energy into heat. It is usual to refer to the above phenomenological description as the "energy cascade".

The large scales fluctuations receive their energy directly from the mean motion and thus are inhomogeneous and anisotropic since their characteristics are determined by the mechanism of generation of the turbulence. Hence the large scales features can not be universal but are related to the particular kind of flow. As a consequence of the chaotic transfer of energy towards small scales the small eddies are not directly influenced by the large scales of the flow. In particular the orienting effects of the mean motion, of the geometry, should became negligibly small for sufficiently small eddies. Hence the statistical characteristics of the small scales of sufficiently large Reynolds number flows should be homogeneous, isotropic and stationary.

In his original work Kolmogorov [40] analyzed the statistical properties of the small scales considering that they are reflected in the relative motion of the fluid particles with respect a fixed particle[4]. In particular he considered the relative velocities: $v(l,\tau) = u(x,t) - u(x_p,t_p)$, where $\tau = t - t_p$ and $l = x - x_p - u(x_p,t_p)(t-t_p)$. As a consequence of the preceding arguments the statistical characteristics of the velocity increments $v(l,t)$ in small space-time region should be homogeneous isotropic, stationary and independent of the choice of the point x_p (i.e. the field u is locally isotropic). These statistical properties should depend on the parameters which describe the process of the energy cascade. Firstly by the rate at which the energy is transferred via the non linear interaction from larger towards smaller scales, secondly by the viscous

[3] where in homogeneous isotropic conditions $u_1^2 = u_2^2 = u_3^2$

[4] Clearly the relative motion is unrelated to the absolute motion which is strongly influenced by the mean flow

dissipation of energy. Clearly if the Reynolds number is sufficiently large so that the energy containing range and the dissipation range do not overlap, the energy injected into the large scales of the flow should be equal to the amount of energy transfer and finally to the energy dissipated into heat. As a consequence the rate of dissipation $\langle\epsilon\rangle$ is determined by the large scales of the flow, which indirectly affect the statistical state of the small scales fluctuations. Hence $\langle\epsilon\rangle$ can be estimated in terms of the mean motion characteristics and in particular through the relation, which is confirmed by experimental analysis [71], $\langle\epsilon\rangle \simeq u^3/L$ which does not involve the viscosity since it is a small scales parameter. In this contest we can consider the

Kolmogorov first similarity assumption: At large Reynolds number the small scale statistical properties are uniquely and universally determined by the scale l, the mean energy dissipation rate $\langle\epsilon\rangle$ and the viscosity ν.

The order of magnitude of the scale at which the viscosity starts to have an appreciable effect should be characterized by a Reynolds number of order one, $\mathrm{Re}_\eta = \eta \mathrm{v}_\eta/\nu = 1$, and using a dimensional estimate for the characteristic velocity of this scale $v_\eta = (\langle\epsilon\rangle l)^{\frac{1}{3}}$, we obtain the subsequent expression for the Kolmogorov scale

$$\eta = \left(\frac{\nu^3}{\langle\epsilon\rangle}\right)^{\frac{1}{4}},$$

which is associated with the smallest dissipative eddies. Consequently according to the first similarity assumption the small scales of large Reynolds number flow are statistically similar, i. e. they are statistically identical when scaled by the Kolmogorov scales. The probability distribution for the dimensionless field $w(\xi,\zeta) = v(\xi\eta, \zeta\tau_\eta)/v_\eta$ should be universal, i.e. the same for all turbulent flows and should not depend on the mechanism associated with the generation of the turbulence. The ratio of the smallest scale to the largest scale is easily determined from the definition of η and from the scaling $\langle\epsilon\rangle \simeq u^3/L$:

$$\frac{L}{\eta} = Re_{\mathrm{L}}^{\frac{3}{4}}$$

and increases with the integral Reynolds number. As a consequence at sufficiently large Reynolds numbers[5] there is a range of scales (very small compared with L and

[5]where the correct meaning to the statement sufficiently large must be attributed on the basis of experimental results

very large compared with η) which is not affected by viscous effects. Therefore we can introduce the

Kolmogorov second similarity assumption: in the limit of infinite Reynolds number all the small scales statistical properties are uniquely and universally determined by $\langle\epsilon\rangle$ and l, independent of ν.

Clearly we may assume that in the limit of vanishing viscosity (for $Re_{\mathrm{L}} \to \infty$) the rate of energy dissipation is finite and equal to the energy flux: $\lim_{\nu\to 0}\langle\epsilon(\nu)\rangle = \langle\epsilon\rangle$, which is confirmed by experimental evidence [71]. For large, but finite Re all the statistics are determined by $\langle\epsilon\rangle$ in the "*inertial range*" $\eta \ll l \ll L$, where the main physical effect is the inertial transfer of energy towards smaller scales without any appreciable dissipation.

2.5 The Kolmogorov equation

In his third 1941 turbulence paper Kolmogorov derived an exact relation for the third order longitudinal structure function stemming from the KH equation and assuming global homogeneity, isotropy and finiteness of the energy dissipation. It is possible to consider a globally isotropic field since the statistical state of the small scales is universal and the resulting relations should be valid for any locally isotropic field, independently of whether or not the turbulence is globally isotropic. Let us now express the KH equation in terms of the longitudinal structure functions $\delta u_\parallel^2$ and $\delta u_\parallel^3$, which are related to $\langle u_\parallel u'_\parallel\rangle$ and $\langle u_\parallel u_\parallel u'_\parallel\rangle$ through the relations:

$$\langle u_\parallel u'_\parallel\rangle = \langle u^2\rangle - \frac{1}{2}\,\delta u_\parallel^2 \qquad\qquad \langle u_\parallel u_\parallel u'_\parallel\rangle = -\frac{1}{6}\,\delta u_\parallel^3\,,$$

so that the equation reads:

$$\frac{\partial\left(\langle u^2\rangle - 1/2\,\delta u_\parallel^2\right)}{\partial t} \;=\; \left(\frac{4}{r}+\frac{d}{d\,r}\right)\left(-\frac{1}{6}\delta u_\parallel^3\right) \;+\; 2\,\nu\,\left(\frac{d^2}{dr^2}\;+\;\frac{4}{r}\frac{d}{d\,r}\right)\left(\langle u^2\rangle - \frac{1}{2}\delta u_\parallel^2\right) \tag{2.20}$$

Observing that if $r \ll L$ the small scale properties should not depend explicitly on time and for globally isotropic turbulence $\partial\langle u^2\rangle/\partial t = -2/3\,\langle\epsilon\rangle$ we have:

$$-\frac{2}{3}\langle\epsilon\rangle = -\frac{1}{6}\left[\frac{d\delta u_\parallel^3}{dr}\;+\;\frac{4}{r}\delta u_\parallel^3\right]\;-\;\nu\;\left[\frac{d^2\delta u_\parallel^2}{dr^2}\;+\;\frac{4}{r}\,\frac{d\delta u_\parallel^2}{dr}\,.\right]$$

If we now integrate over r the final equation reads:

$$\delta u_\parallel^3\;-6\,\nu\,\frac{d\delta u_\parallel^2}{dr}\;=\;-\,\frac{4}{5}\langle\epsilon\rangle\,r\,, \tag{2.21}$$

which gives the exact expression for the third order longitudinal structure function in terms of the separation r plus a viscous correction that vanishes in the inertial range (or equivalently taking the limit $\nu \to 0$ which eliminates any residual viscous diffusion at finite scale),

$$\delta u_\parallel^3 = \;-\,\frac{4}{5}\langle\epsilon\rangle\,r \tag{2.22}$$

which is the Kolmogorov "$4/5ths$ law". This is one of the most important results since it is exact and it is a sort of boundary condition for the theories of turbulence which must satisfy this law or must violate the assumptions on which it is based.

If we now consider the balance equation for the energy spectrum function integrated on the energy containing range, see equation 2.18 and figure 2.1 for a schematic illustration of the following considerations, we find $-W\,(k,t) = \partial/\partial t\,\int_0^k E\,(k)\,dk$ and if we integrate over the dissipation range, see equation 2.19, we find $W\,(k) = \langle\epsilon\rangle$. In the inertial subrange the spectral transfer is the only significant process so that integrating between two wave numbers $k_1 < k_2$ in this range we have: $W\,(k_1) - W\,(k_2) = 0$,

showing that the flux of energy is constant and in particular equal to the dissipation rate $W(k_1) = \langle \epsilon \rangle$. This last relation is the spectral form of the fourth-fifth law and allows us to identify $\delta u_{\parallel}^3 / r$ as the energy flux in physical space.

We note that the Kolmogorov equation was demonstrated only on the basis of global isotropy, since it uses isotropic expression for the triple velocity correlation (see for instance the criticisms in [19] and [44]). However Hill [24] derived the "$4/5ths$ law" by use of local isotropy only. At the moment the experimental evidence confirms the 4/5ths law which is quite general and since this equation involves only velocity differences it is though to be exact for all types of flows, provided that local homogeneity and local isotropy hold [52].

Chapter 3

The Kolmogorov equation

For inhomogeneous flows, such as a channel flow, in addition to the processes characterizing homogeneous isotropic turbulence, i.e. energy cascade and dissipation we have to consider additional effects induced by inhomogeneity, i.e. production and spatial redistribution of energy.

The characteristics of the turbulent fluctuations may change appreciably in different ranges of scales because the local large scales parameters, such as the mean shear, depend on the distance from the wall. As a consequence a complete understanding of these interacting phenomena requires a detailed description of the processes occurring simultaneously in physical space and in the space of turbulent scales. To describe the picture in the space of scales it is necessary to analyze the energy content of a given scale as a function of the spatial position. The proper quantity to consider is the second order structure function $\langle \delta u^2 \rangle$ (see appendix A for nomenclature) which loosely speaking is related to the energy content at a given scale $r = \sqrt{r_\mathrm{i} r_\mathrm{i}}$, and therefore henceforth will be referred to as *scale energy*. The proper tool to perform this kind of analyses is the extension of the Kolmogorov equation 1.1, which is derived in appendix A.

3.1 Homogeneous isotropic turbulence

Equation 1.1, reduces to the classical Kolmogorov equation as homogeneous isotropic conditions are approached. In this limit the derivatives with respect to the mid-point X_c and the contribution of the mean velocity vanish, and the equation reads:

$$\frac{\partial \langle \delta u^2 \delta u_\mathrm{j} \rangle}{\partial r_\mathrm{j}} = -4\langle \epsilon \rangle + 2\,\nu \frac{\partial^2 \langle \delta u^2 \rangle}{\partial r_\mathrm{j} r_\mathrm{j}}\,, \tag{3.1}$$

which expressed in terms of the longitudinal velocity increments is the Kolmogorov equation 2.21. In the inertial range this equation reduces to the fourth-fifths law 2.22 which relates the third order longitudinal structure function to the mean energy dissipation $\langle\epsilon\rangle$. In the absence of intermittency this relation suggests that the main parameter involved in any inertial range scaling should be $\langle\epsilon\rangle$, which is equal to the average energy flux through scales. In this context the scaling behavior of the p-order structure function is assumed to be, on dimensional ground, $\langle\delta u_{\parallel}^{p}\rangle \simeq \langle\epsilon\rangle^{\frac{p}{3}} r^{\frac{p}{3}}$, i.e. the flow is expected to be scale invariant in the inertial range with a unique scaling exponent $h = 1/3$ [19]. However experimental results have show that the scaling laws present exponents $\zeta(p)$ substantially different from the dimensional prediction for large p's. This behavior was essentially related to the random nature of the dissipation field ϵ. When intermittency correction are applied, following for instance the refined Kolmogorov hypothesis [53], the scaling exponents are related to the statistics of the dissipation field. Another phenomenological model, proposed by Parisi and Frisch [19], assumed that the velocity increments possess a continuous range of scaling exponents related to the multi fractal structure of the turbulent field.

Equation 3.1 describes the universal behavior of the small scales $r \ll L$, in fact it neglects the mechanism involved in the production of turbulence and should be valid for any large Reynolds number flows.

3.2 Homogeneous shear flow

Let us now consider the extension of the Kolmogorov equation 3.1 to homogeneous anisotropic flows, where the cascade process is strongly modified by the energy injection associated with the mean velocity gradient. We consider a shear flow with a mean velocity $U = S\,y$ in the x direction, while the mean shear is in the y direction, and u, v are the fluctuation velocity components in the x and y directions, respectively. For an homogeneous shear equation specializes to:

$$\frac{\partial\langle\delta u^2\delta u_i\rangle}{\partial r_i} + \frac{\partial(\langle\delta u^2\rangle S r_y)}{\partial r_x} + 2S\langle\delta u\delta v\rangle = -4\langle\epsilon\rangle + 2\nu\,\frac{\partial\langle\delta u^2\rangle}{\partial r_i\partial r_i}, \tag{3.2}$$

which has been analyzed in detail in [9]. In this work was shown that the inertial transport term on the right hand side of equation 3.2 is the proper generalization of the third order structure function for an anisotropic flow. It clearly shows that the flux

of turbulent kinetic energy in the space of scales is due to both the mean flow and the turbulent fluctuations.

In this case in addition to the two length-scales which are typical of homogeneous and isotropic turbulence, namely the dissipative and the integral scales, the shear introduces a further characteristic quantity, namely the shear scale $\mathrm{L_S}$. Some separations, of the order of the scales where the mean gradient is imposed, are directly affected by the production of energy $2\,S\,\langle \delta u \delta v \rangle$, while other scales are not influenced directly by the mean shear, and follow the classical Kolmogorov equation 3.1. Moreover by comparing the estimate of the velocity fluctuations induced, at a given scales r, by the mean shear, with the estimate given in the inertial range by the Kolmogorov equation $\delta u \simeq \epsilon^{\frac{1}{3}} r^{\frac{1}{3}}$, it is possible to identify a cross-over scale between a production dominated and a cascade dominated ranges:

$$L_{\mathrm{S}} = \sqrt{\frac{\epsilon}{S^3}}\,, \tag{3.3}$$

the production of energy is active at scales larger than the shear scales L_{S}, where the scaling laws described by the refined Kolmogorov-Obhukov theory must fail, while below L_{S} there is a classical inertial range dominated by the transfer of scale energy. Below L_{S} one may model the dynamics by means of equation 3.1 completed with an assigned incoming energy flux at scales of order of L_{S}.

3.3 Scale by scale budget for a simple shear

To account for the additional effects that alter the scale by scale budget in inhomogeneous conditions we consider the generalized equation 1.1, that for a turbulent channel flow specializes to:

$$\begin{aligned} \frac{\partial \langle \delta u^2 \delta u_i \rangle}{\partial r_i} + \frac{\partial \langle \delta u^2 \delta U \rangle}{\partial r_x} \;+\; 2\langle \delta u \delta v \rangle \left(\frac{dU}{dy}\right)^* + \frac{\partial \langle v^* \delta u^2 \rangle}{\partial Y_c} \;= \\ -\; 4\langle \epsilon^* \rangle + 2\nu \frac{\partial^2 \langle \delta u^2 \rangle}{\partial r_i \partial r_i} - \frac{2}{\rho}\frac{\partial \langle \delta p\, \delta v \rangle}{\partial Y_c} + \frac{\nu}{2}\frac{\partial^2 \langle \delta u^2 \rangle}{\partial {Y_c}^2}, \end{aligned} \tag{3.4}$$

which contains all the processes which simultaneously characterize the dynamics of

wall bounded flows both in the space of scales and in physical space. In fact the derivatives with respect to r are associated with the description in the space of scales, while Y_c-derivatives are associated with inhomogeneity.

Equation 3.4 manifests a well defined asymptotic behavior at large scales. At large separations the velocities at the two points are uncorrelated and it easy to show that the equation approaches four times the mid-point average of the single point energy budget for unit mass of fluid, namely

$$\langle u_j \rangle \frac{\partial K}{\partial x_j} = -\rho \langle u_i' u_j' \rangle \frac{\partial U_i}{\partial x_j} + \nu \frac{\partial^2 K}{\partial x_j \partial x_j} - \frac{\rho}{2} \frac{\partial}{\partial x_j} \langle u_i' u_i' u_j' \rangle - \frac{\partial}{x_j} \langle u_j' p' \rangle - \nu \rho \langle \left(\frac{\partial u_i'}{\partial x_j} \right)^2 \rangle \tag{3.5}$$

which is recovered as an asymptotic limit.

Thus equation 3.4 represents the link between the large scales (equation 3.5), and the small scales (equation 3.1) characteristics of the turbulent field. In detail the large scale limit of the divergence of the turbulent flux through scales is

$$\lim_{r \to \infty} \frac{\partial \langle \delta u^2 \delta u_k \rangle}{\partial r_k} = \frac{1}{2} \left(\frac{\partial \langle u^2 u_k \rangle}{\partial x_k} + \frac{\partial \langle u'^2 u'_k \rangle}{\partial x_k'} \right) = \frac{\partial \langle u^2 u_k \rangle^*}{\partial X_{c_k}}, \tag{3.6}$$

reveling that the inhomogeneous contribution represents the large scale boundary condition for the corresponding term in the space of scales, and therefore both the contributions, in the space of scales and in physical space are present, with the same value, in the global kinetic energy balance. For homogeneous flows the right hand side of equation 3.6 is zero, and the divergence in $r-$space of the turbulent component $\langle \delta u^2 \delta u_k \rangle$ of the scale energy flux vanishes as the separation is increased. In this condition the turbulent flux

$$\lim_{r \to \infty} \langle \, \delta u^2 \, \delta u_k \, \rangle = \delta \, \langle \, u^2 \, u_k \, \rangle \tag{3.7}$$

also vanishes. In fact in homogeneous shear flow the energy cascade is initialized by the energy provided by the production term at large separations. Similarly the Kolmogorov

equation 3.1 requires a replenishment of the energy dissipated by the viscous action if we are not dealing with a problem of freely decaying turbulence. This boundary condition on the energy flux is frequently enforced in numerical simulations by introducing an external random force which is homogeneous, isotropic and delta correlated in time.

Chapter 4

The Yaglom equation

In this chapter we will focus on the problem of passive scalar transport in turbulent flows. In particular a passive scalar denotes an advected "*substance*" which has no dynamical effect on the fluid motion. The "*substance*" could be a dye or a pollutant or a temperature field if the density variations due to the temperature differences in the fluid are so small that the buoyancy forces are negligible in comparison with the inertia forces. Since the equation governing the evolution of a passive scalar field is the same, irrespectively of the nature of the scalar, we will take the temperature as representative.

The instantaneous passive temperature field $\tilde{\theta}(x_{\mathrm{i}}, t)$, satisfies the advection diffusion equation:

$$\frac{\partial \tilde{\theta}}{\partial t} + \tilde{u}_{\mathrm{j}} \frac{\partial \tilde{\theta}}{\partial x_{\mathrm{j}}} = \chi \frac{\partial^2 \tilde{\theta}}{\partial x_{\mathrm{j}} \partial x_{\mathrm{j}}} \tag{4.1}$$

where χ is the thermal diffusivity of the fluid. Since the velocity field is not influenced by the scalar, equation 4.1 is linear with respect to $\tilde{\theta}$, and therefore it might be thought that the scalar problem could be easier than the turbulent problem concerning the velocity field. There is, however, a strong numerical support showing that the statistical properties of the scalar are strictly connected with the mixing process itself rather than being inherited from the velocity field [68]. In fact several works (see among others [10]) have shown that the scalar field can presents coherent structures and can show an intermittent behavior even in a purely Gaussian velocity field (which is not intermittent). In this context, since a passive scalar obeying a linear equation, shows distinctive aspects with respect to the velocity field, it is very important to analyze which are the main features which characterize the scale by scale scalar variance budget

and to verify if these characteristics are related to the main features of the velocity field.

4.1 The generalized Yaglom equation

In this section we summarize the procedure to obtain the generalized Yaglom equation, which allows to describe the behavior of a passive temperature field even if the hypotheses of local isotropy is not fulfilled. The experimental evidence [77] have shown that there is a lack of isotropy at both dissipation and inertial scales [77] for the passive scalar and the influence of the larger scales over the smaller ones can not be neglected. To provide a more realistic description of small scales turbulence, especially when asymptotic conditions are not yet reached, it is necessary to consider a generalized form of the scale by scale balance equation, to account for the inhomogeneity and anisotropy of the flow under consideration.

The derivation of the equation is based on the one proposed in [27], and it is analogous to the derivation outlined in appendix A, for the generalized Kolmogorov equation 1.1. We follow the classical Reynolds decomposition for the fluid dynamics variables, for instance the temperature field is decomposed into a mean $\langle\theta\rangle$ and a fluctuating component θ. The evolution equation for $\delta\theta^2 = (\theta' - \theta)^2$ (see appendix A for nomenclature) can be derived if we write the advection diffusion equation for θ at point x_{i} and for θ' at point x'_{i}, then we subtract the two equations and multiply the result for $\delta\theta$. The averaged equation for a steady flow reads

$$\frac{\partial\langle\delta\theta^2\rangle}{\partial t} + \frac{\partial\langle\delta\theta^2\delta u_{\mathrm{j}}\rangle}{\partial r_{\mathrm{j}}} + \frac{\partial\langle\delta\theta^2 u^*_{\mathrm{j}}\rangle}{\partial X_{\mathrm{c_j}}} + \frac{\partial\langle\delta\theta^2\rangle\delta U_{\mathrm{j}}}{\partial r_{\mathrm{j}}} + \frac{\partial\langle\delta\theta^2\rangle U^*_{\mathrm{j}}}{\partial X_{\mathrm{c_j}}} + \tag{4.2}$$

$$2\langle\delta u_{\mathrm{j}}\delta\theta\rangle\frac{\partial\delta\Theta}{\partial r_{\mathrm{j}}} + 2\langle\delta\theta u^*_{\mathrm{j}}\rangle\frac{\partial\delta\Theta}{\partial X_{\mathrm{c_j}}} = 2\chi\frac{\partial^2\langle\delta\theta^2\rangle}{\partial r_{\mathrm{j}}\partial r_{\mathrm{j}}} + \frac{\chi}{2}\frac{\partial^2\langle\delta\theta^2\rangle}{\partial X_{\mathrm{c_j}}\partial X_{\mathrm{c_j}}} - 4\langle\epsilon_\theta\rangle,$$

where $\delta\Theta = \Theta' - \Theta$ denotes the increment of the mean temperature, denoted by the uppercase letter Θ, and $\langle\epsilon_\theta\rangle$ defined as

$$\langle\epsilon_\theta\rangle = \chi\langle\frac{\partial\theta}{\partial x_{\mathrm{i}}}\frac{\partial\theta}{\partial x_{\mathrm{i}}}\rangle, \tag{4.3}$$

is the single point mean rate of destruction of the scalar variance $\langle\theta^2\rangle$, due to the

molecular motion of the fluid that has a smoothing action on the distribution of the scalar.

The generalized equation 4.2 contains the several interacting processes which affect the dynamics of the passive scalar. Besides the classical concept of a variance cascade, the morphology of the field is related to additional processes such as production $2\langle\delta\theta\delta u\rangle\partial\Theta/\partial y$ of scalar fluctuations and inhomogeneous turbulent transport expressed by the $X_{\mathrm{c}}-$derivatives.

The diffusive and mixing properties may change appreciably in dependence of both the molecular Prandtl number $\mathrm{Pr} = \nu/\chi$ (defined as the ratio of the molecular diffusion and viscous time scales) and the boundary conditions. Moreover the local large scales characteristics of the scalar and the velocity fields, which initialize the variance cascade at large separations, are function of the spatial coordinates $X_{\mathrm{c_i}}$ (namely for a channel flow the wall distance). All these inhomogeneous effects are retained in the generalized equation, which allows to describe the dynamics of the scalar field even if asymptotic conditions are not reached and moreover if the large scales anisotropies do not decay down to the small scales.

4.1.1 The Yaglom equation

In the context of local isotropy Yaglom (1949) obtained a fundamental relation for the third order mixed velocity-scalar structure function. This relation stems from the evolution equation for the second order two points scalar correlation function, following essentially the same steps used to obtain the Kármán-Howarth equation. However it is easily to show that the Yaglom equation can be directly recovered from the generalized form 4.2, which for isotropic stationary conditions reads

$$\frac{\partial\langle\delta\theta^2\delta u_{\mathrm{j}}\rangle}{\partial r_{\mathrm{j}}} \;=\; 2\chi\frac{\partial^2\langle\delta\theta^2\rangle}{\partial r_{\mathrm{j}}\partial r_{\mathrm{j}}} \;-\; 4\,\langle\epsilon_\theta\rangle\,. \tag{4.4}$$

If we integrate with respect to r we obtain:

$$\langle\delta u_{\parallel}\,\delta\theta^2\rangle \;=\; 2\chi\,\frac{d\langle\delta\theta^2\rangle}{dr_{\mathrm{j}}} \;-\; \frac{4}{3}\,\langle\epsilon_\theta\rangle\,r. \tag{4.5}$$

As the Kolmogorov equation 2.20 the Yaglom equation 4.5 has been derived on the

basis of global isotropy, but since it involves only increments of the variables, it is thought to be exact for any kind of turbulent field, not necessarily isotropic, provided that local isotropy holds.

4.1.2 Local isotropy at large Péclét numbers

The Kolmogorov similarity hypotheses (see par. 2.4) can be extended to the passive scalar field θ, meaning that under suitable conditions it can be regarded as locally isotropic. However in addition to the parameters characterizing the statistical state of small scales velocity fluctuations we have to consider the molecular diffusivity χ and the mean rate of variance dissipation $\langle \epsilon_\theta \rangle$. In fact, as a consequence of turbulent mixing, there is the formation of distorted and twisted layers with very different temperatures. This process causes the amplification of the local gradients whereas the molecular diffusion has a smoothing action on the distribution of the scalar. Therefore for the description of the small scales properties of the scalar it is necessary to consider the influence of the diffusivity.

Since the advection-diffusion equation 4.1 has the same structure of the Navier-Stokes equations [1], it is possible to describe the balance for $\langle \theta^2 \rangle$ (which is a measure of the variation of the scalar field with respect to its mean value) in the spectral space. An analysis similar to the one performed for the turbulent kinetic energy (see par. 2.3), would lead to the conclusion that at large enough Re and Pe numbers there is a cascade of variance towards smaller scales until the temperature differences are dissipated at a rate $\langle \epsilon_\theta \rangle$. We observe that the $\mathrm{Pe} = \mathrm{UL}/\chi$ number is defined as the ratio of the convection of heat and the molecular conduction (where L should be the scalar integral scale, but we can assume here that is of the same order of the velocity integral scale). Therefore for the scalar we can introduce the equivalent to the first similarity hypothesis

First similarity assumption: At large Reynolds and Péclét numbers the statistical properties of the temperature increments at small scales are uniquely and universally determined by the parameters $\langle \epsilon \rangle$, $\langle \epsilon_\theta \rangle$, ν and χ.

If the Pe number is enough large there exists a *convective subrange* of scales where the only physical effect is the inertial transfer of scalar variance, since the diffusivity is active only at very small scales. However we should note that the viscous and molecular effects became important at different scales. In particular when $\nu \ll \chi$ i.e. $\mathrm{Pr} \ll 1$

[1] meaning that it has an advection and a diffusion term even if it is linear in θ and does not contain the pressure term

the dissipative scale for the scalar according to Corrsin can be estimated as

$$\eta_{\mathrm{c}} = \left(\frac{\chi^3}{\epsilon}\right)^{\frac{1}{4}}, \tag{4.6}$$

while Batchelor (1959) concluded that for $\nu \gg \chi$ the dissipative scalar scale can be estimated as

$$\eta_{\mathrm{b}} = \left(\frac{\nu\chi^2}{\epsilon}\right)^{\frac{1}{4}}. \tag{4.7}$$

Clearly for $\mathrm{Pr} \simeq 1$ the dissipative scale for the velocity and the temperature fields should coincide. However recent results [66] [62] have shown that for $\mathrm{Pr} \simeq 1$ the dissipative scale for the scalar is smaller than that of the velocity, but there isn't yet a general agreement.

Let us consider now the inertial-convective subrange $max\,(\eta, \eta_\theta) \ll r \ll L$, where η_θ represents the dissipation scale of the scalar, irrespective of the Pr number. In this range since the effects of viscosity and diffusivity are negligible, we can introduce for the scalar the equivalent of the second similarity hypotheses

Second similarity assumption: At large Reynolds and Péclét numbers the statistical properties of the temperature increments at small scales are uniquely and universally determined by the parameters $\langle\epsilon\rangle$ and $\langle\epsilon_\theta\rangle$.

Hence the Yaglom equation 4.5 in the inertial-convective subrange assumes a simple form

$$\langle \delta u_{\parallel}\, \delta\theta^2 \rangle = -\frac{4}{3}\langle\epsilon_\theta\rangle\, r, \tag{4.8}$$

which allow to identify $\langle \delta u_{\parallel}\, \delta\theta^2 \rangle / r$ as the constant flux of variance in this subrange. As suggested by this law in the inertial-convective subrange the scaling of the mixed scalar-velocity structure functions should be of the form : $\langle \left(\delta u_{\parallel}\, \delta\theta^2\right)^p \rangle \simeq r^p \langle\epsilon_\theta\rangle^p$, and therefore they should depend only on the mean value of the scalar dissipation. For the scalar structure function, instead, there isn't any exact results stemming from the equation of motions, since the temperature field is coupled with the velocity (see eq. 4.1). However, following the second similarity hypotheses, on dimensional grounds

we can estimate $\langle \delta\theta^p \rangle \simeq r^{p/3} \langle \epsilon_\theta \rangle^{p/6} \langle \epsilon \rangle^{p/6}$. Clearly using an argument á la Landau it should be necessary to consider intermittency correction due to the spotty nature of both the dissipation rates ϵ and ϵ_θ, which are directly connected to the large scales properties of the flow. We can recall that there are many attempts to take into account intermittency corrections, and some exact results are obtained when the velocity field is Gaussian, as described in the Kraichnan model. There are also different models which directly consider the spatial organization of the scalar field into well defined structures, such as ramp-cliffs, see among others [65], which could be directly related to the intermittency of the scaling exponent.

Despite this aspects, the Yaglom equation describes the universal behavior of small isotropic scales, neglecting the details of the production mechanisms of scalar variance.

4.1.3 The Yaglom equation for a mean scalar gradient

In order to reach a steady state it is necessary to replenish the scalar fluctuations destroyed by the action of the dissipation $\langle \epsilon_\theta \rangle$. The simplest way is to introduce an external random forcing term, which should be active only at large scales. An alternative injection mechanism, closer to the typical experimental situation, is to maintain a gradient G of the scalar, so that the evolution equation for the field reads

$$\frac{\partial \theta}{\partial t} + u_{\mathrm{j}} \frac{\partial \theta}{\partial x_{\mathrm{j}}} = \chi \frac{\partial^2 \theta}{\partial x_{\mathrm{j}} \partial x_{\mathrm{j}}} - G v \tag{4.9}$$

where the mean temperature field is $\Theta = G\, y$, G and v are the mean scalar gradient and the fluctuation velocity component in the y direction, respectively. The introduction of a mean gradient selects a privileged direction in the system, and introduces an anisotropic behavior, which is reflected by the presence of a production term in the scale by scale budget

$$\frac{\partial \langle \delta\theta^2 \delta u_{\mathrm{j}} \rangle}{\partial r_{\mathrm{j}}} + 2 \langle \delta u_{\mathrm{j}} \delta\theta \rangle \left(\frac{\partial \delta\Theta}{\partial X_{\mathrm{c_j}}} \right)^* = 2\chi \frac{\partial^2 \langle \delta\theta^2 \rangle}{\partial r_{\mathrm{j}} \partial r_{\mathrm{j}}} - 4 \langle \epsilon_\theta \rangle , \tag{4.10}$$

where an asterisk denotes an average with respect to the mid point, and the velocity field is supposed isotropic. In this case, besides the dissipative scales of the velocity and the scalar fields, we have to consider a new scale associated with the dynamics

induced by the mean gradient G at large scales. At smaller scales we can assume that the behavior of the scalar is correctly described by the Yaglom equation 4.4, provided that local isotropy holds. The crossover scale between convective dominated and production dominated ranges can be estimated by substituting, the order of magnitude of the fluctuations induced at a scale r by the gradient $\delta\theta \simeq G\,r$, in the inertial convective range expression for the mixed structure function $\langle \delta\theta^2 \delta u_{\parallel} \rangle \simeq \langle \epsilon_\theta \rangle\, r$. Using the Kolmogorov estimate for the velocity increments in the inertial range $\delta u_{\parallel} \simeq \langle \epsilon \rangle\, r$, we find

$$L_{\mathrm{G}} \;=\; \left(\frac{\langle \epsilon_\theta \rangle^3}{\langle \epsilon \rangle\, G^6} \right)^{\frac{1}{4}} . \tag{4.11}$$

The production of variance should be active at scales grater than L_{G}, while below L_{G} the classical picture is still valid. Let us now consider the case of a homogeneous shear flow, whose velocity fluctuations are sustained by the action of the local shear S (see par.3.2). In this case the generalized Yaglom equation reads

$$\frac{\partial \langle \delta\theta^2 \delta u_{\mathrm{j}} \rangle}{\partial r_{\mathrm{j}}} \;+\; \frac{\partial \langle \delta\theta^2 S r_{\mathrm{y}} \rangle}{\partial r_{\mathrm{x}}} \;+\; 2 \langle \delta u_{\mathrm{j}} \delta\theta \rangle \left(\frac{\partial \delta\Theta}{\partial X_{\mathrm{c_j}}} \right)^{*} \;=\; 2\chi\, \frac{\partial^2 \langle \delta\theta^2 \rangle}{\partial r_{\mathrm{j}} \partial r_{\mathrm{j}}} \;-\; 4\, \langle \epsilon_\theta \rangle\,, \tag{4.12}$$

where we have an additional convective term, related to δU, which shows that the flux of variance in the space of scales is due to both the mean flow and the turbulent fluctuations. However we should recall that in this case also the velocity field is anisotropic (see par.3.2), and it is affected by a production range at scales $r > L_{\mathrm{S}}$. If $L_{\mathrm{S}} > L_{\mathrm{G}}$ the estimate 4.11 still holds. If $L_{\mathrm{S}} < L_{\mathrm{G}}$ we will have an intermediate range where the dynamics of the scalar is dominated by the convection term, while the velocity is still dominated by the production mechanism. We shall propose a different dimensional prediction for the scale associated with the mean gradient

$$L_{\mathrm{G}} \;=\; \left(\frac{\langle \epsilon_\theta \rangle}{S\, G^2} \right)^{\frac{1}{2}} . \tag{4.13}$$

Clearly this last estimate implies that the Yaglom relation could be used even if the velocity field is not locally isotropic. Hence the validity of 4.13 may be questioned.

However these findings allow us to show that the dynamics of the scalar can be profoundly affected by the scale by scale dynamics of the velocity field.

4.2 Yaglom equation for a turbulent channel flow

Besides the classical description in terms of the cascade of scalar variance for an inhomogeneous flow we have to consider additional effects, related to the spatial transport induced by the inhomogeneity of the field. The diffusive and mixing characteristics of the scalar may change appreciably in different ranges of scales in dependence of both the Pr number and the boundary conditions. Moreover the local large scales characteristics of the scalar and the velocity fields, such as the mean gradients, depend on the geometric location and consequently can lead to both the aforementioned condition: $L_S \ll L_G$ or $L_G \ll L_S$. Hence it is necessary to analyze the dependence of the content of the scalar fluctuations $\delta\theta^2$ of a given scale as a function of the geometric location, namely the wall normal distance y for a turbulent channel flow. In this case the generalized Yaglom equation reads

$$\frac{\partial\langle\delta\theta^2\delta u_j\rangle}{\partial r_j} + \frac{\partial\langle\delta\theta^2\rangle\delta U}{\partial r_x} + \frac{\partial\langle\delta\theta^2 v^*\rangle}{\partial Y_c} + 2\langle\delta v\delta\theta\rangle\left(\frac{\partial\Theta}{\partial y}\right)^* = 2\chi\frac{\partial^2\langle\delta\theta^2\rangle}{\partial r_j\partial r_j} + \frac{\chi}{2}\frac{\partial^2\langle\delta\theta^2\rangle}{\partial Y_c\partial Y_c} - 4\langle\epsilon_\theta\rangle, \tag{4.14}$$

which is the link between the large scales [2] and the small scales (equation 4.4). In particular the same considerations made at the end of the paragraph 3.3 for the generalized Kolmogorov equation are valid for the generalized Yaglom equation.

[2] it can be easily shown that the large scale limit of this equation is twice the mid-point average of the global variance budget

Chapter 5

Velocity field

In this section we will show some results obtained for the velocity field of a turbulent channel flow, which have been discussed in the paper [50]. The computational domain, shown in figure 5.1, is a turbulent channel flow, infinite in the streamwise and spanwise directions. Periodic boundary conditions are applied in the homogeneous directions x and z, and impermeability and no-slip are imposed on the solid walls.

The simulation is carried out with a highly accurate numerical formulation [47], exploiting spectral methods for the spatial discretization of the velocity field, namely Fourier expansion in wall parallel planes and a Chebyshev expansion in the wall normal direction. The time advancement is performed using a mixed Crank-Nicholson/ Runge-Kutta scheme.

The turbulent Reynolds number, based on the channel half height is $\mathrm{Re}_* = \mathrm{u}_*\mathrm{h}/\nu \simeq$

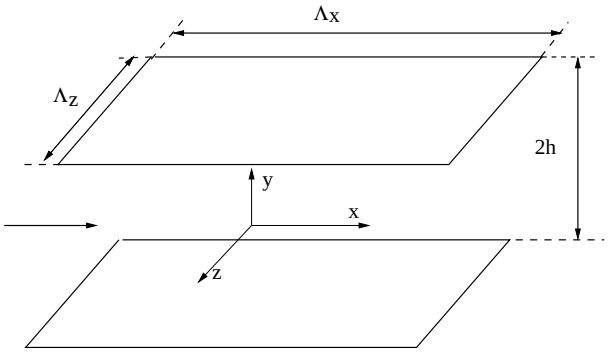

Figure 5.1: Flow configuration and nomenclature for the channel flow. The flow goes from left to right in the direction of the mean flow $U(y)$. The streamwise direction is $x \equiv x_1$. The wall-normal and the spanwise coordinates are $y \equiv x_2$ and $z \equiv x_3$, respectively. The corresponding fluctuation velocity components are denoted by $u \equiv u_1$, $v \equiv u_2$ and $w \equiv u_3$, respectively.

180, where $u_* = \sqrt{\tau_w/\rho}$ is the friction velocity, [1] and τ_w is the viscous stress at the wall. The corresponding bulk Reynolds number is $\mathrm{Re_b} = \mathrm{u_b h}/\nu \simeq 2600$, where u_b is the velocity averaged over the channel section. The results are obtained in a computational domain of size $4h \times 2h \times 2h$, in the streamwise x, spanwise z and wall normal directions y, with a number of grid point equal to $256 \times 129 \times 128$. Therefore the corresponding resolution in wall units (i.e. made dimensionless with respect to u_* and ν) is $\Delta_\mathrm{x}^+ \simeq 2.8$, $\Delta_\mathrm{z}^+ \simeq 2.8$, and Δ_y varying from .05 at the wall to 4.8 at the centerline. The size of the selected computational domain is suited to investigate the spatial structure of the velocity field up to the Kolmogorov dissipative scale.

In this computation, exploiting the homogeneity of the field in wall parallel planes, we can perform the ensemble average of a given quantity in terms of spatial averages. However the dimensions of the domain are close to a minimum channel [29], and therefore the number of spatial structures involved in the spatial averages are reduced. Hence it is necessary also to exploit the temporal ergodicity and therefore long runs with small time steps are required. After reaching a statistically steady state the simulation has been continued for about 2400 eddy-turnover time $T = h/U_\mathrm{cl} = 1,25$, where U_cl is the mean velocity at the channel center. The eddy turn-over time can be identified with a reference time required for a substantial decorrelation of velocity structures. In addition to this we must observe that the life time of the streaks in the viscous sublayer is of the order of more than five hundred inner time units [39] and hence to consider uncorrelated configurations long runs are mandatory.

Finally we want to observe that if on the one hand the DNS allows to analyze the spatial and temporal structure of the components u, v, w and p of the fluctuating fields, on the other allows to treat only small Reynolds number flow, and consequently small Reynolds number effects can not be excluded. Hoverer, concerning the scale by scale budget analyses we are going to perform, we fill that the present findings are able to characterize the scale-dynamics when asymptotic conditions are not reached, and what is more to shed light over the mechanisms that should be necessarily present even in large Reynolds number flows.

5.1 Steady state

A necessary prerequisite to perform a statistical analyses of the flow is to reach a statistically steady state. Then the simulation is continued in order to collect enough fields to perform the turbulent statistics. Traditionally [37] the steady state of the

[1] which provides a natural scale for the velocity in the channel section

channel flow is associated with a linear behavior of the total stress, which is defined as

$$\tau\left(y\right) = \rho\nu\frac{dU}{dy} - \rho\langle uv\rangle\,, \tag{5.1}$$

where the first term on the right hand side is the viscous stress and the second is the Reynolds stress. This relation shows that in addition to the exchange of momentum due to the viscous forces there is a transport induced by the mixing properties of the turbulent flow. Hence as the microscopic motion leads to the appearance of viscous stresses, the additional Reynolds stresses are related to the fluctuating motion.

In a steady state the total shear stress, shown in figure 5.2 is a linear function of the wall normal distance

$$\tau\left(y\right) = \frac{1}{\mathrm{Re}}\frac{dU}{dy} - \langle uv\rangle = \tau_w\left(1 - \frac{\tilde{y}}{h}\right) \tag{5.2}$$

where $\tilde{y} = h - |y|$.

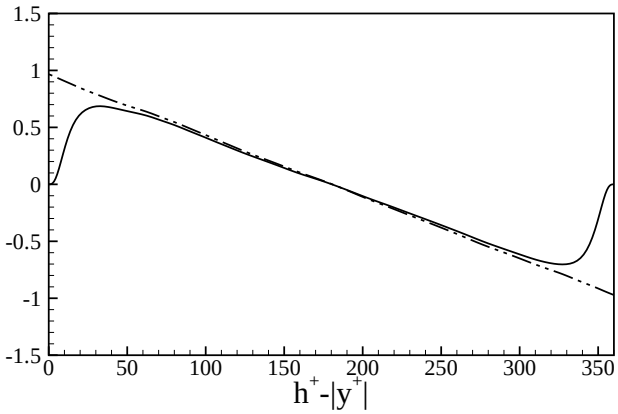

Figure 5.2: Total shear stress, dashed-double dotted line, turbulent component solid line, in the channel section. The quantities are normalized by u_*.

At the wall the boundary conditions impose a zero value of the Reynolds stresses and only the viscous contribution, which enforces the boundary conditions, is present. Hence in a narrow layer next to the wall, we can suppose that the dynamics of the flow can be described by appropriate length and velocity scales, based only on ρ, ν, and τ_w. These are u_* the friction velocity and $\delta_v = \nu/u_*$ the viscous length scale, which allow to introduce a friction or turbulent Reynolds number $\mathrm{Re}_* = \mathrm{u_*h}/\nu = \mathrm{h}/\delta_\mathrm{v}$. This

definition shows that for increasing value of the Reynolds number, and consequently of the turbulent Reynolds number Re_*, the viscous scale becames smaller and smaller and consequently the effect of the viscosity are relegated in the *viscous sublayer* whose thickness diminishes at increasing Re.

We can introduce an additional parameter which is the dimensionless wall normal distance $y^+ = \tilde{y}u_*/\nu$, that can be interpreted as a local Reynolds number, since its magnitude expresses the local importance of the viscous contribution. In fact different regions in the near wall region are traditionally identified on the basis of the value assumed by y^+. For instance away form the wall we can suppose that the viscous contribution to the stresses is negligible, as shown in figure 5.2, and if in addition to this the local wall normal distance is still smaller than h, we can identify the *logarithmic layer* , for $y^+ \gg 1$ and $y^+ \ll h^+$ where

$$-\langle u\, v\rangle \simeq u_*^2 \tag{5.3}$$

the turbulent flux is almost constant and the friction velocity provides the proper scaling factor for the Reynolds stress. Finally the transitional region between the viscosity-dominated and turbulent dominated region of the flow is the *buffer layer*.

5.2 Mean velocity profile

The layers of the near wall region can be characterized in terms of the behavior of the mean velocity profile $U(y)$, shown in figure 5.3.

Using a Taylor series expansion one finds that the mean velocity profile in the viscous sublayer is a linear function of the wall normal distance

$$U^+ = U/u_* = (h - |y|)^+ . \tag{5.4}$$

The upper bound of the viscous sublayer is given by a relation of the type $\delta_\mathrm{v} \simeq \alpha_\mathrm{v}\nu/u_*$, where the constant α_v must be found from experimental data. Clearly the viscous sublayer is not sharply limited but it is smoothly connected with the buffer layer, where the viscous and the Reynolds stresses are of the same order of magnitude. Traditionally α_v is assumed equal to 5, value which is also valid for our simulation.

Using dimensional arguments it is possible to determine the mean velocity profile in the logarithmic layer

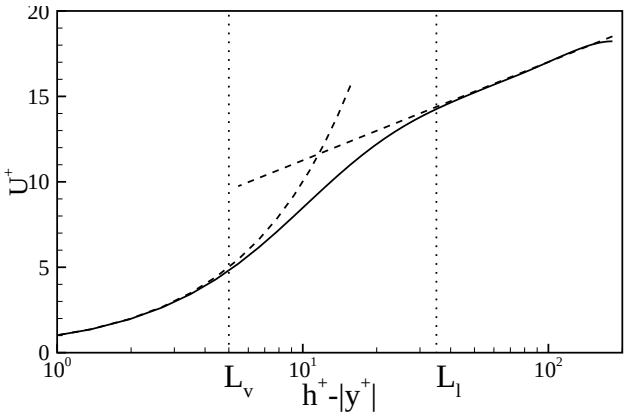

Figure 5.3: Left panel: Mean velocity profile U^+ in viscous units vs distance from the wall $(h - |y|)^+$, solid line. The dashed lines denote the linear and the log-law with a Kármán constant $k = .41$. Classically the near wall region is subdivided into the viscous sublayer $0 \leq (h - |y|)^+ \leq L_{\rm v}^+$, the buffer layer $L_{\rm v}^+ \leq (h - |y|)^+ \leq L_{\rm l}^+$ and the log-layer above $L_{\rm l}^+$ extending up to the bulk region where the mean profile deviates from the log-law. Typically, for Newtonian turbulence, $L_{\rm v}^+ \simeq 5$ and $L_{\rm v}^+ \simeq 30$.

$$U^+ = 1/k \, \log(h - |y|)^+ + \beta \,, \tag{5.5}$$

where k is the Kármán constant. In our simulation $k = .41$ and $\beta = 5.5$, and following [54] and [80] it seems that for larger Reynolds numbers the appropriate values for these constants should be .4 and 5.5, respectively. Clearly the lower boundary of the logarithmic layer is not sharply limited, but traditionally it is assumed to start at $(h - |y|)^+ \simeq 30$. The reader may wish to come back and use figure 6.3 as a schematic visualization of the different regions of the flow to be discussed in the following sections.

5.3 RMS profiles

The left panel of figure 5.4 shows the root mean square velocities $u_{\rm rms} = \sqrt{u^2}$, $v_{\rm rms}$, $w_{\rm rms}$, normalized by the friction velocity u_*. We observe that as a consequence of the impermeability and no slip conditions applied at the walls the limiting near wall behavior of the turbulent intensities can be derived using a Taylor series expansion in terms of $\tilde{y} = (h - |y|)$.

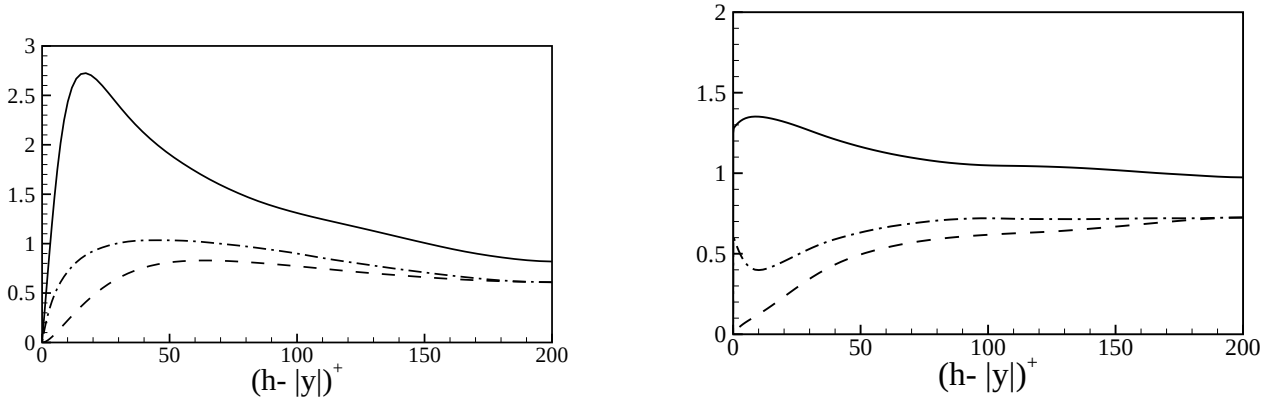

Figure 5.4: Left panel: root mean square velocities vs distance from the wall, $u^+_{\rm rms} : -$, $v^+_{\rm rms} : - \cdot -$, $w^+_{\rm rms} : --$. Right panel: Fluctuation intensities normalized by the kinetic energy, $u^2 : -$, $v^2 : - \cdot -$, $w^2 : --$.

$$\langle u^2 \rangle = b_1 \tilde{y}^2 + O\left(\tilde{y}\right)^3 \qquad \langle v^2 \rangle = b_2 \tilde{y}^4 + O\left(\tilde{y}\right)^5 \qquad \langle w^2 \rangle = b_3 \tilde{y}^2 + O\left(\tilde{y}\right)^3 \qquad (5.6)$$

Since the asymptotic of $\langle v^2 \rangle$ is of two order higher than that of the wall parallel velocities components, we can observe that very close to the wall the flow can be considered as a two components flow, or it may be subject to bi-dimensional effects, but it is not two dimensional since u and w wary in the wall normal direction.

In the logarithmic layer the three intensities are of the same order of magnitude of the friction velocity u_*, and what is more if we normalize the Reynolds stresses by the square of the turbulent kinetic energy $K = .5\left(u^2_{\rm rms} + v^2_{\rm rms} + w^2_{\rm rms}\right)$ these ratios are nearly uniform (see the right panel of figure 5.4). At the channel center the three components nearly approaches the same value, and consequently their anisotropy level is less here than in the other regions of the flow.

This behavior can be partially understood if we consider the evolution equations for the normal Reynolds stresses, specialized for a turbulent channel flow

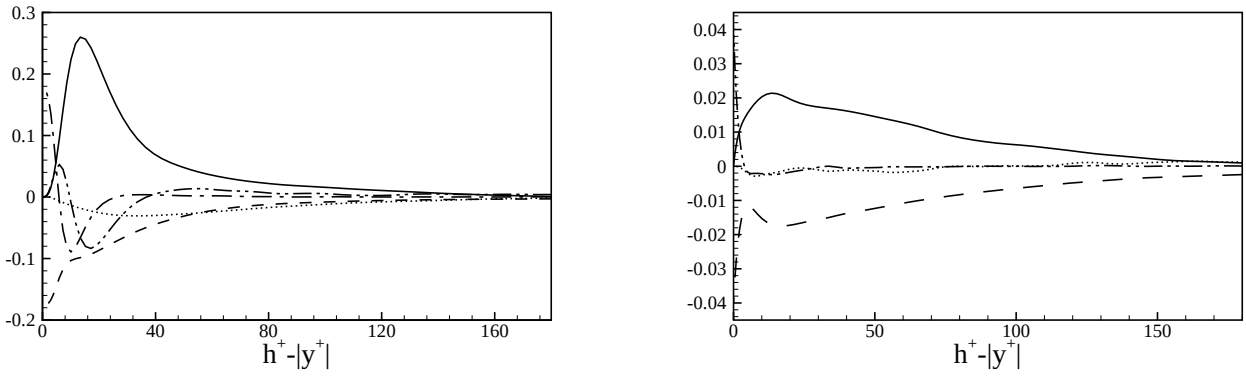

Figure 5.5: Left panel: Budget of $\langle u^2 \rangle$ vs distance from the wall. Production: $-$, viscous diffusion: $- \cdot \cdot -$, turbulent transport: $- \cdot -$, dissipation: $--$, pressure transport:$\cdots$. Right panel: Budget of $\langle w^2 \rangle$ vs distance from the wall. Production (pressure transport): $-$, viscous diffusion: $- \cdot \cdot -$ turbulent transport: $- \cdot -$, dissipation: $--$.

$$
\begin{aligned}
- \quad & \frac{d}{dy}\langle u\, u\, v\rangle + \nu \frac{d^2\langle u\, u\rangle}{dy^2} - \frac{2}{\rho}\langle u \frac{dp}{dx}\rangle - 2\nu\langle \left(\frac{\partial u}{\partial x_{\rm i}}\right)\left(\frac{\partial u}{\partial x_{\rm i}}\right)\rangle - \langle u\, v\,\rangle \frac{dU}{dy} = 0\,, \\
- \quad & \frac{d}{dy}\langle w\, w\, v\rangle + \nu \frac{d^2\langle w\, w\rangle}{dy^2} - \frac{2}{\rho}\langle w \frac{dp}{dz}\rangle - 2\nu\langle \left(\frac{\partial w}{\partial x_{\rm i}}\right)\left(\frac{\partial w}{\partial x_{\rm i}}\right)\rangle = 0\,, \\
- \quad & \frac{d}{dy}\langle v\, v\, v\rangle + \nu \frac{d^2\langle v\, v\rangle}{dy^2} - \frac{2}{\rho}\langle v \frac{dp}{dy}\rangle - 2\nu\langle \left(\frac{\partial v}{\partial x_{\rm i}}\right)\left(\frac{\partial v}{\partial x_{\rm i}}\right)\rangle = 0\,,
\end{aligned}
\tag{5.7}
$$

in order the terms in these balance equations are the turbulent transport rate, the viscous diffusion, the velocity pressure gradient term, the dissipation rate associated with the respective component of the Reynolds stresses, and finally a production term, present only in the equation for the component $\langle u^2 \rangle$.

As a consequence only the streamwise component of the stresses directly receives energy from the interaction of the fluctuations and the mean motion.

As shown in the left panel of figure 5.5 (see [49] for a comparison) the pressure gradient term represents a sink for the streamwise component and is of the same order of the dissipation from the logarithmic layer up to the channel center. We observe that

the velocity pressure gradient term can be decomposed [2] in the following manner:

$$\langle u_{\rm i} \frac{dp}{dx_{\rm i}} \rangle \;=\; \frac{d\langle u_{\rm i}\, p\rangle}{dx_{\rm i}} \;-\; \langle p \frac{du_{\rm i}}{dx_{\rm i}} \rangle \,, \tag{5.8}$$

where the repeated index does not imply summation. The second term on the right hand side is the pressure rate of strain tensor $P_{\rm ij}$, which for incompressibility has a zero trace, and thus its contribution to the turbulent kinetic energy balance is null. Since $-P_{11} = P_{22} + P_{33}$, and P_{11} is a sink for $\langle u^2 \rangle$, P_{22} and P_{33} are production terms for $\langle v^2 \rangle$ and $\langle w^2 \rangle$. Hence the effect of the fluctuating pressure is to extract energy from the streamwise component and to transfer it towards the wall normal and spanwise components.

As a consequence $\langle u^2 \rangle$ is peaked near the wall, where the shear (the production term) is large, at roughly the same location of maximum turbulent kinetic energy production (see the following paragraph). Since the shear diminishes towards the channel center and consequently the local production diminishes, the transfer of energy from $\langle u^2 \rangle$ to the other components leads to a more uniform state.

Finally the right panel of figure 5.6 shows the root mean square pressure fluctuations, which is close to the value obtained in [49]. This confirms the correctness of the solver of the Poisson equation, implemented to evaluate the pressure field, since it is not provided explicitly by the code used.

[2] even of this decomposition is not unique (see [61])

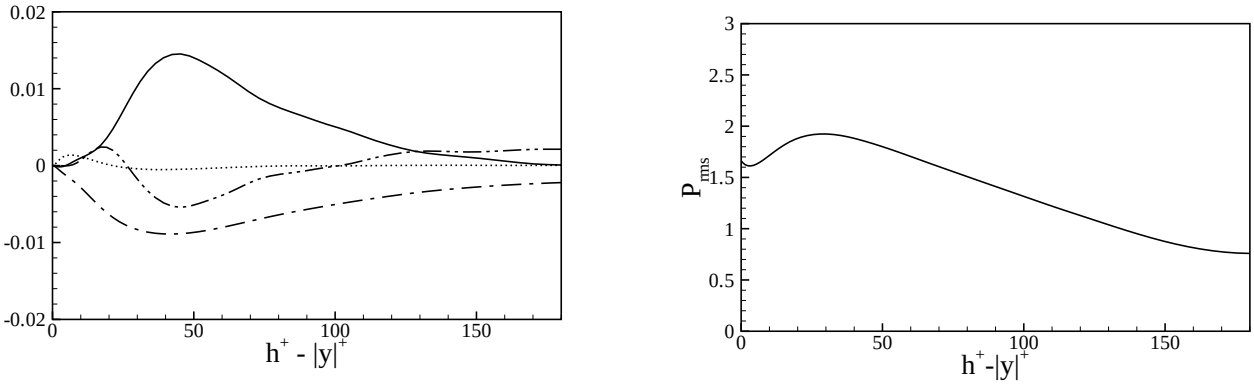

Figure 5.6: Left panel: Budget of $\langle v^2 \rangle$ vs distance from the wall. Production (pressure transport): $-$, viscous diffusion: $- \cdot\cdot -$, turbulent transport: $- \cdot -$, Right panel: root mean square pressure vs distance from the wall, normalized by the friction velocity $p_{\rm rms}/\rho u_*^2$.

5.4 Turbulent kinetic energy balance

The turbulent kinetic energy balance specialized for a turbulent channel flow reads,

$$-\langle uv\rangle\frac{dU}{dy} - \frac{1}{2}\frac{d}{dy}\langle u_i u_i v\rangle + \frac{\nu}{2}\frac{d^2\langle u_i u_i\rangle}{dy^2} - \frac{1}{\rho}\frac{d\langle pv\rangle}{dy} - \langle\epsilon\rangle = 0\,, \tag{5.9}$$

the first term occurs in the balance equation for the mean flow kinetic energy with opposite sign and describes the exchange of energy between the mean and the fluctuating motions. Direct measurements show that for a channel flow this production term is positive at all wall normal distance. As a consequence the flow is self sustained, meaning that it does not need an external mechanism which replenishes the energy dissipated by the viscous action. The last term represents the mean rate of viscous dissipation of kinetic energy into heat (see appendix A). The second, the third and the fourth term lead only to a spatial transfer of energy in the wall normal direction, due to the action of the pressure fluctuations, the fluctuating velocities and the viscous forces, respectively. In fact since through the boundary there is not flux of turbulent kinetic energy if we integrate equation 5.9 over the channel section we find

$$\int_{-h}^{h}\frac{d}{dy}\left(-\frac{1}{2}\langle u_i u_i v\rangle + \frac{\nu}{2}\frac{d\langle u_i u_i\rangle}{dy} - \frac{1}{\rho}\langle pv\rangle\right)dy \;=\; \left[-\frac{1}{2}\langle u_i u_i v\rangle + \frac{\nu}{2}\frac{d\langle u_i u_i\rangle}{dy} - \frac{1}{\rho}\langle pv\rangle\right]_{-h}^{h} = 0\,. \tag{5.10}$$

Hence these contributions can only cause a spatial redistribution or flux of turbulent kinetic energy, without affecting its value.

Let us now introduce an overall spatial flux of turbulent energy

$$\phi(y) = \frac{1}{2}\langle u_i u_i v\rangle - \frac{\nu}{2}\frac{d\langle u_i u_i\rangle}{dy} + \frac{1}{\rho}\langle pv\rangle \tag{5.11}$$

equation (5.9) reads

$$\frac{d\phi(y)}{dy} \;=\; \sigma(y)\,, \tag{5.12}$$

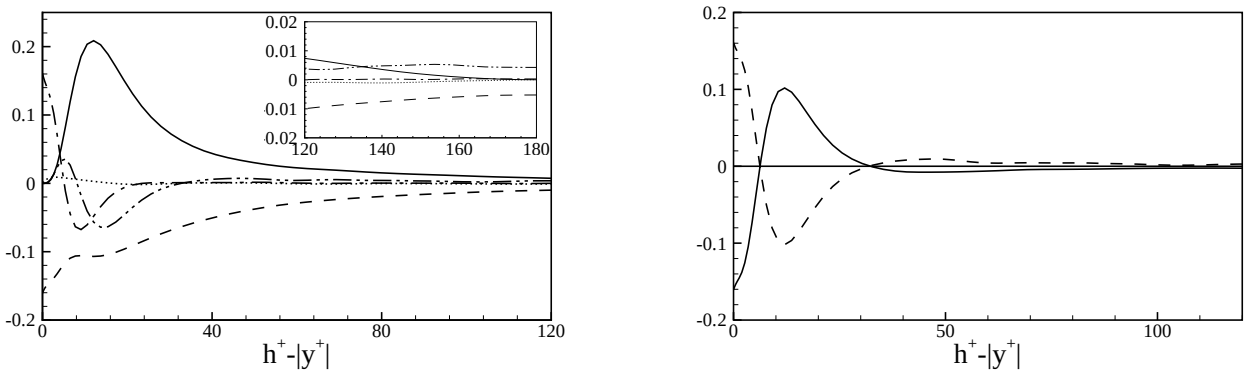

Figure 5.7: Left panel: Turbulent kinetic energy budget vs distance from the wall $(h-|y|)^+$; production:$-$, viscous diffusion:$- \cdot -$, pressure transport $\cdots$, turbulent convection $- \cdot \cdot -$, and dissipation $--$, see equation (5.9). The details of the central region are shown in the inset. Right panel: Turbulent kinetic energy budget vs distance from the wall according to equation (5.12). divergence of the spatial flux ϕ: dashed line, source term σ: solid line.

where $\sigma(y) = \pi(y) - \langle\epsilon(y)\rangle$ is the net amount of turbulent kinetic energy pertaining to a specific location y due to the difference between production $\pi = -\langle uv\rangle dU/dy$ and average dissipation. As a consequence if we integrate equation 5.12 from the wall up to the current value of the wall normal distance $\widehat{y}$ we have

$$\phi\left(\widehat{y}\right) = \int_{-h}^{\widehat{y}} \sigma\left(y\right) dy\,, \tag{5.13}$$

which identifies the flux of energy leaving the layer $-h \leq y \leq \widehat{y}$ to feed the turbulence in the region above.

The different terms of the budget 5.9, normalized by u_*^4/ν are reported in the left panel of figure 5.7 where the inset shows the detailed behavior of the various terms in the core region while in the right panel the balance is shown according to equation 5.12.

As the wall is approached equation 5.9 express a balance between viscous transport and dissipation, according to the fact that the viscous effects are overwhelming in the viscous sublayer.

The peak production occurs within the buffer layer at $(h-|y|)^+ \simeq 12$ (see [37] for a comparison) and around this peak production exceeds dissipation, as also shown by the positive value of σ in the right panel of the figure. This excess of energy is transported away through the spatial flux ϕ, whose divergence is shown in the right

panel of the figure. Pressure transport (see the left panel) is small (as everywhere else in the channel section) while the turbulent convection term transports energy towards the wall and into the logarithmic region. The viscous contribution, instead, transports kinetic energy only towards the wall.

In the logarithmic region the production dissipation ratio should be nearly one (see [54]), and as a consequence the flux ϕ should be constant and its divergence should be zero. Despite the fact that the asymptotic equilibrium state is not reached at the Reynolds number of the present simulation, the energy intercepted in the logarithmic region is only a small fraction of the locally produced by the shear, leaving the gross features unchanged. Since the shear vanishes approaching the channel center, the dissipation exceeds the production, and the sustainment of the turbulence is entirely due to the flux of energy from the buffer. This observation is confirmed by the negative value of the net source σ in the right panel of figure 5.7 and by the inset in the left panel.

The analogy of this spatial transfer of energy and the picture of the energy cascade among different eddies is striking. The viscous sublayer where the bulk of the dissipation occurs is essentially a viscous dominated sublayer, the buffer region plays the role of the production range, the log-layer where the flux is almost constant plays the role of the inertial range. Finally the core receives energy from the spatial flux Φ. The classical cascade of energy from one eddy to another is superimposed on this spatial transfer of energy.

5.5 The scale-energy

The conceptual picture is that of a double transfer of energy both in physical and scale spaces. However the turbulent kinetic energy balance (5.9) alone is not sufficient to describe the effective dynamics of a turbulent flow. Actually, turbulence in wall bounded flows is characterized by several interacting processes, such as energy production, spatial redistribution, energy cascade and dissipation. The relative importance of different phenomena may change significantly depending on the geometrical location (i.e. the distance from the wall) and the range of scales considered. A complete understanding of these interacting phenomena requires a detailed description of the processes occurring simultaneously in the geometric space and in the space of turbulent scales. One should be able to address the energy content of a given scale and evaluate its dependence on the spatial position. The proper quantity to consider is the so called second order structure function defined as $\langle \delta u^2 \rangle$, where $\delta u^2 = \delta u_i \delta u_i$ and

$\delta u_i = u_i(x_s + r_s) - u_i(x_s)$ denotes the fluctuating velocity increment. Loosely speaking, $\langle \delta u^2 \rangle$ measures the amount of fluctuation energy at scale $r = \sqrt{r_s r_s}$ and therefore, following [11], it will be hereafter referred to as scale-energy. From its definition, the scale-energy depends on r - more precisely on the separation vector $r_{\rm i} = x'_{\rm i} - x_{\rm i}$ - and on the location specified by the mid-point $X_{ci} = 1/2(x'_{\rm i} + x_{\rm i})$, see the right panel of figure 5.1 for a sketch of the arrangement.

The left panel of figure 5.8 shows the isolines of the scale-energy on the plane $r_{\rm x} - Y_{\rm c}$ for $r_{\rm y} = r_{\rm z} = 0$, i.e. the function $\langle \delta u^2(r_{\rm x}, 0, 0|Y_{\rm c}) \rangle$, where $Y_{\rm c} = 1/2(y + y')$ is the wall-normal coordinate of the mid-point. Usually, structure functions are plotted as functions of separation, using the wall-normal position as a parameter. In our context, the present - slightly unconventional - representation in terms of isolines in the $r_{\rm x} - Y_{\rm c}$ plane has the advantage of combining, in a synthetic way, the description of the field in physical space ($Y_{\rm c}$) and in the space of turbulent scales ($r_{\rm x}$). The expected small scale asymptotic of the scale energy, given by $\langle \delta u^2 \rangle \simeq \langle (\partial u/\partial x)^2 + (\partial v/\partial x)^2 + (\partial w/\partial x)^2 \rangle \, r_{\rm x}^2$, is consistent with the behavior near the $Y_{\rm c}$ axis of the figure. The near wall asymptotic - i.e. for $|Y_{\rm c}| \simeq h$ - given by $\langle \delta u^2 \rangle \simeq 2 \, \langle \, \delta \tau_{\rm x}^2 + \delta \tau_{\rm z}^2 \, \rangle \, (h - |Y_{\rm c}|)^2/(\rho\nu)^2$, where $\langle \delta \tau_{\rm x/z}^2 \rangle$ denote the mean square fluctuation of the x/z-component of the instantaneous wall shear stress increment at the considered separation, is also apparent near the $r_{\rm x}$-axis. For clarity, $\langle \delta u^2 \rangle$ as a function of the wall-normal distance is also reported in the main part of the right panel of the figure for fixed separations. The plots corresponds to

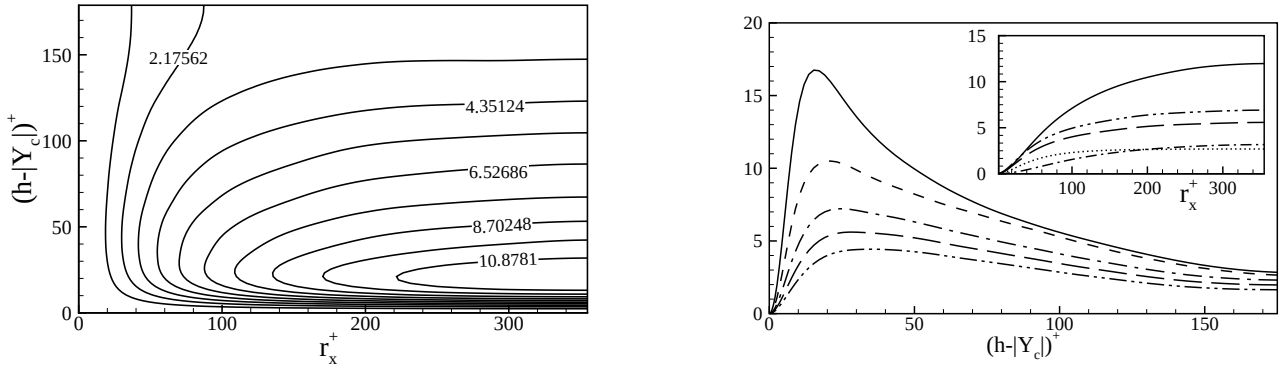

Figure 5.8: Left panel: Isolines of the scale-energy $\langle \delta u^2(r_{\rm x}, 0, 0|Y_{\rm c}) \rangle$, normalized by u_*^2, in the $r_{\rm x}^+ - Y_{\rm c}^+$ plane. Right panel: $\langle \delta u^2(r_{\rm x}, 0, 0|Y_{\rm c}) \rangle$ vs $(h - |Y_{\rm c}|)^+$ for different $r_{\rm x}$, $r_{\rm x}^+ = 55$ (dashed-double dotted line), $r_{\rm x}^+ = 70$ (long dashed line), $r_{\rm x}^+ = 100$ (dashed-dotted line), $r_{\rm x}^+ = 220$ (dashed line). The solid line is $2(u_{\rm rms}^2 + v_{\rm rms}^2 + w_{\rm rms}^2)$. Inset: $\langle \delta u^2(r_{\rm x}, 0, 0|Y_{\rm c}) \rangle$ vs $r_{\rm x}^+$ for different $(h - |Y_{\rm c}|)$, $(h - |Y_{\rm c}|)^+ = 4$ (dashed-dotted line), $(h - |Y_{\rm c}|)^+ = 20$ (solid line), $(h - |Y_{\rm c}|)^+ = 80$ (dashed-double dotted line), $(h - |Y_{\rm c}|)^+ = 100$ (long dashed line), $(h - |Y_{\rm c}|)^+ = 180$ (dotted line).

Y_c-sections of the (r_x, Y_c)-plane shown on the left. Overall the scale-energy presents a maximum in the region of the buffer layer which is sharper for larger separations but becomes smoother as r_x is reduced. The traditional plots showing the r_x-behavior for fixed Y_c are shown in the inset; this plot clearly shows the r_x^2 behavior at small separation for the second order structure function, and the approach to a constant value at large separations. At large separations, where the velocities at the two points are uncorrelated, the limiting behavior is given by $2\,(u_{rms}^2 + v_{rms}^2 + w_{rms}^2)$, i.e. four times the total turbulent kinetic energy pertaining to the considered value of Y_c. This quantity is represented by the solid line as a function of Y_c in the main figure of the panel.

5.6 Fluxes of scale-energy

In [30] there are some comments about the concept of a double cascade of energy. Firstly this author observes that at any given location the energy is transferred to smaller scales, secondly the energy is also transferred from small scales towards larger ones away from the wall. If we suppose that the local isotropy should be recovered at sufficiently small scales in the logarithmic layer, clearly only the large eddies, in particular characterized by a scale $r > L_S$ (see par. 3.2) should be anisotropic and thus responsible for the spatial transfer of scale-energy.

Following this concept it is possible to derive a particular scaling for the energy spectrum in the production range of the logarithmic layer as shown in the works [58], [60] and [67].

To characterize in detail the process of spatial transfer of scale-energy we consider the conservation form of the scale by scale energy budget 3.4:

$$\nabla_r \cdot \mathbf{\Phi}_r\,(\mathbf{r}, Y_c) + \frac{d\Phi_c(\mathbf{r}, Y_c)}{dY_c} = s(\mathbf{r}, Y_c)\,, \tag{5.14}$$

where $\mathbf{r} = (r_x, r_y, r_z)$ and boldface type denotes a three-dimensional vector. The form 5.14 essentially shows that the scale by scale budget can be expressed as a balance between the divergences of two kind of fluxes, the former defined in the space of scales, the latter in physical space and a source term

$$s(\mathbf{r}, Y_c) \;=\; -2\langle \delta u \delta v \rangle\,(dU/dy)^* - 4\langle \epsilon^* \rangle \tag{5.15}$$

that accounts for production and dissipation.

Formally the structure of the two fluxes is the same,

$$\Phi_{\rm c}(\,\mathbf{r},Y_{\rm c}\,) \;=\; \langle\delta u^2 v^*\rangle + \frac{2}{\rho}\langle\delta p\delta v\rangle - \frac{\nu}{2}\frac{d\langle\delta u^2\rangle}{dY_c} \tag{5.16}$$

$$\mathbf{\Phi}_{\rm r}(\,\mathbf{r},Y_{\rm c}\,) \;=\; \langle\delta u^2\delta\mathbf{u}\rangle + \langle\delta u^2\delta\mathbf{U}\rangle - 2\nu\nabla_{\rm r}\langle\delta u^2\rangle\,, \tag{5.17}$$

they are constituted by a turbulent transport and a molecular diffusion term, defined in the corresponding spaces, a pressure transport term present only in $\Phi_{\rm c}$ and a transport due to the mean flow only in $\mathbf{\Phi}_{\rm r}$. The fluxes describe the coupled transfer of scale-energy which occurs simultaneously in physical and in space-scale and in particular Φ_c represents the transfer of scale-energy in the inhomogeneous direction y and is directed towards the wall or towards the outer region according to its sign, while $\mathbf{\Phi}_{\rm r}$ is a vector associated with the transfer of scale-energy through scales.

The integration domain for equation (5.14), corresponding to the constraint $-h \leq y,\, y' \leq h$, i.e. to the geometry of the channel flow, is

$$-h \leq Y_{\rm c} \leq h \qquad -2\,(\,h-|Y_{\rm c}|\,) \leq r_{\rm y} \leq 2\,(\,h-|Y_{\rm c}|\,)\;, \tag{5.18}$$

see the left panel of figure 5.9.

The spatial flux describes the transport of scale-energy in geometric space and is, in principle, a three-dimensional vector - see equation (5.17) - that could be denoted by the boldface type $\mathbf{\Phi}_{\rm c}$. For a channel flow the only non-vanishing component of $\mathbf{\Phi}_{\rm c}$, namely the scalar $\Phi_{\rm c}$ appearing in eq. (5.14), corresponds to a transfer of energy at scale r in y direction.

Actually, after setting $r_{\rm y}=0$ and accounting for the boundary conditions, term by term integration of equation (5.14) from the (lower) wall to the current value of $Y_{\rm c}$,

$$\Phi_{\rm c}(r_{\rm x},0,r_{\rm z}|Y_{\rm c}) \;=\; \int_{-h}^{Y_{\rm c}} \Big[\, s(r_{\rm x},0,r_{\rm z}|\tilde{Y_{\rm c}}) \;-\; \nabla_r\cdot\mathbf{\Phi}_{\rm r}(r_{\rm x},0,r_{\rm z}|\tilde{Y_{\rm c}})\,\Big]\; d\tilde{Y}_{\rm c}\,, \tag{5.19}$$

leads to the interpretation of $\Phi_{\rm c}(r_{\rm x},0,r_{\rm z}|Y_{\rm c})$ as the amount of scale-energy which leaves the region below $Y_{\rm c}$ to feed the portion of the channel above - see the right panel of figure 5.9 for a sketch.

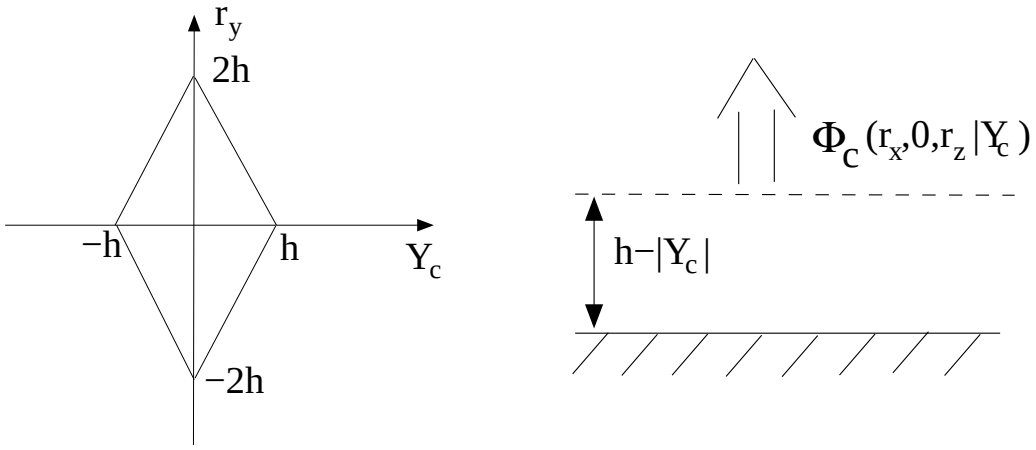

Figure 5.9: Left panel: Integration domain for equation (5.14). Right panel: Physical interpretation of the spatial flux $\Phi_{\rm c}(r_{\rm x}, 0, r_{\rm z}|Y_{\rm c})$.

5.6.1 The r-averaged equation

The classical form of the Kolmogorov 2.21 equation, expressed in terms of longitudinal velocity increments, is the r-average over a sphere of radius r of equation 2.21. Analogously it is possible to consider the r-average form of equation 5.14, that for homogeneous isotropic turbulence at inertial separations reads (see also par. 2.5)

$$\frac{1}{V_r}\int_{\partial B_r} \mathbf{\Phi}_{\rm r}(\mathbf{r}) \cdot \mathbf{n}_r \, dS_r \propto \frac{\langle \delta u_\parallel^3 \rangle}{r} < 0\,, \tag{5.20}$$

where $\mathbf{n}_r$ is the outward normal to the sphere B_r with radius r and frontier ∂B_r. This procedure allows to identify the convection term in the space of scales as representative of the energy flux. A negative value of $\mathbf{\Phi}_{\rm r} \cdot \mathbf{n}_{\rm r}$ implies that scale-energy is transfered from the exterior into the sphere, as described in the classical picture usually referred to as Richardson cascade. However the geometry of the channel makes impossible to average over spheres with radius larger than the distance of their centers from the wall, and would also imply an average over y loosing the information about the local contribution of inhomogeneous fluxes to the balance 5.14. For these reasons instead of considering a $3D$ average of equation 5.14 in the space of scale, we average only along homogeneous directions, considering square domains of side r belonging to wall parallel planes. Hence for a generic quantity q we define a $2D$ average

$$Q_{\rm r}(r, Y_{\rm c}) = \frac{1}{r^2}\int_{-\frac{r}{2}}^{\frac{r}{2}}\int_{-\frac{r}{2}}^{\frac{r}{2}} q(r_{\rm x}, 0, r_{\rm z}|Y_{\rm c})\, dr_{\rm x} dr_{\rm z}\,, \tag{5.21}$$

where the separation vector is defined as $\boldsymbol{r} = (r_x, 0, r_z)$.

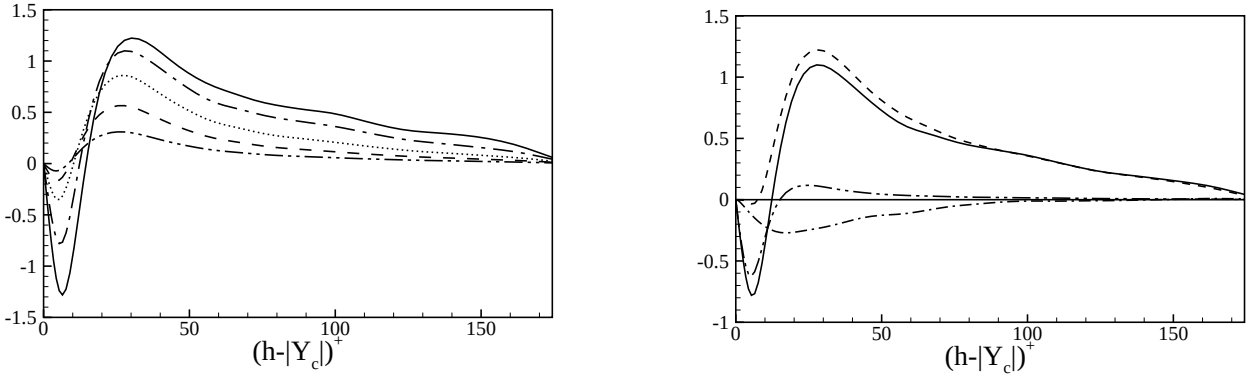

Figure 5.10: Left panel: The r-space average of Φ_c as a function of the distance from the wall $(h - |Y_c|)^+$ for different values of the scale r^+($r^+ = 5$: $- \cdot\cdot -$, $r^+ = 10$: $--$, $r^+ = 20$: $\cdots$, $r^+ = 40$: $- \cdot -$, $r^+ = 120$: $-$). The r-space average is performed on 2D square domains (r_x, r_z), with side r at Y_c =const and $r_y = 0$. Right panel: Different contributions to the r-space average of Φ_c , see equation (5.16), as a function of $(h - |Y_c|)^+$ for fixed separation $r_+ = 40$. Φ_c:$-$, viscous diffusion: $- \cdot\cdot -$, pressure transport :$- \cdot -$, turbulent flux:$--$.

5.6.2 Spatial flux

We start with the analysis of the spatial component of the scale-energy flux. The left panel of figure 5.10 plots the r-space average of $\Phi_c(\mathbf{r}, Y_c)$ as a function of the distance from the wall at different separations r. It is possible to identify two regions, in which the flux is either positive, i.e. transfers scale-energy towards the bulk of the fluid, or negative, i.e. it is directed towards the wall. In both cases the scale-energy is produced in the transitional region between the molecular sublayer and the logarithmic region and is transported, through the spatial flux, to partially sustain the turbulence in the other regions. However the importance of this process will change depending on both the specific scale and the geometric location considered. [3]

The right panel of figure 5.10 displays the different contributions to the r-average of Φ_c at $r^+ = 40$. The spatial flux (solid line) changes sign at $(h - |Y_c|)^+ \simeq 15$, which closely corresponds to the location of the maximum turbulent kinetic energy production. For $(h - |Y_c|)^+ < 15$ the most important contribution is provided by the viscous diffusion term (third term in definition (5.16)), in accordance with the idea that very close to the wall the viscosity plays a central role at all scales. Hence, in this region, the viscosity is active at all scales and there is not a separation between a production and a dissipative range.

[3]This issue will be treated in full detail in the next section.

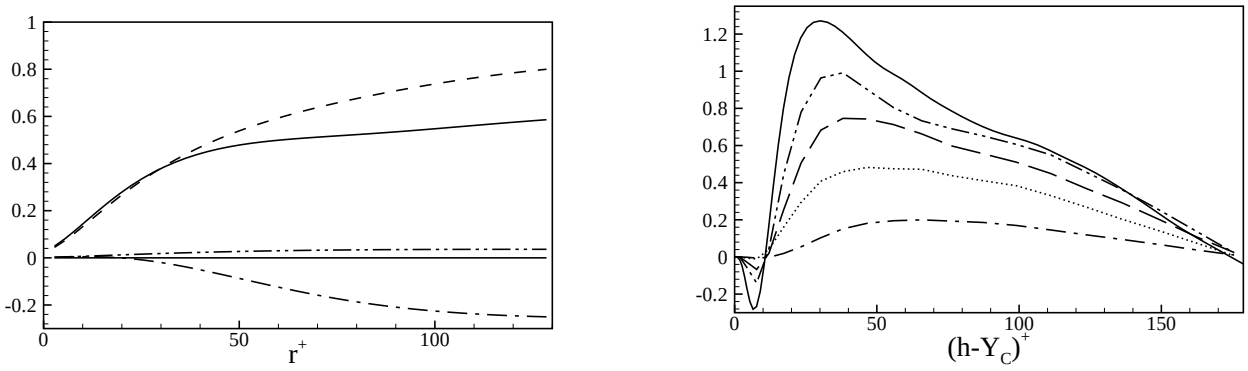

Figure 5.11: Left panel: Different contributions to the r-space average of Φ_c, see equation (5.16), vs. separation r^+ for $(h-|Y_c|)^+ = 80$. Φ_c:−, viscous diffusion:$-\cdots-$, pressure transport :$-\cdot-$, turbulent flux:−−. Right panel: Turbulent transport of scale-energy (non-averaged) $\langle \delta u^2 v^* \rangle$ vs. distance from the wall $(h-|Y_c|)^+$ for different separations, $r_+ = 20$ $-\cdot-$, $r_+ = 40$ $\cdots$, $r_+ = 80$ −− , $r_+ = 170$ $-\cdots-$. The solid line corresponds to twice the turbulent energy flux $(1/2\langle\, u^2\, v\,\rangle)$, see eq. (5.9), according to the limiting behavior (5.22).

For $(h-|Y_c|)^+ > 15$ the most important contribution is provided by the turbulent transport term, since the effect of viscosity is less relevant at increasing wall normal distances. The effect of the pressure transport term appears negligible quite in the entire channel section, with exception of the buffer region.

Now we analyze the same quantities at a typical location within the logarithmic layer at $(h-|Y_c|)^+ \simeq 80$ in function of the separation r, see the left panel of figure 5.11. We should observe that at large scales all the term approaches a constant value. In fact at large scales the velocities at the two points are uncorrelated (see par. 3.3) and consequently the large scale limit of the different components of the flux Φ_c are

$$\begin{aligned}
\lim_{r\to\infty} \langle \delta u^2 v^* \rangle &= \langle u^2 v \rangle\,, \\
\lim_{r\to\infty} \frac{2}{\rho} \langle \delta p \delta v \rangle &= \frac{4}{\rho} \langle p\ v \rangle\,, \\
\lim_{r\to\infty} \frac{\nu}{2} \frac{d\,\delta u^2}{dY_c} &= \nu \frac{d\,u^2}{dY_c}\,;
\end{aligned}$$

these large scale limits correspond to twice the respective components of the spatial flux of global energy, see definition 5.11.

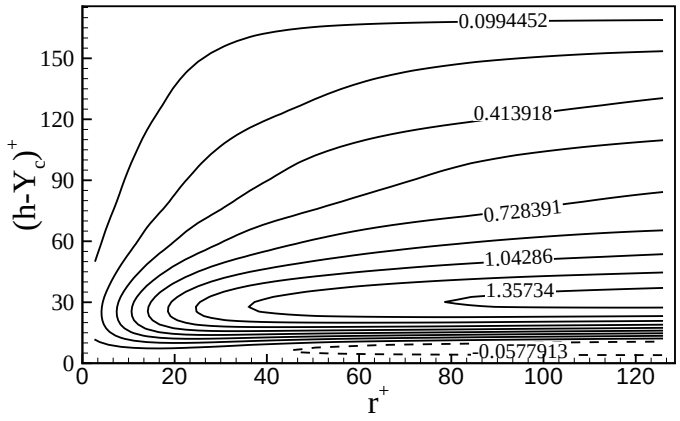

Figure 5.12: The r-space average of the turbulent transport of scale-energy $\langle \delta u^2 v^* \rangle$, normalized by u_*^3, as a function of the distance from the wall $(h - |Y_c|)^+$ and of the scale r^+. The uniformly spaced contour levels are shown by solid and dashed lines for positive and negative values, respectively.

It appears, as expected, that the turbulent component of the flux is the leading term at all scales, since the effect of viscosity is prominent only in the viscous sublayer next to the wall.

Let us now consider in more detail the turbulent component of the spatial scale-energy flux $\langle \delta u^2 v^* \rangle (r_x, 0, 0 | Y_c)$ as a function of the longitudinal component of the separation vector and not averaged. This quantity is addressed in the right panel of figure 5.11. The figure clearly shows that the large scale limit of this scale-energy component is twice the global convective component of the kinetic energy flux, (solid line in the figure, see definition 5.11). The turbulent component is present at all scales, even if its contribution is less than the viscous contribution in the viscous sublayer, see the left panel of figure 5.11. What is more it seems that in the log-layer the scale-energy flux manifests a trend to form a plateau. Actually as the Reynolds number is increased, $\langle u^2 v \rangle$ is known to approach a constant value in the log-layer, [54]. If this is the case, at Reynolds numbers larger than the one of the present simulation, it is expected that $\langle \delta u^2 v^* \rangle$ at each scale approaches a constant value in the logarithmic layer. As a consequence, the log-layer should be asymptotically traversed by an almost constant flux of scale-energy, meaning that at each scales it does not need a replenishment of energy by the action of the spatial flux, which does not interfere with the local dynamics.

Figure 5.12 shows the isocontours of the r-average of $\langle \delta u^2 v^* \rangle$, as a function of the current scale r and the spatial location Y_c. The turbulent component of the spatial flux

reaches a maximum between the buffer and the log-layer and decreases both towards the wall and towards the channel center. This decrease implies that the scale-energy carried by the flux is progressively released to the fluctuations. This decrease is limited in the log-layer, according to the aforementioned asymptotic constance of the spatial flux in this region. At small separations vanishingly values of the turbulent flux are attained, meaning that the spatial flux is effectively due only to the larger scales of the flow. What is more a little contribution of the flux at large scales is present in the viscous sublayer, as in the turbulent kinetic energy balance (see par. 5.4) the convective term carries a little amount of energy towards the wall. In this region at small separations the turbulent component of the flux is negligible and the main contribution is the viscous one (not shown in the figure). It clearly appears that the buffer layer is a sort of *engine* for the scale-energy, since it is the preferred location for the scale energy (see also par. 5.5), and for the turbulent component of the spatial flux.

5.7 Scale by scale budget

When applying the r-averaging operator (5.21), the contribution from the second term on the left hand side of equation (3.4) vanishes altogether, since $\delta U = 0$ when $r_\mathrm{y} = 0$. The r-averaged form of the equation then follows as

$$T_\mathrm{r}(r, Y_\mathrm{c}) + \Pi(r, Y_\mathrm{c}) + T_\mathrm{c}(r, Y_\mathrm{c}) = E(r, Y_\mathrm{c}) + D_\mathrm{r}(r, Y_\mathrm{c}) + P(r, Y_\mathrm{c}) + D_\mathrm{c}(r, Y_\mathrm{c}) \qquad (5.22)$$

where each term corresponds to the appropriate term in (3.4). Specifically, T_r gives the inertial contribution to the scale-energy flux in r-space, which is proportional to $\langle \delta u_\parallel^3 \rangle / r$ for homogeneous isotropic turbulence. Π arises from the first contribution of the source term s, which is due to production. This term is the production term already present in the homogeneous shear flow. T_c is the inertial contribution to the spatial flux of scale-energy and it is strictly associated with inhomogeneity. E is the term related to dissipation which arises from the second contribution to the source s. D_r and D_c are the diffusive components of the flux in r-space and in geometric space, respectively, and, finally, P is an inhomogeneous contribution related to the pressure-velocity correlation.

Equation 5.22 can be recast in a simple form. We observe that the amount of scale energy which is effectively available at a given geometric location Y_c is provided by

the local production Π plus all the terms corresponding to a spatial transfer of scale-energy towards (or from) the location considered. By considering the overall turbulent transport in the wall normal direction we can define an effective production

$$\Pi_{\mathrm{e}}(r,\, Y_{\mathrm{c}}) \,=\, \Pi(r,\, Y_{\mathrm{c}}) \,+\, T_{\mathrm{c}}(r,\, Y_{\mathrm{c}}) \,-\, P(r,\, Y_{\mathrm{c}}) \;. \tag{5.23}$$

Clearly, the single contributions are not positive definite, while their sum must be positive since it represents the only production mechanism of the flow. Analogously, the contributions of diffusive nature can be added to form a modified dissipation rate,

$$E_{\mathrm{e}}(r,\, Y_{\mathrm{c}}) \,=\, E(r,\, Y_{\mathrm{c}}) \,+\, D_{\mathrm{r}}(r,\, Y_{\mathrm{c}}) \,+\, D_{\mathrm{c}}(r,\, Y_{\mathrm{c}})\,, \tag{5.24}$$

as the sum of the actual dissipation and the diffusive fluxes of scale-energy in physical and r-space, respectively. With these definitions, the r-averaged balance is expressed in more concise form as

$$T_{\mathrm{r}}(r,\, Y_{\mathrm{c}}) \,+\, \Pi_{\mathrm{e}}(r,\, Y_{\mathrm{c}}) \,=\, E_{\mathrm{e}}(r,\, Y_{\mathrm{c}})\,, \tag{5.25}$$

to be read as: transfer across scales plus effective production equals effective dissipation.

In the following, equation (5.25) and the different contributions to effective production and dissipation will be addressed on the basis of the traditional topology of the flow, see figure 6.3 and related caption.

5.7.1 The log-layer

The left panel of figure 5.13 shows the detailed balance (5.25) for a typical location within the log-layer $(h - |Y_{\mathrm{c}}|)^{+} = 80$. Let us now spend few words about the format of this figure. In the left panel the effective production term $-\,\Pi_{\mathrm{e}}$ with a minus sign is represented by the solid line, the transfer term $-\,T_{\mathrm{r}}$ by the dashed-dotted line, and the effective dissipation E_{e} by the dashed line.

The sum $\Pi_{\mathrm{e}} + T_{\mathrm{r}}$ is given by the filled symbols, and as expressed in the balance 5.25, this sum must be equal to E_{e}. The little discrepancy is due to the statistical error, which is small as appears from the figure.

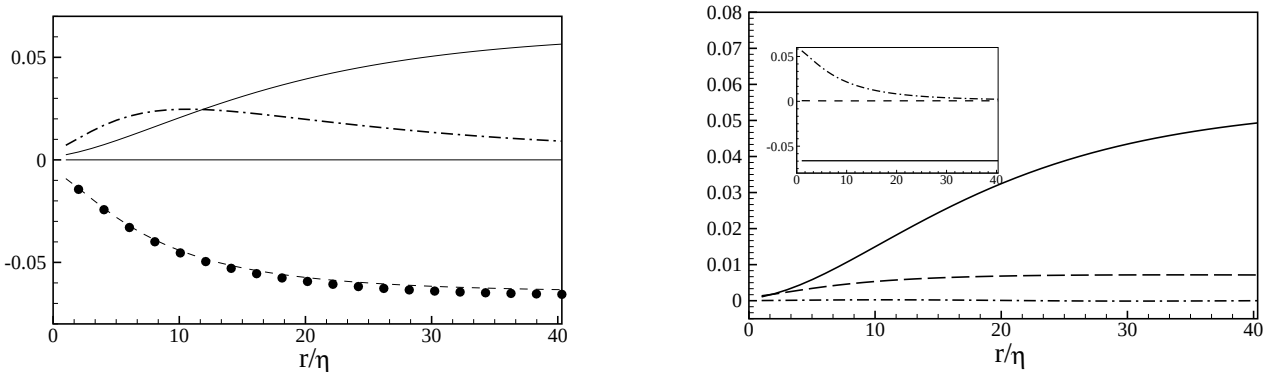

Figure 5.13: Detailed balance (5.25) in the log-layer, $(h - |Y_c|)^+ = 80$. Left: The sum $(T_r + \Pi_e)$ is represented by the filled symbols, E_e is given by the dashed line. The solid line is $-\Pi_e$, the dash-dotted line corresponds to $-T_r$. Right: The different contributions to the effective production, $-\Pi_e$, eq. (5.23), plotted as functions of the scale r, namely production $-\Pi$ (solid line), turbulent transport $-T_c$ (dashed line) and pressure transport $-P$ (dash-dotted line) - note that the sign of each term has been changed. In the inset, the various terms of the effective dissipation E_e, eq. (5.24): dissipation E (solid line) and diffusion of scale-energy in physical and in r-space, D_c (dashed line) and D_r (dash-dotted line), respectively. All the terms are normalized by u^{*4}/ν.

The right panel shows the different contributions to the effective production 5.23, where as in the left panel all the quantities are plotted with a minus sign, and the inset shows the different contributions to the effective dissipation. In describing the different regions we have decided to start with the log-layer which presents strongly analogies with the case of a homogeneous shear, as we shall see in this paragraph.

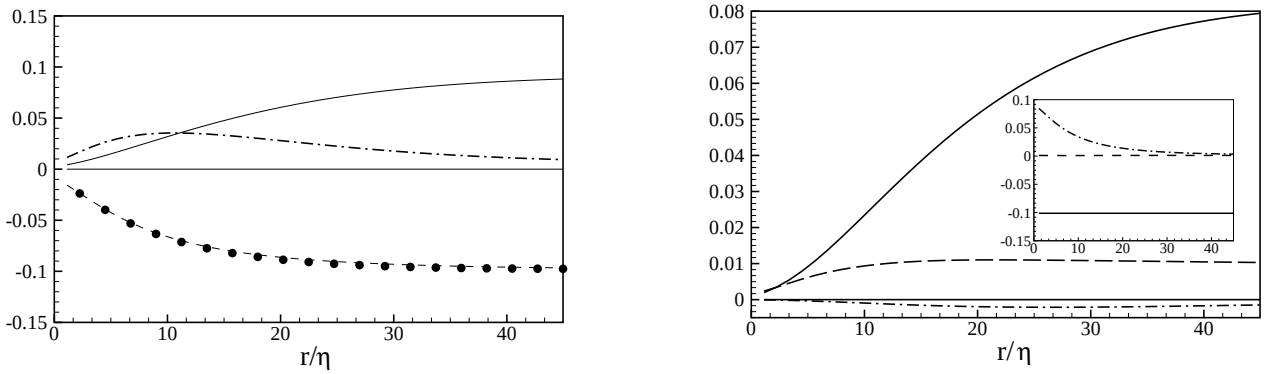

Figure 5.14: Detailed balance (5.25) at $(h - |Y_c|)^+ = 60$ (log-layer). See caption of figure 5.13.

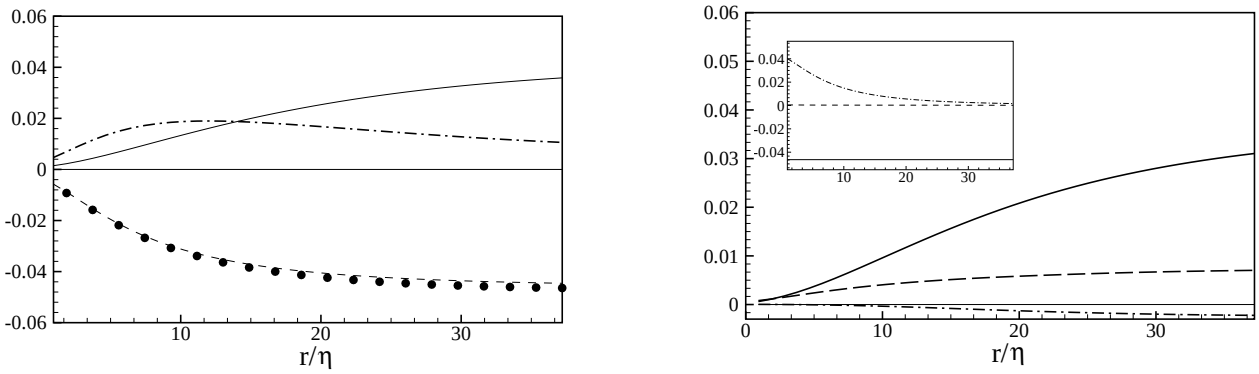

Figure 5.15: Detailed balance (5.25) at $(h-|Y_c|)^+ = 100$ (upper log-layer). See caption of figure 5.13.

The effective production Π_e, shown in the right panel of figure 5.13 is essentially coincident with the local production term Π, since turbulent T_c and pressure transport are negligible at quite all scales. This observation is also confirmed by the analysis of figures 5.14 and 5.15, which display the balance at $(h-|Y_c|)^+ = 60$ and $(h-|Y_c|)^+ = 100$, respectively. The inset shows that the inhomogeneous contribution to the diffusive flux of scale-energy D_c is negligible at all scales, while the diffusive contribution in the space of scales D_r is equal to the dissipation term E at zero separation and is negligible at large scales, where the effective dissipation E_e is equal to the local dissipation term E.

This behavior is analogous to the behavior of the homogeneous shear flow, as discussed in [9], and can be easily understood from the analysis of the Kolmogorov equation for this flow (see par. 3.2). In fact in the log-layer the effects of viscosity are negligible and the local shear does not present a sharp variation in function of the wall normal distance. What is more it is also transversed by an almost constant flux of scale-energy, meaning that the latter does not interact with the local dynamics. As a consequence the large scale features, which initialize the cascade through scales, are nearly the same for both the log-layer and the homogeneous shear flow. In both cases the sum of inertial component of the flux across scales, T_r (i.e. the energy cascade term), and production Π balances dissipation plus diffusion across scales.

The detailed budget (5.25) is represented in the left panel of figure 5.13, which plots the sum $(T_r + \Pi_e)$ in comparison with E_e. At large scales the local production term Π (since $\Pi_e \simeq \Pi$) balances the local dissipation E (since $E_e \simeq E$), while at small scales the cascade across scales term T_r balances the effective dissipation E_e.

Apparently at large separations the production overwhelms the cascade term, and

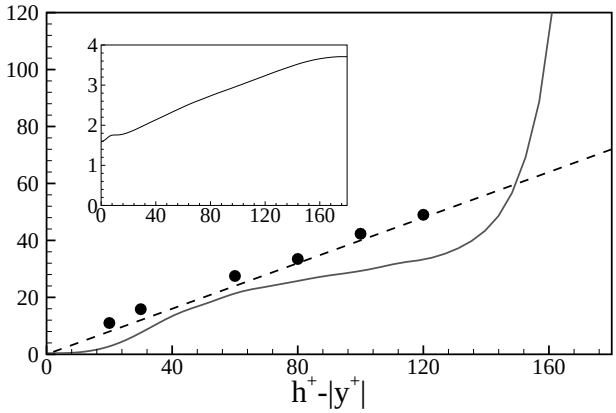

Figure 5.16: The solid line gives $L_{\rm s} = \sqrt{\epsilon/S^3}$ (in wall units) vs distance from the wall. The dashed line corresponds to $k\,(h-|y|)^+$ and the circles denote the crossover scale $\ell_{\rm c}^+$ between production and energy cascade term in viscous units, see equation (5.26). The inset is the Kolmogorov scale η^+ vs distance from the wall.

$\Pi > T_{\rm r}$ down to a cross-over scale $\ell_{\rm c}(Y_{\rm c})$ defined by the condition

$$\Pi(\ell_{\rm c}, Y_{\rm c}) \;=\; T_{\rm r}(\ell_{\rm c}, Y_{\rm c}) \;. \tag{5.26}$$

According to the classical equilibrium theory for the log-layer, the local dissipation can be estimated in terms of production of turbulent kinetic energy, $\langle\epsilon(y)\rangle \simeq u_*^3/(k\,y)$. By comparing the order of magnitude of the fluctuations induced at scale r by the shear, $\delta u_{\rm S}(r) \simeq Sr$, with that typical of the classical Kolmogorov-like inertial range, $\delta u_{\rm K}(r) \simeq \langle\epsilon\rangle^{1/3} r^{1/3}$, one is led to expect the cross-over between production-dominated and cascade-dominated range to occur at the shear scale $L_{\rm S} = \sqrt{\langle\epsilon\rangle/S^3}$. Given the estimate for the dissipation, since $S(y) \simeq u_*/(ky)$, one finds the classical prediction $\ell_c(Y_{\rm c}) \simeq kY_{\rm c}$. The cross-over scale (5.26) as function of the distance from the wall is reported in figure 5.16, which shows a remarkable agreement with the dimensional prediction. The classical Kolmogorov scale $\eta = (\nu^3/\epsilon)^{1/4}$ is shown in the inset of the same figure. It increases from the wall to the channel center, and is sufficiently large to achieve a well resolved DNS.

Above the cross-over scale the turbulent fluctuations are sustained by the shear, i.e. by the local production term, while, below the cross-over scale, the turbulent fluctuations are sustained by the flux of scale-energy, i.e. by the cascade of scale-energy, which is terminated at viscous separation by the dissipation. This picture is analogous to the budget of the homogeneous shear flow, even if a substantial difference must be considered. The log-layer is traversed by an almost constant flux of scale-energy directed towards the bulk region of the flow. However the large scales shape of the

turbulent component of the spatial flux $\langle \delta u^2 v^* \rangle$ is imposed by the turbulent transport term of the single point turbulent kinetic energy equation, see the discussion concerning the right panel of figure 5.11. Since this latter is supposed to became constant, in the logarithmic-layer at large Reynolds number flows, (as discussed in [54]), the analysis of our results - see figure 5.11 - suggests that the same asymptotics should be reproduced by the turbulent transport of scale-energy in physical space. Hence its divergence T_c should be null in the log-layer as in the case of the homogeneous shear. The fact that its divergence is sufficiently small in comparison with the other terms of the budget - see the right panels of figures 5.13,5.14,5.15- but it is not exactly null suggests that it can be regarded as a finite Reynolds number effect. In general for the assessment of finite Reynolds number effects the review paper [20] and the work [63] are worth mentioning.

According to the above picture, the log-region appears as an equilibrium layer of essentially inviscid nature across which the scale-energy is found to flow with no effective interference with the local dynamics, and the inhomogeneity which characterizes the wall bounded flow is reduced.

5.7.2 The bulk region

In paragraph 5.4 we observed that the shear diminishes towards the center of the channel and consequently the production term of the global kinetic energy K becomes smaller and smaller, and vanishes exactly at the centerline. In the bulk region the dissipation is essentially balanced by the flux of turbulent kinetic energy from the buffer. This behavior is essentially reproduced in a scale by scale context. Let us analyze figure 5.17 which shows a comparison between the divergence T_c of the spatial flux Φ_c and the local production term Π in the bulk region of the flow. The figure clearly shows that, approaching the channel center, the production of scale-energy is still predominant at large scales, while a significant amount of scale-energy at small scales begins to be supplied by the wall normal turbulent flux, see the left panel of figure 5.17. Reaching the centerline the production should exactly vanish uniformly through the entire range of scales, so that the entire amount of scale-energy carried by the spatial flux now feeds the turbulence, see the right panel of figure 5.17 giving the relevant components of the effective production on the symmetry line. It appears clearly that the effective production term Π_e coincides with the inhomogeneous contribution T_c, since also the pressure transport is negligible at the centerline. The inset shows the different contributions of the effective dissipations. The inhomogeneous diffusion D_c is negligible at all scales, while the diffusion in the space of scales D_r is active only at

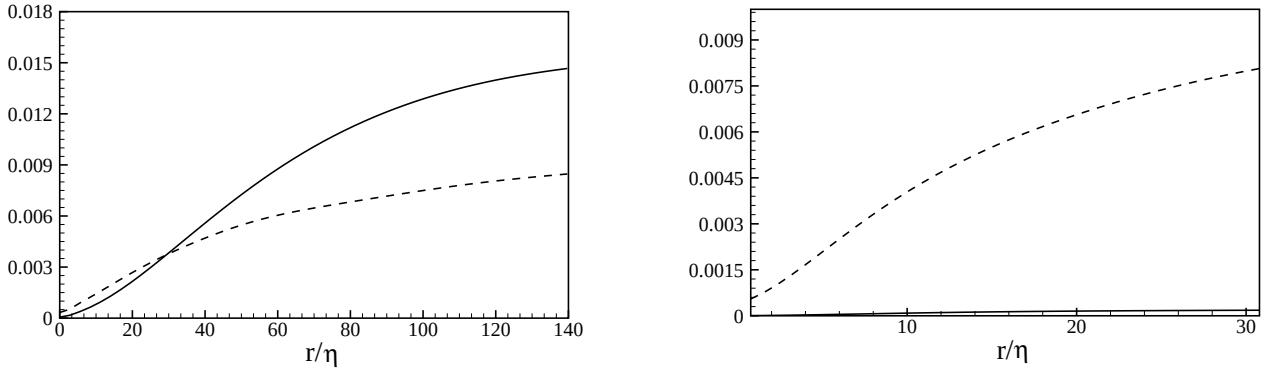

Figure 5.17: Production Π (solid line) and turbulent flux T_c (dashed line) of scale-energy in the bulk region of the turbulent channel flow. Left: $(h-|Y_c|)^+ = 130$. Right: Centerline, $(h-|Y_c|)^+ = 180$.

small scales.

The detailed balance at the centerline, $(h-|Y_c|)^+ = 180$, is shown in the left panel of figure 5.18. The effective production, which is given by the transport term T_c, is less at quite all scales than the divergence of the cascade term T_r. In fact the large scale limit of the effective production, given essentially by T_c, is equal to the limit of the turbulent flux across scales T_r,

$$\lim_{r\to\infty} T_r(r,h) \;=\; \lim_{r\to\infty} \Pi_e(r,h)\,, \tag{5.27}$$

and this common limit is given by twice the turbulent flux of global kinetic energy (see par. 3.3). Despite this common limit it appears that each scales receives more

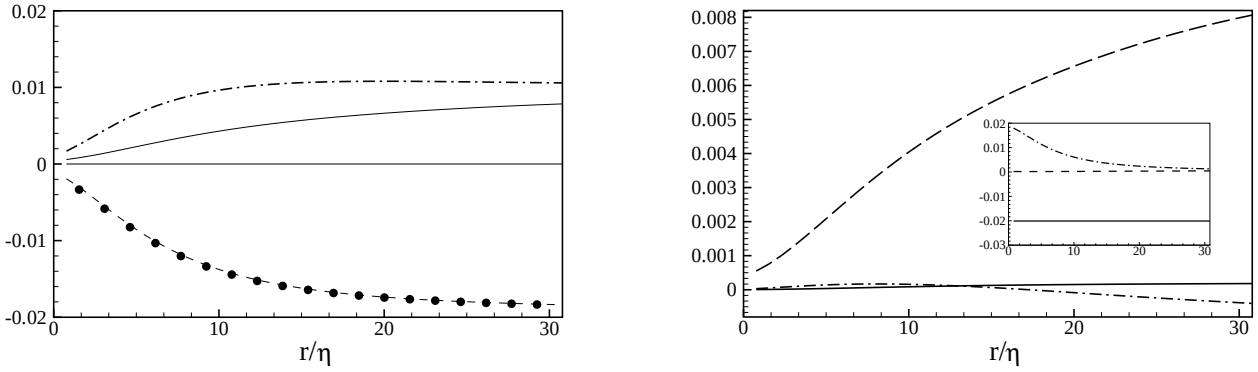

Figure 5.18: Detailed balance (5.25) in the bulk region, $(h-|Y_c|)^+ = 180$. See caption of figure 5.13 for definitions and symbols.

energy from the cascade mechanism than by the spatial flux, which plays the role of initiator of the cascade at large scales.

5.7.3 The viscous sublayer

The presence of the walls impose a well definite behavior in the viscous sub-layer. It is possible to suppose that the Kolmogorov and the integral scales become of the same order of magnitude as the wall is approached and consequently there is not a separation of scales between dissipative and production ranges. The effect of viscosity should dominate the scale by scale behavior.

Despite the central role played by the viscous component of the spatial flux of turbulent kinetic energy, see figure 5.10, its divergence, i.e. its Y_c-derivative D_c, shown in the inset of the right panel in figure 5.19, provides only a small contribution to the effective dissipation, significant mostly at large scales. Concerning small scales, as everywhere else in the channel, the behavior of E_e is determined by the actual dissipation and by the scale-diffusion D_r.

The different components of the effective production are shown in the right panel of figure 5.19. The effective production is mainly due to the local production term,

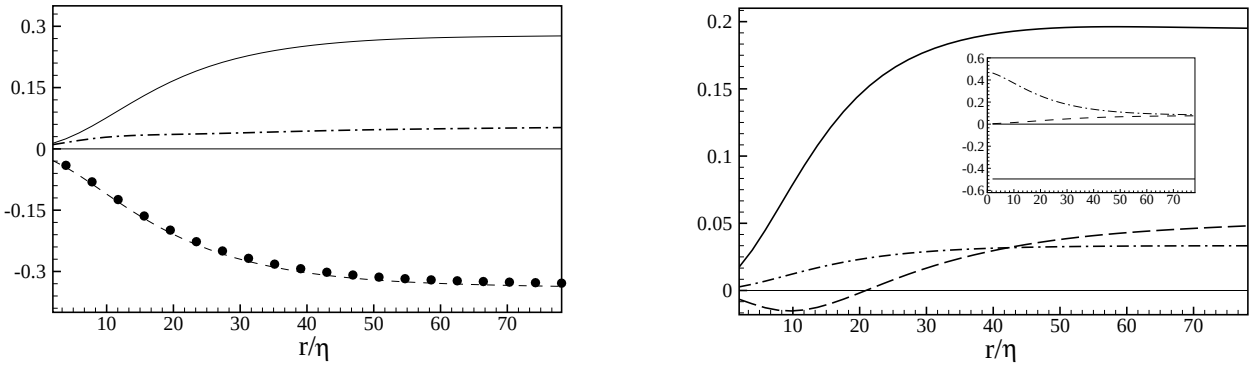

Figure 5.19: Detailed balance (5.25) in the sublayer, $(h - |Y_c|)^+ = 3$. Left: The sum $(T_r + \Pi_e)$ is represented by the filled symbols, E_e is given by the dashed line. The solid line is $-\Pi_e$, the dash-dotted line corresponds to $-T_r$. Right: The different contributions to the effective production, $-\Pi_e$, eq. (5.23), plotted as functions of the scale r, namely production $-\Pi$ (solid line), turbulent transport $-T_c$ (dashed line) and pressure transport $-P$ (dash-dotted line) - note that the sign of each term has been changed. In the inset, the various terms of the effective dissipation E_e, eq. (5.24): dissipation E (solid line) and diffusion of scale-energy in physical and in r-space, D_c (dashed line) and D_r (dash-dotted line), respectively. Notations and symbols, same as in the caption of figure 5.13, are repeated here for convenience.

even if the contribution of the divergence of the turbulent T_c and pressure transport P_c are not negligible. Actually, despite the fact that turbulent and pressure transport contributions to Φ_c are relatively small in the viscous sublayer their strong Y_c dependence generates a non-negligible divergence and contributes a significant part of Π_e. The detailed scale by scale balance is shown in the left panel of figure 5.19. The contribution of the scale-energy cascade term T_r is negligible at all scales, and essentially the effective production balances the effective dissipation. In this region the inhomogeneous effects, induced by the presence of the wall, are not negligible, even if most of the energy required for the sustainment of the turbulent fluctuations is generated locally. The inertial transfer across scales plays a less significant role, and we can suppose that this behavior should be reproduced at large Reynolds number, since the strong viscous effects prevent the development of asymptotic conditions.

5.7.4 The buffer layer

According to the classical description in terms of global parameters, the buffer layer is identified as the region where the local production of turbulent kinetic energy exceeds the local dissipation and the excess of energy is drained from the buffer to feed the other regions of the flow, see par. 5.4. What is more it is a transitional region between the viscosity-dominated and turbulent-dominated regions of the flow, and as a consequence we can suppose that at increasing wall normal distance the scale by scale budget presents a smooth transition from the near wall asymptotics to an essentially inviscid scaling. This smooth transition is reproduced in the different terms of the scale-energy balance, as shown by the comparison of figure 5.20, deeply within the buffer, with figure 5.21, close to the viscous sub-layer, and with figure 5.22, in the low log-layer, respectively.

Let us now analyze the different components of the effective production, shown in the left panel of figure 5.20. The divergence of the inhomogeneous spatial flux T_c is opposite in sign with respect to the local production Π. Hence T_c reduces the amount of scale-energy per unit time which is locally made available. Namely, it exactly corresponds to the scale-energy which is drained from the specific location to contribute to the feeding of the adjacent regions. The effect of the inhomogeneous pressure transport is negligible as in almost all the channel section.

The insets of figures 5.21, 5.20, and 5.22, show the different contributions of the effective dissipation E_e. It is clear that the contribution of the inhomogeneous diffusion in the physical space becomes negligible as the distance from the wall is increased, while the contribution of the viscous diffusion in the space of scales is significant only

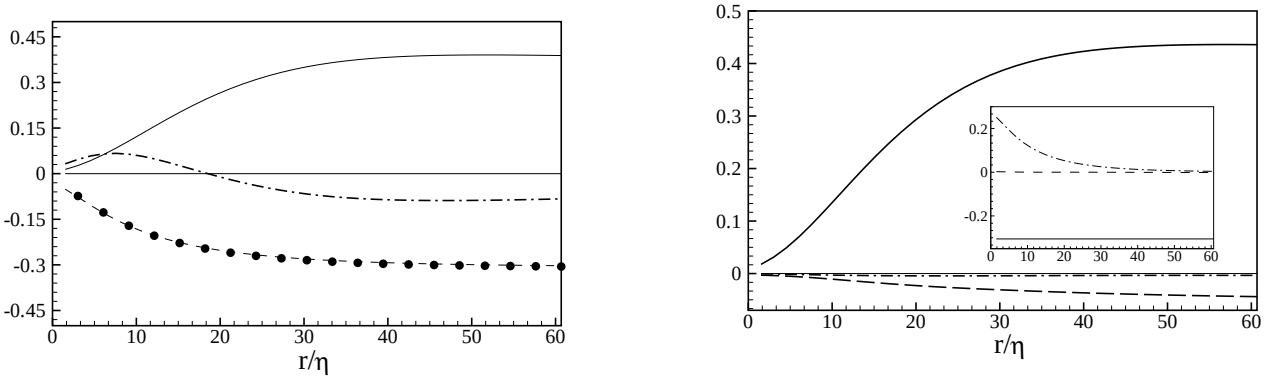

Figure 5.20: Detailed balance (5.25) in the buffer layer, $(h - |Y_c|)^+ = 20$. See caption of figure 5.19 for definitions and symbols.

at small scales. However we should observe that in the low buffer region, see the left panel of figure 5.20, D_c has a non vanishing contribution at large scales, according to its asymptotics. In fact the large scale limit of D_c and D_r is the same and is equal to twice the diffusion term of the turbulent kinetic energy (see par. 5.4 and 3.3).

Let us now consider the detailed scale by scale budgets shown in right panel of figures 5.21, 5.20, and 5.22.

A peculiar aspect of the buffer layer is the turbulent transport across scales T_r, which changes its nature from same sign of the local production at small scales to the opposite sign at large scales - in the figures, the sign of both T_r and Π_e has been changed for better readability of the plots. This behavior should be interpreted in the sense of a classical cascade of scale-energy occurring in the small scales which turns

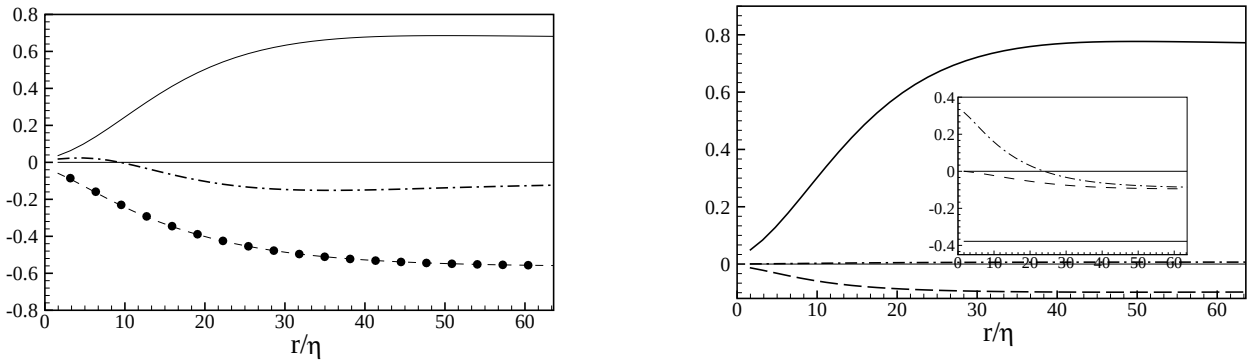

Figure 5.21: Detailed balance (5.25) at $(h - |Y_c|)^+ = 10$ (buffer layer). See caption of figure 5.19 for definitions and symbols.

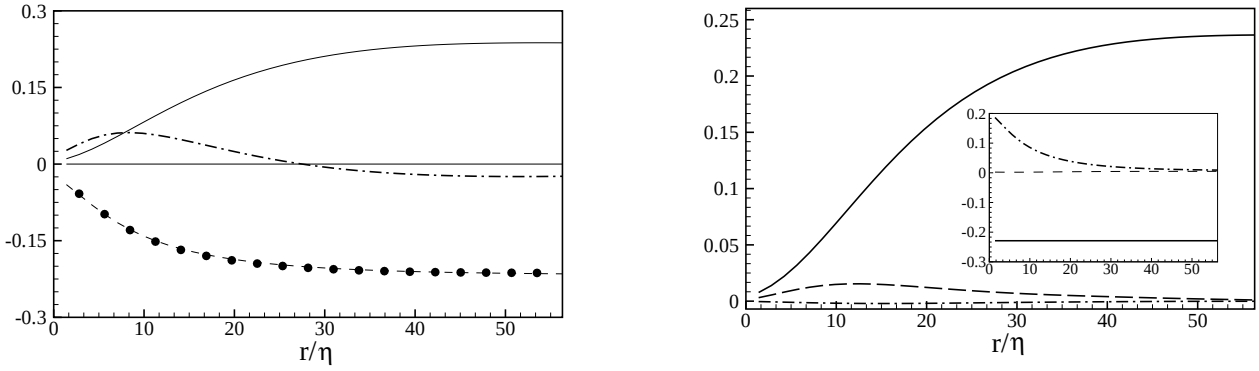

Figure 5.22: Detailed balance (5.25) at $(h - |Y_c|)^+ = 30$ (upper buffer layer). See caption of figure 5.19 for definitions and symbols.

into a reverse cascade at large separations. Actually, the asymptotics of the turbulent flux across scales (3.6), by linking the large scale behavior of T_r to the transport term of turbulent kinetic energy, implies a positive limit (negative in the figure where T_r and Π_e are plotted with the opposite sign) as r increases, i.e. a reverse cascade.

At this regard we shall mention the work [17] in which a spectral analysis of the process of energy transfer across wall parallel scales of motion is performed. In particular this work considers the instantaneous energy transfer due to modes belonging to well defined spectral regions. One of the main findings is that in the buffer region the largest scales and the smallest scales gain energy while the intermediate scales lose energy.

We can suppose that the different features which characterize the buffer layer, namely the ability to provide a replenishment of energy to the other region of the flow and the reverse transfer of scale-energy should be strictly related. Maybe they could be related to the dynamics of the coherent structures which are demanded to built-up of Reynolds stresses and present a well definite cycle consisting of regeneration of relatively extended structures with quasi-periodic breakdown to small scale turbulence, [64], [22].

Chapter 6

Passive scalar field

In this section we present some results concerning the transport of a passive scalar field in a turbulent channel flow. We analyze the results of three Direct Numerical Simulations (DNS), which give access to the instantaneous values of the variables. As a drawback, DNS can manage only small Reynolds and Péclét numbers flows. The computational domain, shown in figure 6.1, as already discussed in chapter 5, is a turbulent channel flow infinite in the streamwise and the spanwise directions. Periodic boundary conditions are applied in homogeneous directions for both the velocity and the passive scalar fields, with impermeability and no-slip on the solid wall.

A number of experimental and numerical studies, see among others [33], [35], [34], and [15], have shown that different boundary conditions and different molecular Prandtl numbers $\mathrm{Pr} = \nu/\chi$ (where ν is the kinematic viscosity of the fluid and χ its thermal diffusivity) profoundly affect the mechanism of heat transfer. These analysis have proved very useful for the development of turbulence models for the scalar, since they provide qualitative and quantitative data about relevant quantities, such as the turbulent Prandtl number and the turbulent heat fluxes.

As anticipated, we discuss here the mixing process based on three different simulations. In the first one, the Prandtl number is $\mathrm{Pr} = 0.71$, which corresponds to standard value for air. Each wall is kept at a constant temperature, with dimensionless antisymmetric boundary conditions prescribed as -1 and 1 on the upper and the lower wall, respectively. The second simulation, keeping the same Prandtl number of the first one, is characterized by different boundary conditions at the walls, which better corresponds to practical applications. We prescribe a constant value of the thermal flux at each wall, without enforcing any constraint on the fluctuating temperature. This is particularly interesting, since most of the simulations performed in the past considered zero temperature fluctuations at the wall. Hence these simulations could not account for the thermal patterns appearing rightly at the wall, which, on the contrary, were

subject of close scrutiny in a number of experimental works (see e.g. [72]). However strictly isoflux wall boundary conditions were considered in the works [46] and [72]. The boundary conditions, in this case, are symmetric with respect to the centerline, i.e. at both walls the flux is directed towards the interior of the domain, as shown in figure 6.1

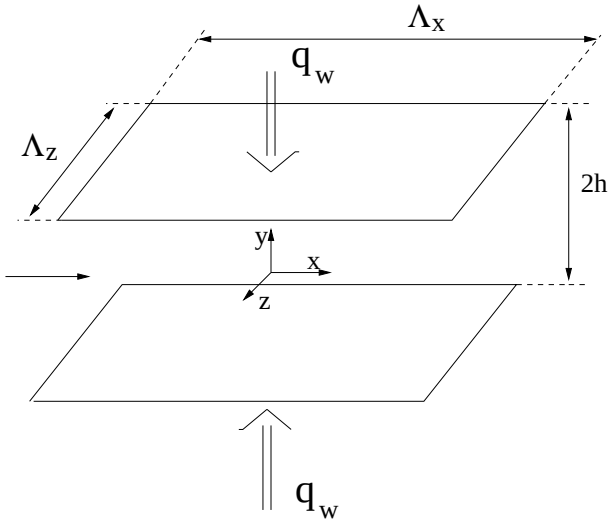

Figure 6.1: Flow configuration and nomenclature for the channel flow. The flow goes from left to right in the direction of the mean flow $U(y)$. The streamwise direction is $x \equiv x_1$. The wall-normal and the spanwise coordinates are $y \equiv x_2$ and $z \equiv x_3$, respectively. The corresponding fluctuation velocity components are denoted by $u \equiv u_1$, $v \equiv u_2$ and $w \equiv u_3$, respectively. q_w represents the wall normal heat flux imposed at the boundaries.

For this kind of wall boundary conditions we decided to realize another simulation at $\mathrm{Pr} = 2$ to understand how the flow is influenced by the different scalar dynamics at increased Pr numbers.

The computations are based on the same high order numerical formulation described for the velocity field in chapter 5. The solver has been modified to include the evolution equation for the passive scalar field, which at each time step is evaluated together with the advancement of the velocity field.

6.1 Parameters

Concerning the velocity, the three simulations were started from the same fully developed turbulent field. Stemming from the same initial data, the velocity field is statistically identical in the three simulations, to be sure that any observed difference

is due to the different conditions and parameters used for the scalar. Concerning the passive scalar, the initial condition was arbitrarily selected as the linear solution of the diffusion equation for the constant temperature case, and as a parabolic profile for the isoflux wall boundary conditions. The turbulent Reynolds number based on the channel half height h is $\mathrm{Re}_* = \mathrm{u}_*\mathrm{h}/\nu = 200$ (where $u_* = \sqrt{\tau_w/\rho}$ is the friction velocity, and τ_w the viscous stress at the wall). The computational domain is of size $2\pi h \times 2h \times \pi h$ in the streamwise x, wall normal y and the spanwise z directions respectively, with a number of grid points equal to $256 \times 129 \times 128$. The resolution in wall unit (i.e. made dimensionless with respect to u_* and ν) is $\Delta x^+ = 4.9$, $\Delta z^+ = 4.9$ and Δy^+ varying from .05 at the wall to 4.8 at the centerline. The size of the computational domain and the spatial resolution are suited to investigate the spatial structure of velocity and scalar fields up to dissipative scales which arise for the values of the parameters here considered. Actually, [36], [37], [49] can be taken to ascertain that our resolution is sufficiently fine to capture the dissipative effects both for the velocity, and for the passive scalar field. In fact in the case $\mathrm{Pr} < 1$, the Corrsin estimate implies that the dissipative scale for the scalar η_c field [1] should be larger than that of the velocity field, $\eta_\mathrm{c} = \eta/(\mathrm{Pr})^{3/4}$, where η is the Kolmogorov scale. In the case $\mathrm{Pr} > 1$, instead, see [14], according to Batchelor prediction $\eta_\mathrm{c} = \eta/(\mathrm{Pr})^{1/2}$, η_c is smaller than η. These estimates suggest that for our simulations the dissipative scales for the scalar and the velocity field are of the same order of magnitude. The results discussed are averaged over $N = 2000$ large eddy turn-over times $T = h/U_{cl}$, where U_{cl} is the average velocity at the centerline. For each simulation about 100 statistically uncorrelated configurations of the channel has been dumped to the disk to perform the statistical analysis.

Given the translational invariance in the wall parallel directions, and the steadiness in time, we can perform the ensemble average of a given quantity in terms of spatial and temporal averages. It is not strictly necessary that the temporal sample is excessively long, since the computational domain is large enough to contain a sufficient number of spatial structures. Nevertheless we performed a sensitivity analysis to show that our statistics is sufficient for the observables we are going to discuss.

Clearly the analysis, limited by moderate values of the Reynolds and Prandtl numbers, prevents the observation of asymptotic conditions. However the present findings could be of help to analyze the relation between mixing processes at different scales and large scales properties of both scalar and velocity fields, and on some mechanisms that may be operating in large Reynolds and Prandtl numbers flows.

[1] see par. 4.1.2

6.2 The equation for the passive scalar

In the simulations performed with the iso-flux wall boundary conditions (here after referred to as CF) the wall heat flux is constant in time and in the streamwise and the spanwise directions. As a consequence of the global heat balance for the thermal field, the continuous supply of heat at the walls gives rise to a linear increment of the mean temperature in the streamwise direction. To account for the heating of the fluid in the context of a numerical method conceived for periodic fields, we adopt a decomposition of the instantaneous temperature field $T(x, y, z, t)$ into the instantaneous field $\tilde{\theta}(x, y, z, t)$ deprived of the contribution stemming from the mean streamwise gradient and the contribution due to the mean streamwise gradient $\partial\langle T\rangle/\partial x$. The instantaneous field reads $T(x, y, z, t) = -\tilde{\theta}(x, y, z, t) + a\, x$, where $\partial\langle T\rangle/\partial x = a$. Here and henceforth ensemble averaged quantities are denoted by $\langle\cdot\rangle$. The instantaneous temperature field $\tilde{\theta}$ can be decomposed into a mean Θ and a fluctuating part θ, consequently the total field can be expressed as

$$T(x, y, z, t) = -\theta(x, y, z, t) - \Theta(y) + a\, x = -\theta(x, y, z, t) + \langle T\rangle . \tag{6.1}$$

The constant a can be easily evaluated through the integration over y of the evolution equation of the mean temperature $\langle T\rangle$

$$\frac{\partial\langle T\rangle}{\partial t} + U_{\mathrm{j}}\frac{\partial\langle T\rangle}{\partial x_{\mathrm{j}}} = \chi\frac{\partial^2\langle T\rangle}{\partial x_{\mathrm{j}}\partial x_{\mathrm{j}}} - \frac{\partial\langle u_{\mathrm{j}}\theta\rangle}{\partial x_{\mathrm{j}}}, \tag{6.2}$$

which after the substitution 6.1, specialized for a turbulent channel flow, reads

$$a\, U = -\chi\frac{\partial^2\Theta}{\partial^2 y} + \frac{\partial\langle v\theta\rangle}{\partial y}. \tag{6.3}$$

If we now integrate equation 6.3 over the entire channel section, i.e. from $-h$ up to h we find

$$a = \frac{-2\,\chi d\Theta/d\,y|_h}{\int_{-h}^{h} U(y)\, d\,y} = \frac{q_w}{U_{\mathrm{b}}}, \tag{6.4}$$

where U_{b} is the bulk velocity, and q_w is the heat flux at the lower wall, which is equal in modulus and opposite in sign to the flux imposed at the upper wall, see figure 6.1.

With the above transform the evolution equation for the passive scalar field $\tilde{\theta}$ reads

$$\frac{\partial \tilde{\theta}}{\partial t} - a\, u + u_i \frac{\partial \tilde{\theta}}{\partial x_{\rm i}} = \chi \frac{\partial^2 \tilde{\theta}}{\partial x_{\rm i} \partial x_{\rm i}}\,, \tag{6.5}$$

with the boundary conditions $d\tilde{\theta}/dy|_h = -q_w/\chi$, and $d\tilde{\theta}/dy|_{-h} = q_w/\chi$.

Let us now consider the inner scaling, which is a normalization with respect to suitable quantities [2]: the friction velocity u_* (see par. 5.1), the friction length ν/u_* and $\Theta_* = \chi \partial\Theta/\partial y|_w / u_*$, where $\partial\Theta/\partial y|_w$ is the gradient of mean temperature at the wall. The evolution equation for the passive scalar field in wall units reads,

$$\frac{\partial \tilde{\theta^+}}{\partial t^+} - \frac{1}{{\rm Re}_*} \frac{u^+}{U_{\rm b}^+} + \tilde{u_i}^+ \frac{\partial \tilde{\theta^+}}{\partial x_{\rm i}^+} = \frac{1}{\rm Pr} \frac{\partial^2 \tilde{\theta^+}}{\partial x_{\rm i}^+ \partial x_{\rm i}^+}\,, \tag{6.6}$$

with the boundary conditions $d\tilde{\theta^+}/dy^+|_h = -{\rm Pr}$, and $d\tilde{\theta^+}/dy^+|_{-h} = {\rm Pr}$. This last equation, for fixed Reynolds and Prandtl numbers, is independent of the specific value of the wall normal heat flux q_w, meaning that at varying q_w the dimensionless solution is exactly the same.

6.3 Steady state

A necessary prerequisite to perform a statistical analyses of the flow is to reach a statistically steady state. Then the simulation is further continued in order to collect enough fields to perform the turbulent statistics.

The steady state is usually associated with a well defined profile of the wall normal heat flux. For a fully developed temperature field the mean temperature is governed by equation 6.5, where the constant a is zero for the CT (constant wall temperature) case. If we now integrate equation 6.3 from the lower wall up to the current value of y, we obtain

$$\chi \frac{\partial \Theta}{\partial y} - \langle v\, \theta \rangle \;=\; q_w \;-\; a \int_{-h}^{y} U d\, y\,, \tag{6.7}$$

in the CF cases and

[2] which will be rigorously introduced in the next section

$$\chi \frac{\partial \Theta}{\partial y} - \langle v\,\theta \rangle \;=\; const \;=\; q_w\,, \tag{6.8}$$

in the CT case. In this case relation 6.8 shows that the wall normal heat flux is constant in all the channel section and in particular this constant is the diffusive heat flux at the wall q_w. Let us also observe that the total heat flux is negative, since it is directed from the upper wall towards the lower wall.

The first term on right hand side of equations 6.7 and 6.8 represents the molecular heat flux, and the second term the turbulent heat flux. As a consequence in addition to the exchange of heat due to the thermal diffusivity there is a convective transport due to the fluctuating field. In all cases, see figures 6.2, at the wall the turbulent transport is zero and the flux is entirely due to the molecular contribution.

Hence in narrow layer next to the wall we can assume that the dynamics of the scalar field can be described by means of appropriate length, velocities, and temperature scales, based only on ρ, ν, τ_w, which characterize the near wall behavior of the velocity field and χ, q_w, which characterize the near wall behavior of the temperature field. These scales are the friction velocity u_*, and the friction temperature $\Theta_* = q_w/u_*$.

Away from the wall the diffusive contribution of the flux is negligible. Consequently

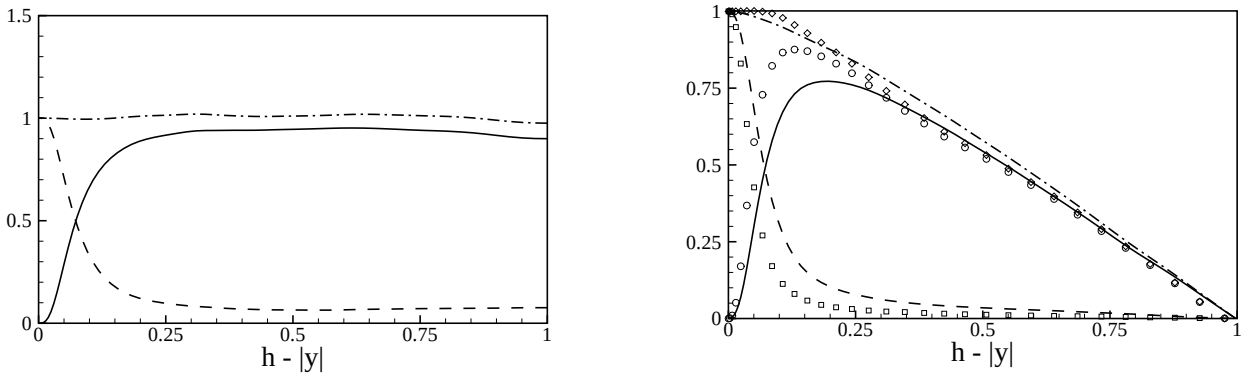

Figure 6.2: Right panel: Total heat flux at the lower wall for the CT case vs wall normal distance dashed-dotted line, diffusive heat flux $\mathrm{Pr}^{-1}\,\mathrm{d}\Theta^+/\mathrm{d}y^+$ dashed line, turbulent component $-\langle v^+\,\theta^+\rangle$ solid line. Left panel: Total heat flux for the CF cases vs wall normal distance. Diffusive heat flux at the lower wall $\mathrm{Pr}^{-1}\,\mathrm{d}\Theta^+/\mathrm{d}y^+$ dashed line for $\mathrm{Pr} = 71$, and open squares for $\mathrm{Pr} = 2$. Turbulent component $-\langle\, v^+\,\theta^+\rangle$ solid line for $\mathrm{Pr} = .71$ and open circles for $\mathrm{Pr} = 2$. Contribution due to the mean streamwise gradient $1 - Int/Re_*$ (where Int corresponds to the integral in 6.10) dashed-dotted line for $\mathrm{Pr} = .71$, diamonds for $\mathrm{Pr} = 2$.

for the CT case in the core region the flux is constant and equal to

$$-\langle v\,\theta\rangle = \Theta_*\,u_*\,, \tag{6.9}$$

which shows that $\Theta_*\,u_*$ provides the proper scaling factor for the heat flux away from the wall. The dimensionless expressions for the total heat fluxes easy follow

$$\begin{aligned}
\frac{1}{\mathrm{Pr}}\frac{\partial\Theta^+}{\partial y^+} - \langle v^+\,\theta^+\rangle &= 1 - \frac{1}{\mathrm{Re}_*}\int_{-h^+}^{y^+}\frac{U^+}{U_\mathrm{b}}d\,y^+\,, \\
\frac{1}{\mathrm{Pr}}\frac{\partial\Theta^+}{\partial y^+} - \langle v^+\,\theta^+\rangle &= 1
\end{aligned} \tag{6.10}$$

valid in the CF case and in the CT case, respectively. In the CF cases away from the wall relation 6.10 shows that the turbulent heat flux is not constant. In this case, the analysis of the right panel of figure 6.2 show that at increasing Pr numbers the contribution of the molecular heat flux is confined to a progressively narrow region next to the wall and rapidly decreases with respect to the turbulent component. The latter presents a maximum at a location closer to the wall at increasing Pr numbers.

6.4 Mean temperature profiles

The layers which characterize the near wall regions for the passive scalar can be easily characterized in terms of the behavior of the mean temperature profiles.

Let us observe that in the CF cases since the boundary conditions impose a wall normal thermal heat flux entering into the domain, the mean temperature $\langle T\rangle$ is maximum at the wall and diminishes towards the channel center, while the definition for Θ, see equation 6.1, gives a mean temperature which increases from the wall towards the middle region. The dimensionless mean temperature is defined as an over temperature with respect to the wall value,

$$\Theta^+\left(y^+\right) = \frac{\langle T_\mathrm{w} - T\rangle}{\Theta_*} = \frac{\Theta - \Theta_w}{\Theta_*}\,, \tag{6.11}$$

where $\langle T_\mathrm{w}\rangle$ is the mean temperature at the walls. We note that this definition for Θ^+ is valid for both the CF and CT wall boundary conditions.

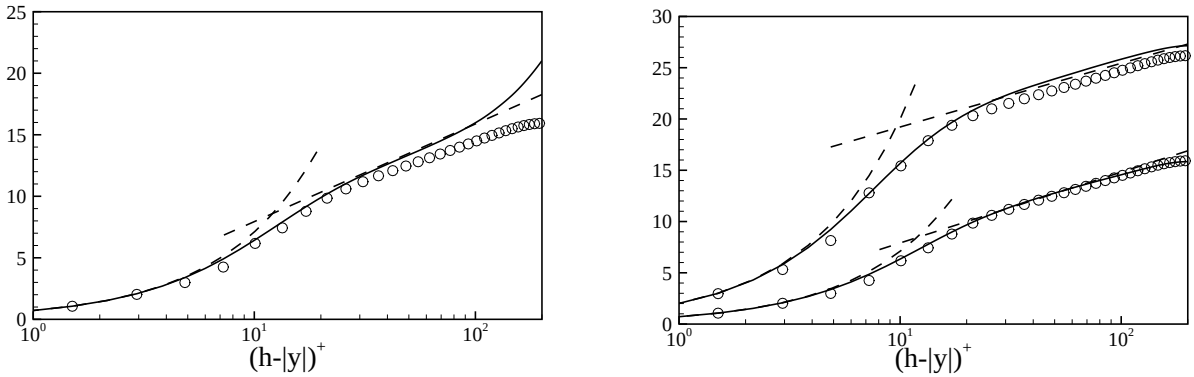

Figure 6.3: Left panel: Mean temperature profile in CT case vs distance from the wall. The dashed lines denote the linear and the log-law with a constant $\alpha = .29$. Right panel: Mean temperature profile (Pr = .71 lower line, Pr = 2 upper line) in the CF cases vs wall normal distance. The constants of the logarithmic profiles are $\alpha = .4$ for Pr = .71 and $\alpha = .37$ for Pr = 2. The open circles denote Kader's formula.

For small values of the wall normal distance the mean temperature profile can be easily obtain using a Taylor series expansion with respect to $y^+ = (h - |y|)^+$. The wall normal mean temperature derivatives can be evaluated recurring to the relations 6.10, which gives the following values

$$\frac{d\Theta^+}{d\,y^+}|_w \;=\; \mathrm{Pr}$$

$$\frac{d\Theta^+}{dy^{+2}}|_w \;=\; \mathrm{Pr}\frac{\mathrm{d}\,\langle \mathrm{v}\,\theta\rangle}{\mathrm{d}\,\mathrm{y}^+}\,|_{\mathrm{w}} = \left[\langle\theta^+\frac{\mathrm{d}\,\mathrm{v}^+}{\mathrm{d}\,\mathrm{y}^+} \;+\; \mathrm{v}^+\frac{\mathrm{d}\,\theta^+}{\mathrm{d}\,\mathrm{y}^+}\rangle\right]_{\mathrm{w}} = 0$$

$$\frac{d^3\Theta^+}{dy^{+3}}|_w \;= \mathrm{Pr}\;\left[\langle\frac{\mathrm{d}\theta^+}{\mathrm{dy}^+}\frac{\mathrm{dv}^+}{\mathrm{dy}^+} + \theta^+\frac{\mathrm{d}^2\mathrm{v}^+}{\mathrm{dy}^{+2}} + \frac{\mathrm{dv}^+}{\mathrm{dy}^+}\frac{\mathrm{d}^2\theta^+}{\mathrm{dy}^{+2}} \;+\; \mathrm{v}^+\frac{\mathrm{d}^2\theta^+}{\mathrm{dy}^{+2}}\rangle\right]_{\mathrm{w}} = 0$$

$$\frac{d^4\Theta^+}{dy^{+4}}|_w \;\neq\; 0$$

in the CT case, and

$$\frac{d\Theta^+}{d\,y^+}|_w \;=\; \mathrm{Pr}$$

$$\frac{d^2\Theta^+}{dy^{+2}}|_w \;=\; \mathrm{Pr}\,\frac{\mathrm{d}}{\mathrm{d}\,\mathrm{y}^+}\left[-\left\langle \mathrm{v}\,\theta\right\rangle \;-\; \frac{1}{\mathrm{Re}_*}\int_{-\mathrm{h}^+}^{\mathrm{y}^+}\frac{\mathrm{U}^+}{\mathrm{U_b}}\mathrm{d}\,\mathrm{y}^+\right]_{\mathrm{w}} \;=\; 0$$

$$\frac{d^3\Theta^+}{dy^{+3}}|_w \;\neq\; 0$$

for CF wall boundary conditions.

Consequently the mean velocity profiles can be represented by

$$\Theta\left(y^+\right) \;=\; \mathrm{Pr}\,(\mathrm{h}-\mathrm{y})^+ \;+\; \mathrm{c}_4\,(\mathrm{h}-\mathrm{y})^{+4} \;+\; \cdots \tag{6.12}$$

in the CT case, and

$$\Theta\left(y^+\right) \;=\; \mathrm{Pr}\,(\mathrm{h}-\mathrm{y})^+ \;+\; \mathrm{c}_3'\,(\mathrm{h}-\mathrm{y})^{+3} + \cdots \tag{6.13}$$

for the CF boundary conditions.

As a consequence the mean temperature profiles can be considered linear next to the wall for all the cases analyzed. This region identifies the *diffusive sublayer*, above which there is a transitional region where the molecular and the turbulent diffusion are of the same order of magnitude. Clearly the boundary of the diffusive sublayer is not sharply delimited and presents a strong dependence on the Pr number. In fact in the case of very small Pr numbers [3], the value of the molecular diffusivity is very large if compared to the molecular viscosity and the diffusive sublayer is expected to be thicker than the viscous sublayer. While at large Pr numbers [4], the diffusive sublayer should be embedded by the viscous sublayer.

There are many attempts to relate the thickness of the two molecular sub layers. For instance as reported in [53] for $\mathrm{Pr} \gg 1$ in the case of CT boundary conditions the subsequent estimate may hold: $\delta_\theta \simeq \delta_v \mathrm{Pr}^{(-1/3)}$, where δ_v and δ_θ represents the thickness of viscous and diffusive sub layers, respectively.

[3] for example liquid metals, like mercury

[4] for example ordinary liquids

In our simulations a graphic estimate of the diffusive sublayer thickness gives the values $\delta_\theta \simeq 7$ for the CT and CF cases with $\mathrm{Pr} = .71$ and $\delta_\theta \simeq 4$ for the CF case with $\mathrm{Pr} = 2$. These values are in good agreement with previous findings (see for instance [6] [34]), and confirm the reduction of the diffusive sublayer at increasing Pr. In particular our results show that the thickness of the diffusive sub layer is not profoundly affected by the type of boundary conditions for a given Pr number.

A simple expression for the mean temperature profile can be obtained also for sufficiently large value of y^+. If $y^+ \gg max\,(\delta_v,\, \delta_\theta)$ the effects of molecular viscosity and molecular diffusivity on the scalar field are negligibly small and the dimensional analysis gives a logarithmic profile for the mean temperature

$$\Theta^+\left(y^+\right) \,=\, \frac{1}{\alpha}\,\log(h-|y|)^+ \,+\, \beta\,, \tag{6.14}$$

Concerning the values of the constants in the mean temperature profile there is no general agreement since previous experimental and numerical studies have shown a broad scatter ([78], [34]). However our CT profile, shown in the left panel of the figure, displays a constant $\alpha = .29$ analogous to the value obtained in the simulation [34]. Let us observe that the mean temperature profile agrees fairly well with the formula suggested by Kader [32] in the range $y^+ \leq 30$. This formula is based on the interpolation of several experimental data in a wide range of variation of Re and $\mathrm{Pr} \subset (6\times 10^{-3} \div 40\times 10^3)$, and explicitly reads

$$\Theta^+\left(y^+\right) = \mathrm{Pr}\,\mathrm{y}^+\mathrm{e}^{-\Gamma} \,+\, \{2.12\,\log\left[\left(1\,+\,\mathrm{y}^+\right)\frac{1.5\,(2-\mathrm{y/h})}{1\,+2\,(1\,-\,\mathrm{y/h})^2} \,+\, \beta\left(\mathrm{y}^+\right)\right]\}\mathrm{e}^{-1/\Gamma}$$

$$\beta\left(y^+\right) \,=\, \left(3.85\mathrm{Pr}^{-1/3} \,-\, 1.3\right)^2 \,+\, 2.12\log\mathrm{Pr}$$

$$\Gamma \,=\, \frac{10^{-2}\,(\mathrm{Pr}\,\mathrm{y}^+)^4}{1\,+\,5\,\mathrm{Pr}^3\,\mathrm{y}^+}\,,$$

which shows a strong variability of the constant of the logarithmic profile in function of the Pr number. This formula, as also noted in [23], is better fitted by profiles symmetric with respect to the centerline. In fact in the CF simulations, see right panel of figure 6.3, the agreement with the Kader's formula is remarkable for both Pr. Moreover it is apparent the wider extension of the diffusive sublayer for $\mathrm{Pr} = .71$.

6.5 Root mean square temperature profiles

One of the most-demanding characteristics which can be evaluated through a DNS, required by scalar turbulent models, (see for example [16]), is the asymptotic $\theta_{\rm rms} = \langle\sqrt{(\theta-\Theta)^2}\rangle$ value in the near wall region. The root mean square temperature fluctuations are shown in figure 6.4. Apparently the boundary conditions profoundly affect the intensity of the turbulent scalar field for all the channel section, imposing different limiting behaviors as the wall is approached in the CT and CF cases. Expanding the fluctuating temperature fields in Taylor series it is easily to show that $\theta_{\rm rms}$ is dominated by a linear term in the CT case i.e. $\theta_{\rm rms} = cost\,(h-|y|)+O((h-|y|)^3)$ and by a constant term i.e. $\theta_{\rm rms} = \theta_w + O((h-|y|)^2)$ in the CF cases, where θ_w is the rms value of the temperature fluctuations at the wall.

For case CT, see the left panel of figure 6.4, most of the simulations performed up to now, see among others [15], [48] and [6], have shown that the $\theta_{\rm rms}$ profile is characterized by two maxima, one located in the near wall region and the second at the centerline. The presence of the latter is supposedly related to the non vanishing values of the mean temperature gradient and turbulent heat flux at the channel center. In particular it is known that for Pr numbers less than one the absolute maximum of the $\theta_{\rm rms}$ profile is located at the channel center, as also shown by the result of our simulation.

At increasing Pr numbers, as shown in [57], the maximum at the channel center becomes smaller than the maximum in the buffer layer. The effective reasons for the this behavior are not fully understood yet. Presumably the differences in the temperature variance profile at increasing Pr numbers are strictly related to the increase of the relative importance of the turbulent heat flux in the buffer region and the decrease of the mean temperature gradient at the channel center.

In the CF cases, instead, as shown in the right panel of figure 6.4, the variance reaches its minimum at the centerline - a behavior similar to that of the root mean square velocity components (see par. 5.3)- since both the turbulent wall normal heat flux and the mean gradient are negligible in this region. For our simulations the variance at the wall is in good agreement with the results of other published works, see among others [46] and [72]. This agreement confirms the accuracy of the present findings, since the wall value of the temperature variance is known to be particularly sensitive to the wall normal resolution.

As shown in the plots on the right panel, the range where the variance is constant decreases at increasing Pr numbers, and the location of its maximum moves towards the wall. This displacement of the maximum can be easily understood in terms of the

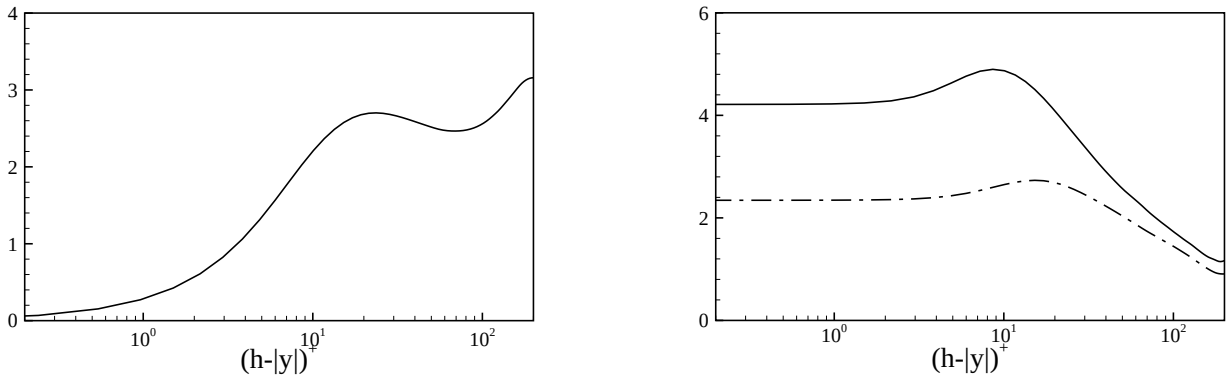

Figure 6.4: Left panel: scalar variance profiles in the CT case (dashed line) vs wall normal distance. Right panel: scalar variance profiles in the CF cases (Pr = .71 dashed-dotted line and Pr = 2 solid line) vs wall distance. All the quantities are normalized by Θ_*.

temperature variance budget, to be analyzed in the following sections.

6.6 Correlation coefficients

The relation between velocity and temperature fields is of profound interest for the development of both scalar turbulence models and of experimental measurement techniques. The similarity is used on the one hand to develop model for the passive heat transfer which are directly derived from models for the velocity field. On the other it allows to deduce the properties of the velocity field through images of the passive scalar, following a procedure often used in the context of experimental investigation of the near wall region. However, as we shall see, this procedure may be misleading, since the images are highly distorted and give traces of the velocity field only to a first approximation, even at Pr $\simeq 1$.

Usually to examine the relation between the velocity and the temperature fluctuations one considers the correlation coefficients:

$$C_{uv} = \frac{-\langle u\, v\rangle}{\theta_{\rm rms}\, u_{\rm rms}} \qquad C_{u\,\theta} = \frac{-\langle v\, \theta\rangle}{\theta_{\rm rms}\, u_{\rm rms}} \qquad C_{u\,\theta} = \frac{\langle u\, \theta\rangle}{\theta_{\rm rms}\, u_{\rm rms}} \tag{6.15}$$

which are shown in figure 6.5.

From of figure 6.5 we observe that independently of wall boundary conditions and of the molecular Pr number, our DNS results show a correlation coefficient $C_{u\theta}$ higher than

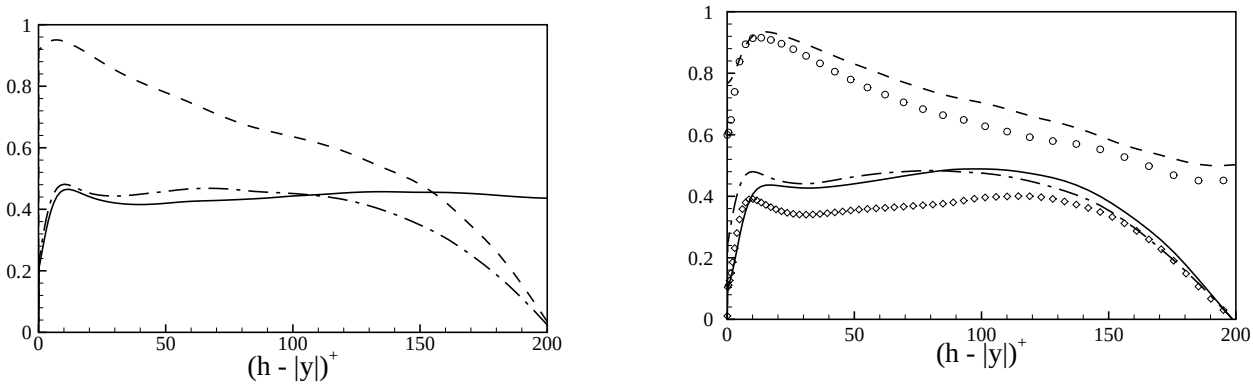

Figure 6.5: Left panel: Correlation coefficients at the lower wall vs wall normal distance for CT wall boundary conditions. C_{uv} dashed-dotted line, $C_{u\theta}$ dashed line, $C_{v\theta}$ solid line. Right panel: Correlation coefficients at the lower wall vs wall normal distance for CF wall boundary conditions. C_{uv} dashed-dotted line. $C_{u\theta}$ dashed line, for Pr = .71, and open circles for Pr = 2. $C_{v\theta}$ solid line for Pr = .71, and open diamonds for Pr = 2.

$C_{v\theta}$ in all the channel section. In the CT case, see the left panel of the figure, and [48], the correlation $C_{u\theta}$ is antisymmetric with respect to the centerline and consequently should be exactly zero there. The positive value of this correlation coefficient shows that at the lower wall positive temperature fluctuations are associated with positive streamwise velocity fluctuations. $C_{u\theta}$ is close to unity near the wall, with a peak value of $\simeq .96$ at $(h - |Y_c|)^+ \simeq 13$, and decreases towards zero at the channel center. $C_{v\theta}$ agrees quite well with C_{uv} in the near wall region, while in the center of the channel the presence of a non vanishing mean temperature gradient induces a substantially different behavior for the correlation coefficients. In particular in the near wall region there is a strong similarity between the streamwise velocity and then temperature field, while as the channel center is approached (say for $y^+ \gg 160$) the temperature field has a higher correlation with the vertical component of the fluctuation velocity.

In the CF cases, instead, as shown in the right panel of figure 6.5, the correlation coefficients between the temperature and the streamwise velocity are higher than the others in all the channel section. Moreover at the channel center $C_{u\theta}$ does not vanish unlike the other two correlation coefficients. It is interesting to observe that our findings suggest, as shown in the right panel of figure 6.5, that at increasing Pr number the correlation coefficient $C_{u\theta}$ decreases in nearly all the channel section, while its peak value $\simeq .94$ at $(h - |Y_c|)^+ \simeq 15$, seems not to vary substantially for the values of Pr number under consideration.

At increasing Pr also $C_{v\theta}$ diminishes in nearly all the channel section, but in the

middle region of the channel it seems to be less affected by the different value of the Pr number. In the near wall region the value of the correlation coefficient $C_{v\theta}$ for the CT and the CF cases displays a similar behavior. This suggests that the wall normal heat flux and the Reynolds stresses are generated by similar mechanisms. However away from the wall these coefficients are very different in dependence of the wall boundary conditions, as also reported in [41].

The behavior of the streamwise velocity fluctuation is very similar to that of the passive scalar at least near the wall, as also noted in [36], and consequently a turbulent model for $\langle \theta u \rangle$ should be similar to that for $\langle u^2 \rangle$ and one for $\langle \theta\, v \rangle$ should be similar to that for $\langle u\, v \rangle$. In particular this correspondences have lead to the refinement of some Reynolds averaged scalar flux modeling [1], in a way which gives results closer to that of a DNS.

6.7 Coherent structures

Since wall boundary conditions profoundly affect the statistics of the temperature fluctuations, it seems natural to expect that the instantaneous structures of the scalar field should present substantial differences with respect to the instantaneous structure of the velocity field. Figure (6.6) shows instantaneous streamwise velocities and temperature fluctuations at $(h - |y|)^+ \simeq 3.8$, for a mean flow directed from left to right (positive x direction). The well established streaky structure of the fields is clearly visible.

The simplest conceptual model relates the streaks, see [64] for a comprehensive review, to the presence of counter rotating pairs of vortices whose axis is nearly parallel to the streamwise direction. These vortices should cause a transfer of low momentum fluid away from the wall region and high momentum fluid towards it. In the former case the instantaneous velocity is smaller than the mean value and the associated structure is called a low speed streak. The intermediate regions between low speed streaks are called high speed streaks, since there the streamwise velocity exceeds the mean velocity. Even if the streaks are not steady and not uniformly distributed they represent an organized and simply recognizable patterns.

Thinking of temperature as a passive scalar, it looks reasonable to assume that the thermal patterns should reflect the structure of the velocity field. As clearly visible in figure 6.6, for all the simulations performed, the low speed streaks are associated with low temperature streaks and high speed streaks with high temperature ones. However the thermal patterns are not merely footprints of the velocity field, in fact they appear more elongated and also their spatial distribution seems to be Pr number dependent.

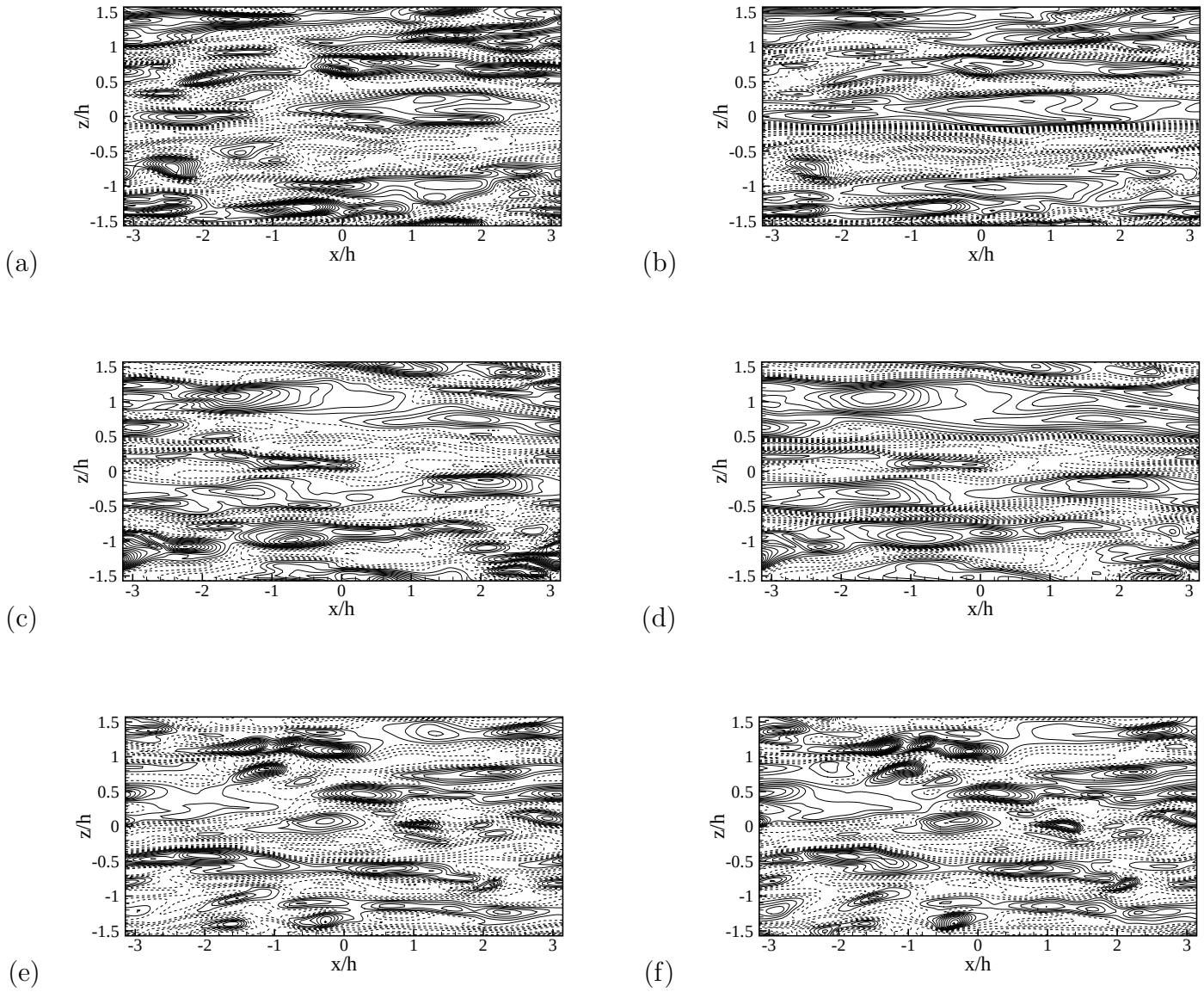

Figure 6.6: Streamwise velocity fluctuation (left panels) and fluctuating temperature (right panels) in the CF case Pr = 2 (a),(b), in the CF case Pr = .71 (c),(d), and at the lower wall in the CT case (e),(f). All the maps are at $(h - |y|)^+ \simeq 3.8$. Solid/dashed line represent positive/negative values respectively.

Moreover the simultaneous images of the streamwise velocity and the temperature field are more similar in the CT case, with respect to a visual inspection.

To clarify this aspect we evaluate the mean spanwise separation of the streaks as the double of the location of the first negative peak in the spanwise correlation

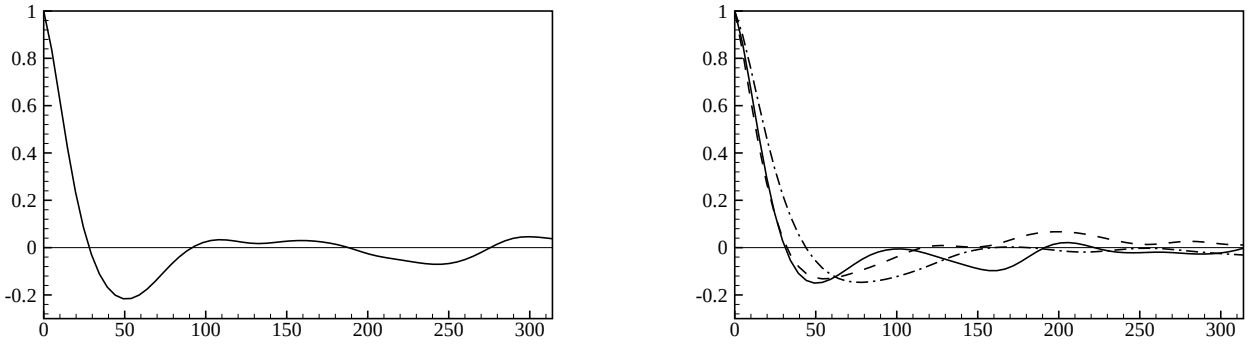

Figure 6.7: Two-point spanwise correlation of velocity fluctuations (left panel) and temperature fluctuations (right panel) vs $r_{\rm z}^+$, in CT case solid line, CF case Pr = .71 dashed-dotted line, CF case Pr = 2 dotted line, at $(h - |y|)^+ \simeq 3.8$.

$$R_{uu}\,(r_{\rm z},\, y) \;=\; \frac{\langle u\,(x,\, y,\, z)\; u\,(x,\, y,\, z \,+\, r_{\rm z})\rangle}{u^2_{\rm rms}}\,, \tag{6.16}$$

for the streamwise velocity fluctuations, and

$$R_{\theta\theta}\,(r_{\rm z},\, y) \;=\; \frac{\langle \theta\,(x,\, y,\, z)\; \theta\,(x,\, y,\, z \,+\, r_{\rm z})\rangle}{\theta^2_{\rm rms}} \tag{6.17}$$

for the temperature fluctuations.

A graphic estimate based on the left panel of figure (6.7), shows that the mean spanwise spacing of the velocity streaks is about $\Lambda^+ \simeq 100$ in wall units, in good agreement with other studies (see [37]), while the mean spanwise spacing of the scalar streaks, as appears from the analysis of the right panel of the same figure, strongly depends on both the value of the Pr number and the boundary conditions. Let us observe that in the CT case similar boundary conditions are applied to both velocity and temperature fields (meaning that the value of the velocity and the temperature are fixed at both walls). In addition the evolution equation 6.5 for the passive scalar field and that for the streamwise fluctuation velocity component are very similar in structure. The main differences are the pressure gradient term, which is absent in the equation for the passive scalar and the numerical values of the respective diffusion coefficients. However neglecting the contribution of the pressure gradient term and observing that in the CT case with Pr = .71 the thermal diffusivity has quite the same order of magnitude of the molecular viscosity, we should aspect a great correspondence

between the velocity and the thermal streaks. This is confirmed by our DNS results which show a thermal streaks spanwise spacing $\Lambda_\theta^+ \simeq 104$ quite similar to Λ^+.

The diffusive behavior of the thermal field is affected by the boundary conditions. In the CF cases the boundary conditions do not impose a zero value of the temperature fluctuations at the wall, that are transported by the normal velocity similarly to the streamwise velocity fluctuations. Let us observe, as shown in the right panel of figure 6.7, that the mean spanwise spacing of the thermal streaks $\Lambda_\theta^+ \simeq 140$ for Pr = .71 is larger than Λ^+ (see also [2]), thus the scalar field seems to be much more diffusive than the velocity field even in the case of Pr = .71, which is very close to unity.

Independently of the boundary conditions at increasing Pr the effects related to thermal diffusivity become less relevant (see [6], [73]). As a consequence, the numerical studies performed up to now, show that the scalar is directly transported by the wall normal velocity fluctuations and assumes a spatial organization analogous to that of v. Since the spanwise correlation length of v is shorter that Λ^+ the mean spanwise spacing of the thermal streaks diminishes, resulting $\Lambda_\theta^+ \simeq 110$ in the CF case for Pr = 2.

6.8 Temperature variance budgets

Turbulence models based on the second moment equation, usually require the substitution of the unknowns with terms modeled on the basis of appropriate closure hypothesis. For this purpose (see for instance [3]) the analysis of the temperature variance budgets, at different Pr numbers and with different wall boundary conditions, prove to be very useful.

In the CF case the turbulent variance budget, specialized for a turbulent channel flow reads

$$-2\langle\theta v\rangle\frac{d\Theta}{dy} - \frac{d}{dy}\langle v\theta^2\rangle + \chi\frac{d^2\langle\theta^2\rangle}{d^2y} - 2\langle\epsilon_\theta\rangle + 2\,a\langle u\theta\rangle = 0\,, \tag{6.18}$$

which is also valid for the CT wall boundary conditions if the constant a is set to zero. The first term occurs in the balance for the mean temperature variance, with opposite sign and describes the exchange of variance between the mean and the fluctuating motion. Direct measurements show that for a channel flow this production term is positive at all wall normal distances. As a consequence, the scalar fluctuations are self sustained, meaning that they do not need an external mechanism which replenishes the thermal fluctuations dissipated by the molecular action. This rate of molecular destruction of

temperature variance is represented by the fourth term $\langle \epsilon_\theta \rangle = \chi \langle d\theta/dx_\mathrm{i}\ d\theta/dx_\mathrm{i} \rangle$ (see par. 4.1.2). The last term on left hand side is an additional production term due to the presence of the streamwise mean temperature gradient. The second and the third term lead only to a spatial transfer of variance in the wall normal direction, due to the action of the fluctuating velocities and the molecular diffusion respectively. In fact the boundary conditions (both in the CT and in CF cases) impose a zero flux of the scalar variance at the entire boundary of the channel. If we integrate this contribution over the channel section we find

$$\int_{-h}^{h} \left[-\frac{d}{dy}\langle v\theta^2 \rangle + \chi \frac{d^2\langle \theta^2 \rangle}{dy^2} \right] dy \;=\; \left[-\langle v\theta^2 \rangle + \chi \frac{d\langle \theta^2 \rangle}{dy} \right]_{-h}^{h} \;=\; 0\,. \tag{6.19}$$

Hence these contributions can only cause a spatial redistribution or flux of variance in the inhomogeneous direction, thereby affecting in a substantial way the local balance.

Let us now introduce an overall spatial flux of variance, in the same manner as done for the turbulent kinetic energy,

$$\phi_\theta(y) = \langle v\theta^2 \rangle - \chi \frac{d\langle \theta^2 \rangle}{dy}\,. \tag{6.20}$$

Equation (6.18) then reads

$$\frac{d\phi_\theta\,(y)}{dy} \;=\; \sigma_\theta(y)\,, \tag{6.21}$$

where $\sigma_\theta(y) = \pi_\theta(y) \,-\, 2\,\langle \epsilon_\theta(y) \rangle$ is the net amount of excess production of variance (in principle positive or negative) pertaining to a specific location y due to the difference between production $\pi \;=\; -\,2\,\langle v\theta \rangle d\Theta/dy \,+\, 2\,a \langle u\,\theta \rangle$ and average dissipation. As a consequence if we integrate equation 5.12 from the wall to the current value of the wall normal distance $\widehat{y}$ we have

$$\phi_\theta\,(\widehat{y}) = \int_{-h}^{\widehat{y}} \sigma_\theta\,(y)\,dy\,, \tag{6.22}$$

which identifies the flux of variance leaving the layer $-h \leq y \leq \widehat{y}$ to feed the turbulent scalar fluctuation in the region above.

The different terms of the budget 6.18, normalized by $u_*^2\theta_*^2/\nu$ are reported in the left panels of figure 6.8. The inset, if present, shows the detail of the various terms in the core region, while the right panels show the net source term σ_θ, which has the same value of the divergence of the spatial flux ϕ_θ.

The turbulent kinetic energy balance 5.9, and the temperature variance budget 6.18 have very similar structures. The main differences are essentially the pressure transport term, present in equation 5.9, and absent in equation 6.18, the different value of the respective diffusion coefficients, and the terms involved in the production. However, since in our simulations the value of the Pr number is not very different from unity and the velocity and the scalar field are highly correlated, we can expect that there may be a qualitative agreement between the behavior of turbulent kinetic energy and scalar variance.

Let us first analyze the balance in the CT case, shown in panel (a) of figure 6.8. For these wall boundary conditions, as a consequence of the presence of a nonzero mean gradient at the channel center, production and dissipation are approximately in balance except than in the near wall region where, similarly to the turbulent kinetic energy balance, the molecular diffusion balances the dissipation.

The peak production occurs within the buffer layer at approximately $(h - |Y_c|)^+ \simeq 15$ and it is easy to show that its maximum value in wall units should be equal to $\mathrm{Pr}/2$. Recurring to relation 6.8 for the wall normal heat flux, the production term can be expressed as

$$\Pi_\theta^+ \;=\; -\,\langle v^+\,\theta^+\rangle \frac{d\,\Theta^+}{d\,y^+} \;=\; \left(1 \,-\, \frac{1}{\mathrm{Pr}}\frac{d\,\Theta^+}{d\,y^+}\right)\,\frac{d\,\Theta^+}{d\,y^+}\,. \tag{6.23}$$

To find the maximum value of the production, we remember that a necessary condition is to have a zero value for its first derivative with respect to y^+. Consequently, if we impose the aforementioned condition

$$\frac{d\,\Pi_\theta^+}{d\,y^+} \;=\; \frac{d^2\,\Theta^+}{d\,y^{+2}}\,\left(1 \,-\, \frac{2}{\mathrm{Pr}}\frac{d\,\Theta^+}{d\,y^+}\right) \;=\; 0\,, \tag{6.24}$$

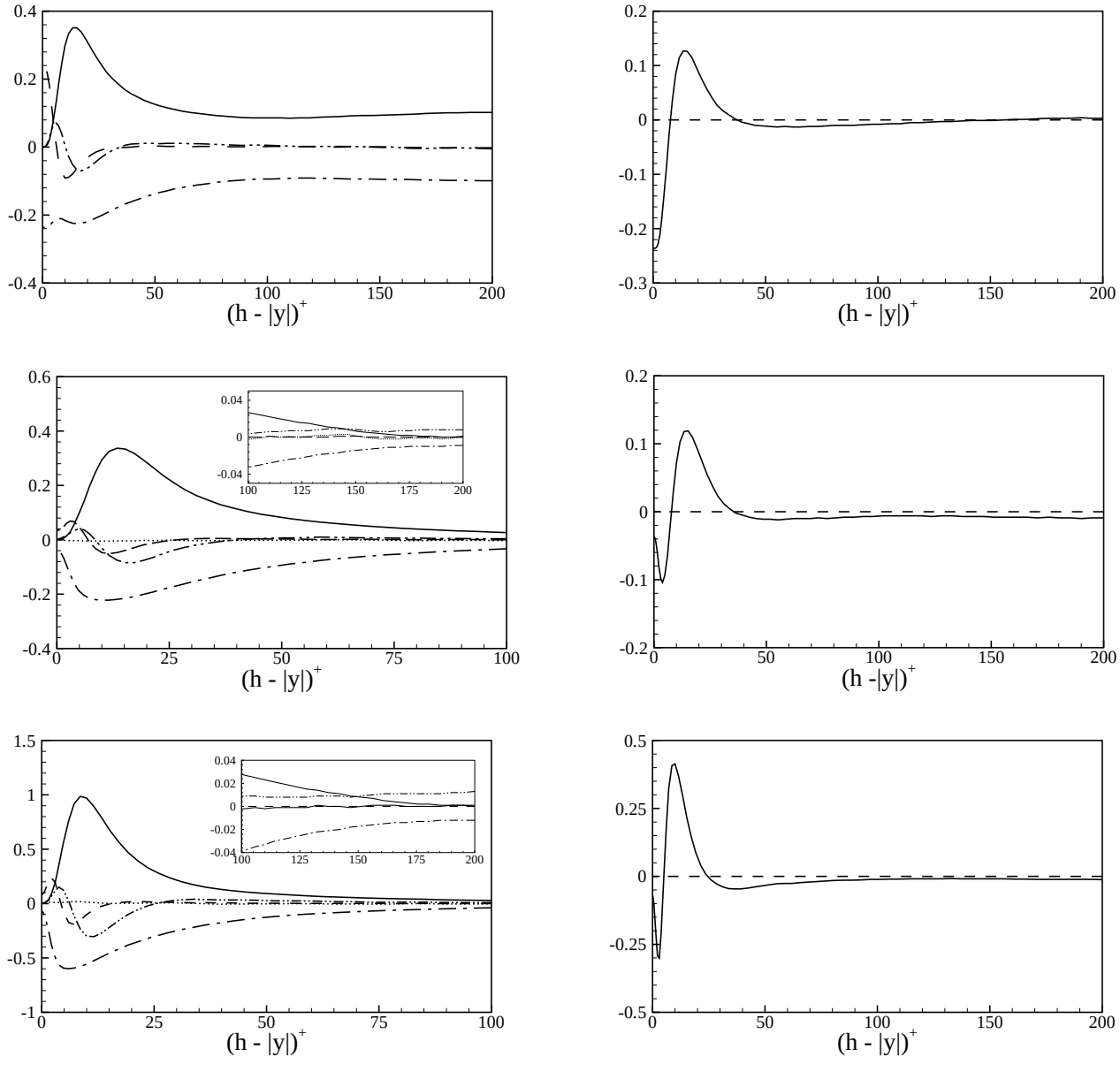

Figure 6.8: Left panels: Budgets of the scalar variance, see equation (6.18), in the CT case (a), in the CF cases Pr=.71 (b) and Pr=2 (c). production: $-$, dissipation: $-\cdot-$, molecular diffusion: $--$, turbulent convection: $-\cdot\cdot\cdot-$, streamwise production: $\cdots$. Right panels: associated productions term σ_θ vs wall normal distance.

we find that the maximum production is $max(\Pi_\theta^+) = \mathrm{Pr}/2$ at the location where $\langle v^+\theta^+\rangle = 1/2$. Hence at increasing Pr numbers the peak increases and moves toward the wall. Around the peak production exceeds dissipation, as also shown by the positive value of σ_θ in the right panel of the figure. This excess of energy is transported away

by the spatial flux ϕ_θ, whose divergence represents the net source term σ_θ.

At the wall dissipation is balanced by the molecular diffusion, which is the leading term in the diffusive sub layer, as the viscous diffusion dominates the turbulent kinetic energy balance in the viscous sub layer. We can say that the qualitative analogy between the turbulent kinetic energy balance (see equation 5.9 and figure 5.7) and the temperature variance budget seems to extend up to the lower logarithmic layer (say $(h - |Y_c|)^+ < 40$).

In fact for the CT case the boundary conditions, which impose the value of the temperature at the walls, are similar to that of the velocity field and moreover the value of the molecular Prandtl number close to one, indicates that the molecular diffusivity is of the same order of magnitude of the viscosity. In the middle of the channel, instead, the budgets are substantially different due to the presence of a non vanishing mean temperature gradient. As a consequence the production term is not negligible in the middle region of the channel and the production-dissipation ratio is nearly one from the logarithmic layer up to the centerline. The small imbalance between production and dissipation, shown by the positive value of the net source term σ_θ (see the right panel of figure 6.8), is equal to the divergence of the spatial flux Φ_θ. However this divergence is negligible with respect to the local values of production and dissipation, and the flux can then be considered as substantially constant.

Let us now consider the temperature variance budgets for the CF wall boundary conditions, shown in the right panels (b) and (c) of figure 6.8. We observe that the production due to the streamwise mean temperature gradient -last term in equation 6.18- is negligibly small with respect the production due to the wall normal mean gradient. In fact even if the correlation between u and θ is higher than that between v and θ (see par. 6.6), it results $d\langle T^+\rangle/dx^+ \ll d\Theta^+/dy^+$. In the diffusive sub layer the molecular diffusion balances the dissipation, but they do not reach their absolute maxima here, as the respective counterparts of the turbulent kinetic energy balance. The peak production occurs in the buffer layer, at locations $(h - |Y_c|) \simeq 15$ for $\mathrm{Pr} = .71$ and $(h - |Y_c|) \simeq 9$ for $\mathrm{Pr} = 2$, respectively.

If we follow the same arguments used in the evaluation of the maximum value of the production term for the CT wall boundary conditions we obtain a more complex expression, since in this case the wall normal heat flux (see relation 6.7) depends also on the mean streamwise temperature gradient,

$$\Pi_\theta^+ \;=\; -\,\langle v^+\,\theta^+\rangle \frac{d\,\Theta^+}{d\,y^+} \;=\; \left(1 \;-\; \frac{1}{\mathrm{Pr}}\frac{d\,\Theta^+}{d\,y^+} \;-\; \frac{1}{\mathrm{Re}_*}\int_{-h^+}^{y^+} \frac{U^+}{U_\mathrm{b}} d\,y^+\right) \frac{d\,\Theta^+}{d\,y^+}\,, \qquad (6.25)$$

and consequently the zeros of the first derivative are

$$\frac{d\,\Pi_\theta^+}{d\,y^+} = \frac{d^2\,\Theta^+}{d\,y^{+2}}\left[\left(1 - \frac{2}{\mathrm{Pr}}\frac{d\,\Theta^+}{d\,y^+}\right) - \left(\frac{1}{\mathrm{Re}_*}\int_{-h^+}^{y^+}\frac{U^+}{U_\mathrm{b}}d\,y^+ + \frac{U^+}{U_\mathrm{b}\,\mathrm{Re}_*}\right)\right] = 0\,, \quad (6.26)$$

Clearly if the terms in the second brackets are negligibly small the maximum production value should also be in this case equal to Pr/2. Since usually the peak value of the production occurs at small wall normal distances we can suppose that this additional contribution is effectively negligible. In fact as shown by our results, in left panels (b) and (c), the prediction Pr/2 for the maximum value of Π_θ^+ seems to be reasonably satisfied.

The peak production occurs for both Prs in the buffer layer. Here the excess of production, shown also by the positive value of the net source terms in right panels (b) and (c) of figure 6.8, originates an inhomogeneous flux ϕ_θ of variance. The turbulent component of which transports the scalar variance towards the wall and the logarithmic region, while the diffusive component, instead, transports the variance only towards the wall.

Moving towards the channel center the qualitative behavior of the temperature variance budget is more similar to the behavior of the turbulent kinetic energy balance. This similarity is essentially due to the analogies between both the wall normal stress and the wall normal turbulent heat flux, and the mean velocity and temperature gradients. It is possible to identify a region of similarity, where the production dissipation ratio is nearly one, and consequently the divergence of the spatial flux is quite zero, see the right panels of figure 6.8. Even if the asymptotic equilibrium state is clearly not reached at the Reynolds and Prandtl numbers of the present simulations, we can say that the flux of variance is negligible with respect to the local production of variance.

Also in this case in the core region dissipation exceeds production, and the fluctuations of the scalar are sustained by the spatial flux of variance, which is originated in the buffer layer.

6.9 The scale-variance

Using the tools developed in the preceding chapters we are able to analyze in a scale by scale context the analogies and the differences between the velocity and the temperature

fields. In particular also for the temperature field the conceptual picture is that of a dual transfer of variance both in the inhomogeneous direction and among eddies with different sizes. Clearly the temperature variance budget alone is not sufficient to describe the dynamics of the field at different molecular Prandtl numbers and with different boundary conditions. The analyses performed up to now shows that the local large scale characteristics of the velocity and the temperature fields, such as the mean gradients, vary substantially in function of the wall normal distance. Since these large scale characteristics are involved in the mechanisms of production, we can suppose that they could affect appreciably the mixing properties of the scalar in different ranges of scales. Consequently it is necessary to analyze the dependence of the content of the scalar fluctuations at a specific scale, described by the second order structure function $\langle \delta\theta^2 \rangle = (\theta(x_s + r_s) - \theta(x_s))^2$, on the wall normal distance. Hereafter $\langle \delta\theta^2 \rangle$ will be referred to as scale-variance.

In figure 6.9 we show the scale variance $\langle \delta\theta^2(r_{\mathrm{x}}, 0, 0|Y_{\mathrm{c}}) \rangle$ as a function of the streamwise separation, and of $Y_{\mathrm{c}} = (y + y')/2$, which is the wall normal distance of the mid-point. The right panels show $\langle \delta\theta^2 \rangle$ as a function of the separation, using the wall normal distance as a parameter, while in the left panels $\langle \delta\theta^2 \rangle$ is shown as a function of the current geometric location Y_{c} using the current scale as a parameter. The figure explicitly addresses only the CT case and the CF case at Pr = 2., since the behavior at Pr = .71 is qualitative analogous.

From the analysis of the right panels of figure 6.9 it appears clearly that the small scale behavior of $\langle \delta\theta^2 \rangle \simeq (d\theta/dx)^2 \; r_{\mathrm{x}}^2$ is accurately captured, giving further confidence on the resolution of the simulations. At large separations, where the values of the scalar at the two points x and x' are uncorrelated, the limit of $\delta\theta^2$ is equal to $2\,\theta^2_{\mathrm{rms}}$. This large scale limit is clearly reproduced by the results of the present simulations, since the curves at large separations approach a constant value equal to twice the θ^2_{rms} pertaining to the corresponding geometric location.

The left panels of figure 6.9 show that the shape of $\langle \delta\theta^2 \rangle$ is almost similar at different separations while their absolute values increase at increasing scales. In particular the scale-variance presents a relative or an absolute maximum, which becomes sharper at increasing separations, at about the same location where θ_{rms} reaches the corresponding absolute or relative maximum.

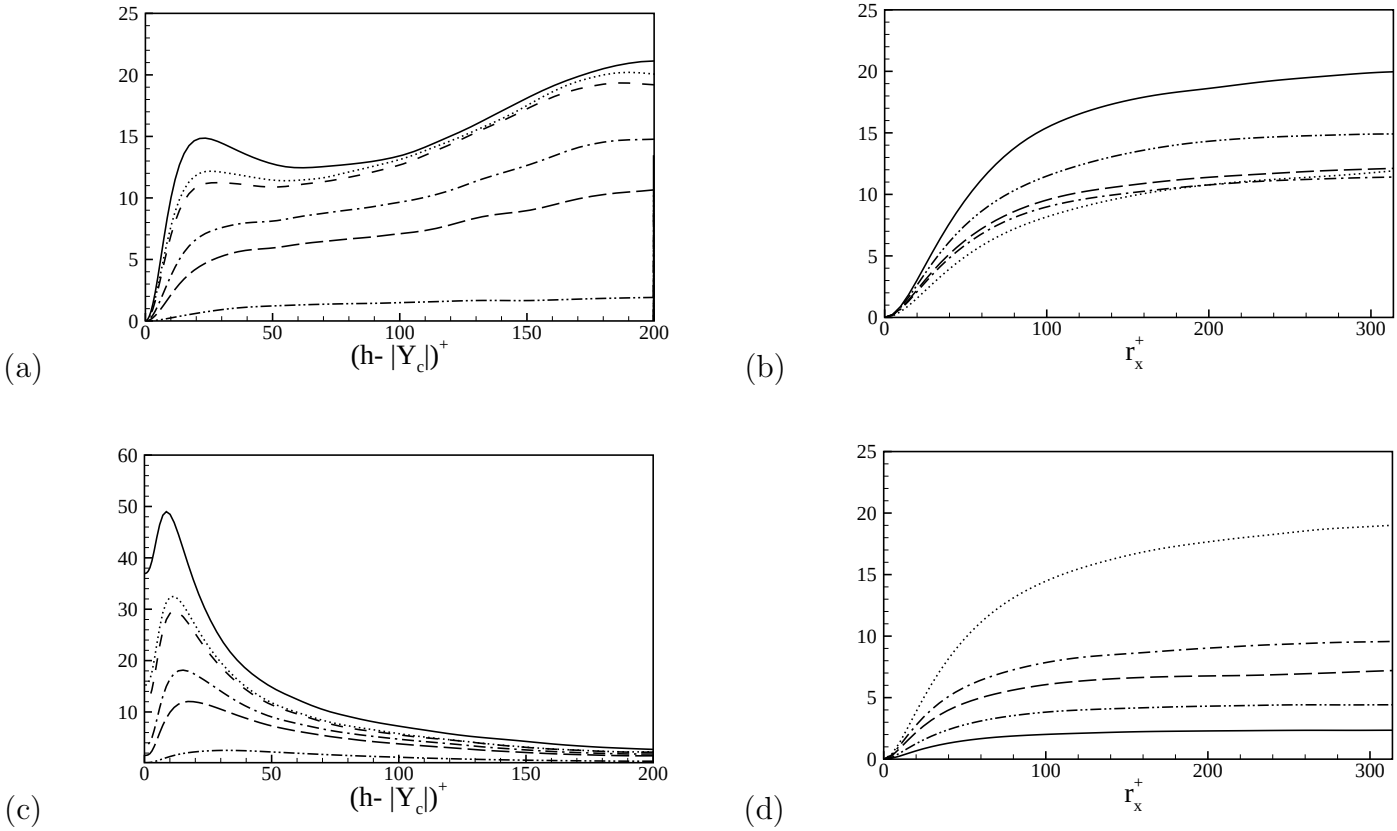

Figure 6.9: Left panels: Isolines of the scale-variance $\langle \delta\theta^2(r_\mathrm{x}, 0, 0|Y_\mathrm{c})\rangle$, normalized by θ_*^2, vs $(h - |Y_\mathrm{c}|)^+$ for different r_x, in the CT case (a) and in the CF case Pr = 2 (c). $r_\mathrm{x}^+ = 14$ (dashed-double dotted line), $r_\mathrm{x}^+ = 53$ (long dashed line), $r_\mathrm{x}^+ = 88$ (dashed-dotted line), $r_\mathrm{x}^+ = 240$ (dashed line). $r_\mathrm{x}^+ = 926$ (dotted line). The solid line is $2(\theta_\mathrm{rms}^2)$. Right panels: $\langle \delta\theta^2(r_\mathrm{x}, 0, 0|Y_\mathrm{c})\rangle$ vs r_x^+ for different $(h - |Y_\mathrm{c}|)$, in the CT case (b) and in the CF case Pr = 2 (d). $(h - |Y_\mathrm{c}|)^+ = 10$ (solid line), $(h - |Y_\mathrm{c}|)^+ = 31$ (dashed-double dotted line), $(h - |Y_\mathrm{c}|)^+ = 80$ (long dashed line), $(h - |Y_\mathrm{c}|)^+ = 180$ (dashed dotted line).

6.10 Fluxes of scale-variance

In paragraph 5.6 we observed that if local isotropy is recovered at sufficiently small scales, only the largest eddies, in particular characterized by a scale $r > L_\mathrm{S}$, should be responsible for the inhomogeneous transfer of scale-energy. Clearly an analogous observation holds for the passive scalar, i.e. if the temperature field recovers local isotropy at sufficient small scales, only the largest ones can be involved in the spatial transfer of scale-variance.

Before analyzing in more detail the spatial flux of scale-variance, let us consider the

scale by scale variance budget (6.18)

$$\frac{\partial\langle\delta\theta^2\delta u_{\rm j}\rangle}{\partial r_{\rm j}} + \frac{\langle\delta\theta^2\rangle\delta U}{\partial r_{\rm x}} + \frac{\partial\langle\delta\theta^2 v^*\rangle}{\partial Y_{\rm c}} + 2\langle\delta v\delta\theta\rangle\left(\frac{\partial\Theta}{\partial y}\right)^* - 2\,a\langle\delta\theta\,\delta u\rangle = 2\chi\frac{\partial^2\langle\delta\theta^2\rangle}{\partial r_{\rm j}\partial r_{\rm j}} + \frac{\chi}{2}\frac{\partial^2\langle\delta\theta^2\rangle}{\partial Y_{\rm c}\partial Y_{\rm c}} - 4\,\langle\epsilon_\theta\rangle\,, \quad (6.27)$$

where additional term $2\,a\,\langle\delta\theta\delta u\rangle$, due to mean streamwise temperature gradient, is present only in the CF cases. Clearly in the large scales limit, see par. 3.3, this term approaches $4\,a\langle u\,\theta\rangle$, which is twice the value of the streamwise production of the global variance budget (see eq. 6.18). From the analysis of the temperature variance budget the term $2\,\langle u\,\theta\rangle$ is found to be negligible, and since the production mechanisms are essentially active at large scales, we may suppose that the streamwise production of scale-variance should be negligible at all scales. This prevision will be fully satisfied in the detailed scale by scale analysis discussed in the following paragraphs.

The process of spatial transfer of scale-variance is better characterized by addressing the conservation form of the scale-variance budget (6.27),

$$\nabla_r\cdot\mathbf{\Phi}_{\boldsymbol{\theta}\rm r}\,(\mathbf{r},Y_{\rm c}) + \frac{d\Phi_{\theta\rm c}(\mathbf{r},Y_{\rm c})}{dY_{\rm c}} = s_\theta(\mathbf{r},Y_{\rm c})\,, \quad (6.28)$$

where $\mathbf{r} = (r_{\rm x}, r_{\rm y}, r_{\rm z})$ and boldface type denotes a three-dimensional vector. The form 6.28, in analogy with the conservation form of the scale-energy budget 5.14, essentially shows that the scale-variance balance can be expressed in terms of the divergence of the flux of scale-variance in the space of scales $\mathbf{\Phi}_{\boldsymbol{\theta}\rm r}$, of the flux $\Phi_{\theta\rm c}$ in geometrical space, and a source term

$$s_\theta(\mathbf{r},Y_{\rm c}) = -2\langle\delta\theta\delta v\rangle\,(d\Theta/dy)^* - 4\langle\epsilon_\theta^*\rangle + 2\,a\,\langle\delta\theta\delta u\rangle\,, \quad (6.29)$$

which express the local net production of scale-variance, i.e. the production term deprived of the local dissipation. Formally the structure of the two fluxes is the same,

$$\Phi_{\theta \mathrm{c}},(\mathbf{r},Y_{\mathrm{c}}) \;=\; \langle \delta\theta^2 v^* \rangle - \frac{\chi}{2}\frac{d\langle \delta\theta^2 \rangle}{dY_c} \tag{6.30}$$

$$\mathbf{\Phi}_{\boldsymbol{\theta}\mathrm{r}}(\,\mathbf{r},Y_{\mathrm{c}}) \;=\; \langle \delta\theta^2 \delta\mathbf{u} \rangle - 2\chi\nabla_{\mathrm{r}}\langle \delta\theta^2 \rangle\,, \tag{6.31}$$

they are constituted by a turbulent transport and a molecular diffusion term, defined in the corresponding spaces. These fluxes describe the coupled transfer of scale-variance which occurs simultaneously in physical and in space-scale and in particular Φ_c represents the transfer of scale-variance in the inhomogeneous direction y and is directed towards the wall if it is negative or towards the outer region if it is positive, see par. 5.6. $\mathbf{\Phi}_{\mathrm{r}}$, instead, is a vector associated with the transfer of scale-variance through scales.

The classical form of the Yaglom equation, expressed in terms of longitudinal velocity and temperature increments, is the r-average over a sphere of radius r of equation 6.28, as we discussed in par. 4.1.1. Analogously if we perform an r-average of equation 6.28, for a homogeneous isotropic turbulent-scalar field, at inertial separations we recover

$$\frac{1}{V_r}\int_{\partial B_r} \mathbf{\Phi}_{\boldsymbol{\theta}\mathrm{r}}(\mathbf{r}) \cdot \mathbf{n}_r \, dS_r \;\propto\; \frac{\langle\, \delta u_{\parallel}^2 \, \delta\theta \,\rangle}{r} < 0\,, \tag{6.32}$$

where $\mathbf{n}_r$ is the outward normal to the sphere B_r with radius r and frontier ∂B_r. A negative value of $\mathbf{\Phi}_{\mathrm{r}} \cdot \mathbf{n}_{\mathrm{r}}$ implies that scale-variance is transfered from the exterior into the sphere, as described in the classical picture of the cascade of variance towards smaller scales. Nevertheless for the same reasons outlined in par. 5.6 for the velocity field, we consider the average of a generic quantity q as $2D$ average over square domains of side r belonging to wall parallel planes,

$$Q_{\mathrm{r}}(r,Y_{\mathrm{c}}) = \frac{1}{r^2}\int_{-\frac{r}{2}}^{\frac{r}{2}}\int_{-\frac{r}{2}}^{\frac{r}{2}} q(r_{\mathrm{x}},0,r_{\mathrm{z}}|Y_{\mathrm{c}})\, dr_{\mathrm{x}} dr_{\mathrm{z}}\,, \tag{6.33}$$

where the separation vector is defined as $\boldsymbol{r} = (r_x, 0, r_z)$.

6.10.1 Spatial flux

We start with the analysis of the spatial component of the scale variance flux $\Phi_{\theta c}$. The left panels of figure 6.10 show, for each simulations, the r-average of Φ_c (see definition 6.33) as a function of $(h - |Y_c|)^+$ at different separations. For the CF cases, in analogy with the spatial flux of scale energy analyzed in par. 5.6.2, panels (c) and (e) of figure 6.10 show that for all separations it is possible to identify two regions where the flux of scale-variance is either positive, i.e. transfers scale-variance towards the bulk of the fluid, or negative, i.e. it is directed towards the wall. For all scales the scale-variance is produced in the transitional region between the molecular sublayer and the logarithmic region and is transported, through the spatial flux, to partially sustain the scalar fluctuations in the other regions. A comparison between figure 6.10 (c) and (e) allows to analyze the effect of different molecular Pr numbers, though very close to unity, on the spatial flux. In particular at increasing Pr the changes in sign of the flux occurs at a location closer to the wall.

The mechanisms involved in the sustainment of turbulence are profoundly affected by the wall boundary conditions as appears clearly from panel (a) of figure 6.10 which shows the r-average of $\Phi_{\theta c}$ in the CT case. The spatial flux of scale-variance assumes a negligible value from the upper logarithmic layer up to the channel centerline, where it should be exactly null as prescribed by the asymmetry with respect to the centerline. In this case the transport of scale variance generated in the buffer layer is limited to the near wall region of the flow, meaning that in the outer region the sustainment of the fluctuations of the scalar should be mainly due to the local production related to the presence of a non vanishing mean gradient. This issue will be analyzed in full detail in the following paragraphs. The right panels of figure 6.10 show, for each of the simulations performed, the different contributions to the r-average of Φ_c for a fixed separation $r^+ = 88$. For each simulations the change in sign of the spatial flux corresponds roughly to the location of maximum variance production and above this location the main contribution is provided by the turbulent flux. Below the most important contribution is provided by the diffusive component of the spatial flux, which confirms the hypothesis that very close to the wall the diffusivity should be active at all scales.

Dually the same analysis can be performed at a fixed Y_c^+ in function of the separation r^+. As shown in the left panels of figure 6.11 at a typical location within the logarithmic layer, for all the scales the main contribution is represented by the turbulent flux, relegating the effect of the diffusivity to the diffusive sub layers.

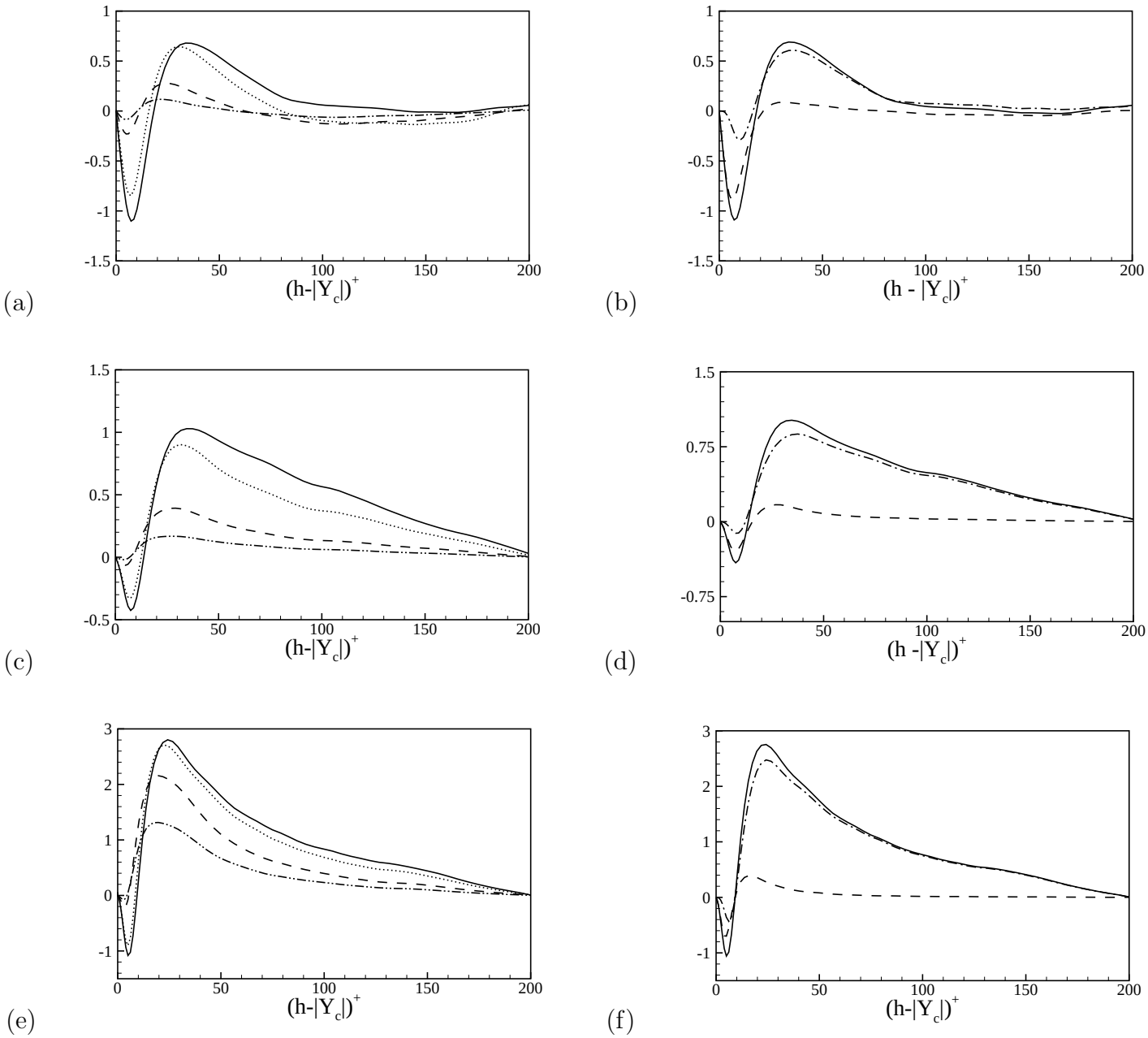

Figure 6.10: Left panels: r-average of $\Phi_{\theta c}$, normalized by $\Theta_*^2 u_*$ vs wall distance at different r^+ ($r^+ = 4 - \cdot\cdot -$, $r^+ = 14 - -$, $r^+ = 53\ \cdot\cdot$, $r^+ = 122-$) in the CT case (a), in the CF case Pr = .71 (c), in the CF case Pr = 2 (e). Right panels: Different contributions to the averaged form of $\Phi_{\theta c}$ (see definition 6.31), vs wall normal distance at fixed $r^+ = 88$, molecular diffusion $--$, turbulent flux $- \cdot -$, total $\Phi_{\theta c}$ $-$ in the CT case (b), in CF case for Pr = .71 (d), and in CF case for Pr = 2 (f).

At large scales the turbulent component of the spatial flux approaches a constant value, which is equal to the turbulent component of the spatial flux Φ_θ of the global variance budget (see eq. 6.18), $\lim_{r\to\infty}\langle\delta\theta^2 v^*\rangle = \langle\theta^2\, v\rangle$.

Let us now analyze in more details the turbulent component $\langle\delta\theta^2\, v^*\rangle\,(r_{\mathrm{x}},\, 0,\, 0|\, Y_{\mathrm{c}})$ of the scale-variance spatial flux, reported in right panels of figure 6.11, as a function only of the longitudinal separation vector r_{x}, and not averaged over wall parallel planes.

The solid lines represent the large scale limit of this term, i.e. the turbulent transport of the global temperature variance. In the CT case, as shown in panel (b), the turbulent spatial flux of scale-variance seems to approach a constant value from the logarithmic layer up to the centerline. This behavior is essentially due to the boundary conditions which determine the large scale local properties of the flow. In fact in the analysis of the global temperature variance budget we observed that the equilibrium layer, where the production dissipation ratio is nearly one, extends from the logarithmic layer up to the channel center. This imply that in the same region the divergence of the spatial flux is null and the flux itself should be constant. In particular our findings show that there the spatial flux Φ_θ is negligible[5]. Since this global flux represents the large scale limit of $\langle\delta\theta^2 v^*\rangle$, it is reasonable to assume that this contribution should be negligible also at smaller scale [6].

In the CF cases, instead, a trend towards a constant value in the equilibrium layer, which, in this case, nearly coincides with the logarithmic layer, could be detected less clearly. This behavior is very similar to the behavior of the scale-energy spatial flux analyzed in paragraph 5.6.2. Here we noted that at increasing Reynolds numbers $\langle u^2\, v\rangle$ is supposed to approach a constant value in the logarithmic layer and consequently also $\langle\delta u^2\, v^*\rangle$ is supposed to approach a constant value in this region. Similarly we can expect that at large Péclét numbers the flux of global temperature variance approaches a constant value in the equilibrium layer, and this properties should be inherited by the scale flux $\langle\delta\theta^2 v^*\rangle$, which should approach a constant value at each scales.

At this regard let us observe that in the CF case with $\mathrm{Pr} = 2$, as shown in panel (f) of figure 6.11, this trend is more easily detectable than in the CF case with $\mathrm{Pr} = .71$, as shown in panel (d) of the same figure.

In figure 6.12 the contours of the r-averaged form of $\langle\delta\theta^2\, v^*\rangle$ are shown as a function of the current scale r and the geometric location Y_{c}. We report the CF case only for $\mathrm{Pr} = 2$, since for the lower Prandtl number the same considerations hold. For the CF case this contribution, shown in the right panel of figure 6.12 reaches its maximum

[5] this is not clearly shown in the figure. Maybe a larger statistical sample is needed

[6] Since it is also reasonable to assume that this flux decreases at decreasing scales

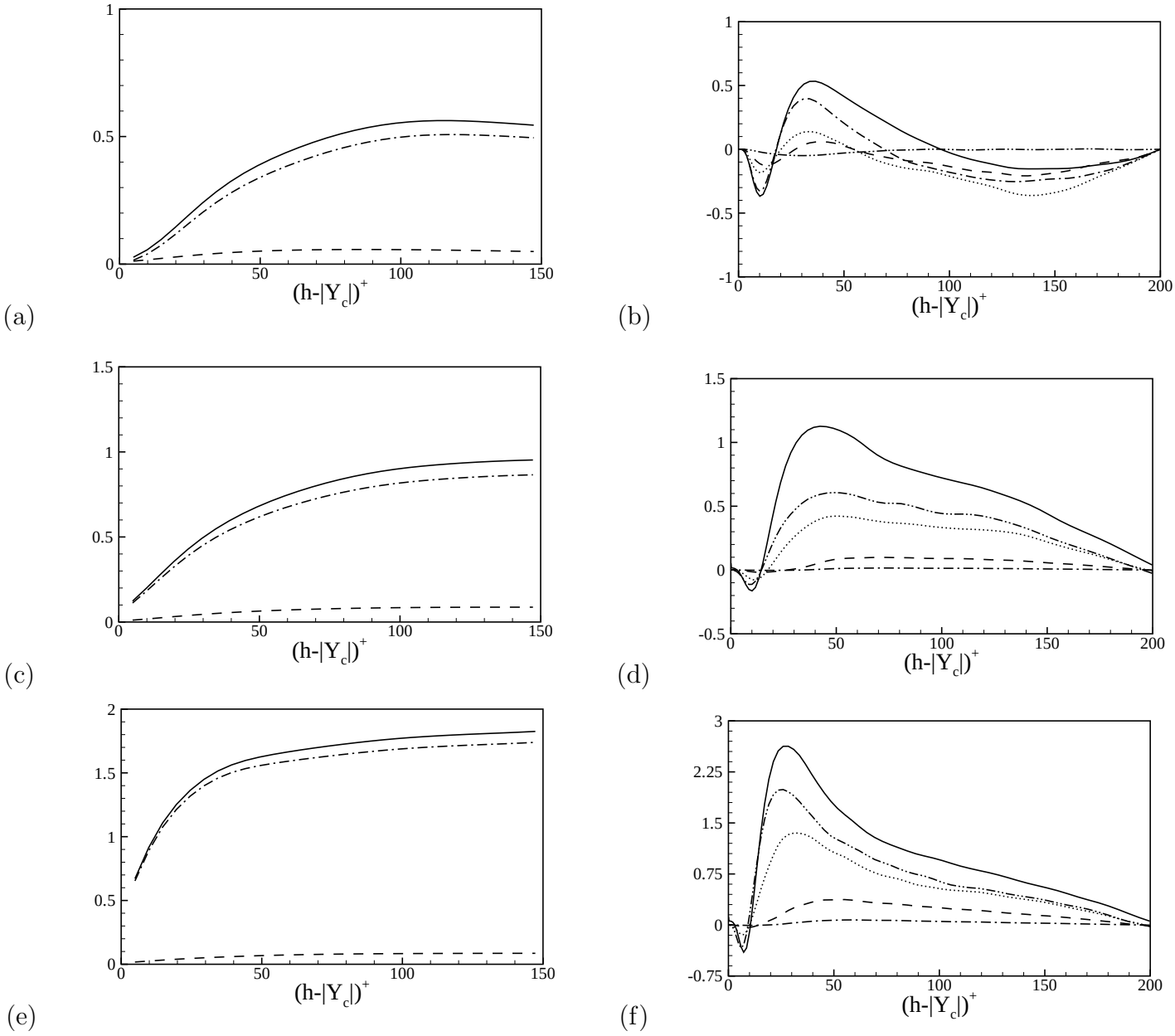

Figure 6.11: Left panels: Different contributions to the-averaged form of $\Phi_{\theta c}$. (see definition (5.14)), vs r^+ at fixed $(h - Y_c)^+ = 50$, molecular diffusion: $--$, turbulent flux: $-\cdot-$, $\Phi_{\theta c}$: $-$ in the CT case (a), in the CF case Pr = .71 (c), and in the CF case for Pr = 2 (e). Right panels: Non averaged turbulent transport $\langle \delta\theta^2 v^* \rangle$ vs wall normal distance for different separations in the CT case (b), in the CF case Pr = .71 (d), and in the CF case for Pr = 2 (f) at $r^+ = 4$ dashed-dotted line, $r^+ = 14$ dashed line, $r^+ = 53$ dotted line, $r^+ = 137$ dashed-double-dotted line. The solid line corresponds to the turbulent variance flux $\langle v\theta^2 \rangle$, see eq. 6.18.

in the buffer region, for roughly all scales, and decreases both towards the wall and towards the outer region.

This decrease means that the scale-variance carried by the flux is progressively released to partially sustain the local scalar fluctuations. Clearly if the asymptotic conditions were reached in the logarithmic layer, the flux should be almost constant, and as a consequence it should not interact with the local dynamics of the scalar fluctuations. What is more a little contribution of the flux at large scales is present in the diffusive sublayer, as in the temperature variance balance (see par. 6.8) the convective terms carries a little amount of variance towards the wall. In this region at small separation the turbulent component of the flux is negligible and the main contribution is the diffusive one (not shown in the figure).

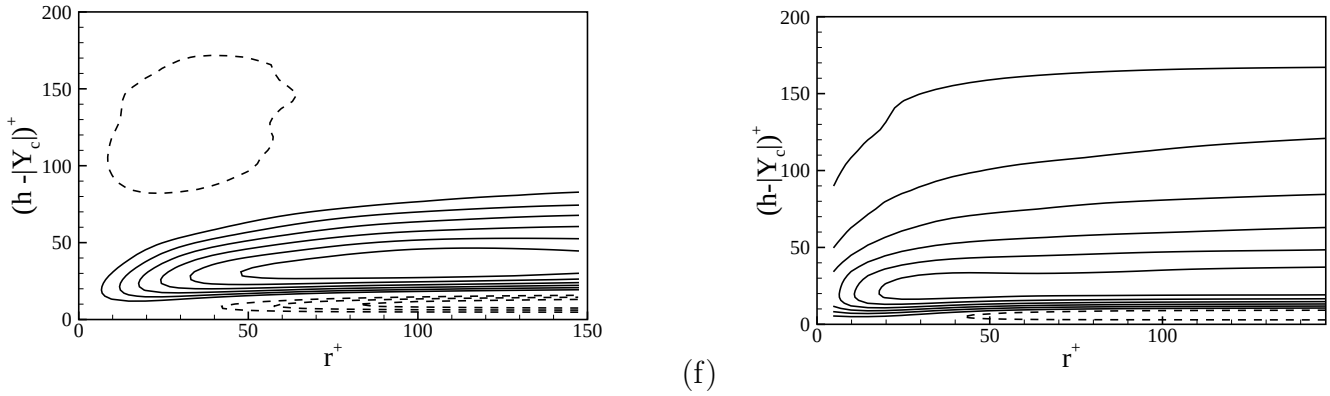

Figure 6.12: Iso-contours of the turbulent contribution to the r-averaged form of $\Phi_{\theta c}$ as a function of wall normal distance $(h - |Y_c|)^+$ and of the separation r^+, in the CT case left in the CF case Pr = 2 right, Solid/dashed contours represent positive and negative values respectively.

Also in the CT case (see the left panel of figure 6.12) the turbulent flux is built-up in the buffer layer, but its partial action of sustainment is limited to the lower part of the logarithmic layer and to the large scales of the diffusive sub layer. In fact, as we anticipated, in the equilibrium layer the turbulent component of the spatial flux of scale-variance should be negligible at all scales.

6.11 Scale by scale budget

The scale by scale variance budget 6.27 can be recast in a simpler form, as already done for the scale-energy budget, see par. 5.7.

Let us observe that when the wall normal component of the separation vector r_{y} is zero the second term on the left hand side of equation 6.27 vanishes since $\delta U = 0$ for $r_{\mathrm{y}} = 0$. After the application of the average operator 6.33 to equation 6.27 we obtain

$$T_{\theta \mathrm{r}}(r, Y_{\mathrm{c}}) \; + \; \Pi_{\theta}(r, Y_{\mathrm{c}}) \; + \; \Pi_{\mathrm{s}}(r, Y_{\mathrm{c}}) \quad + \quad T_{\theta \mathrm{c}}(r, Y_{\mathrm{c}}) \; =$$

$$E_{\theta}(r, Y_{\mathrm{c}}) \quad + \quad D_{\theta \mathrm{r}}(r, Y_{\mathrm{c}}) \; + \; D_{\theta \mathrm{c}}(r, Y_{\mathrm{c}}) \, , \tag{6.34}$$

which corresponds term by term to equation 6.27. In particular $T_{\theta \mathrm{r}}$ is associated with the inertial contribution of the flux through scales. Π_{θ} is the production term of scale variance which arise due to the presence of a wall normal mean gradient of the scalar. Π_{s} is an additional production term related to the presence of a mean streamwise gradient, and consequently absent in the CT case. $T_{\theta \mathrm{c}}$ is the inertial contribution to the spatial transfer of scale-variance and arises from the inhomogeneity of the field. E_{θ} is the mean scalar dissipation and finally $D_{\theta \mathrm{r}}$ and $D_{\theta \mathrm{c}}$ are the divergences of the molecular components of the fluxes in the space of scales and in geometrical space respectively. Let us observe that the effective amount of scale-variance available at a given location Y_{c} is provided by the local production $\Pi + \Pi_{\mathrm{s}}$ plus the scale-variance which is received or released due to the interaction with the overall inhomogeneous spatial flux $\Phi_{\theta \mathrm{c}}$. Consequently we can define the effective production, as the amount of scale-variance pertaining to the specific geometric location, $\Pi_{\theta \mathrm{e}}(r, \, Y_{\mathrm{c}}) \; = \; \Pi_{\theta}(r, \, Y_{\mathrm{c}}) \; + \; T_{\theta \mathrm{c}}(r, \, Y_{\mathrm{c}}) \; + \; \Pi_{\mathrm{s}}(r, \, Y_{\mathrm{c}})$. Clearly the single contributions are not positive definite, but to have a self sustained scalar field the sum must be positive since it represents the only production mechanism of the temperature fluctuations. Analogously, adding together the contributions of diffusive nature we can define an effective dissipation rate, $E_{\theta \mathrm{e}}(r, \, Y_{\mathrm{c}}) \; = \; E_{\theta}(r, \, Y_{\mathrm{c}}) \; + \; D_{\theta \mathrm{r}}(r, \, Y_{\mathrm{c}}) \; + \; D_{\theta \mathrm{c}}(r, \, Y_{\mathrm{c}})$. With these definitions, the r-averaged balance is expressed in a more concise form as

$$T_{\theta \mathrm{r}}(r, \, Y_{\mathrm{c}}) \; + \; \Pi_{\theta \mathrm{e}}(r, \, Y_{\mathrm{c}}) \; = \; E_{\theta \mathrm{e}}(r, \, Y_{\mathrm{c}}) \, , \tag{6.35}$$

which can be read as: transfer across scales plus effective production equals effective dissipation.

6.11.1 The logarithmic region

Figure 6.13 shows for each simulation the detailed balance 6.35 at a typical location within the logarithmic layer, namely $(h - |Y_c|)^+ = 100$. Concerning the figures we will use the same format adopted in the description of the scale by scale budget for the velocity field, which is described in par. 5.7.1. We observe that the sum $T_{\theta r} + \Pi_{\theta e}$, represented by the filled symbols in the figure, must be equal to $E_{\theta e}$ in order to have well converged datasets. Clearly this condition is completely satisfied in our simulations, since the symbols are almost on the top of the lines corresponding to the effective dissipation term. For each case the effective production, shown in the left panels of figure 6.13 is essentially due to the local production term Π_θ since the inhomogeneous turbulent transport $T_{\theta c}$ is negligible, and in the CF cases, shown in panels (d) and (f) of the figure, the streamwise production term is almost null. The insets show that the inhomogeneous molecular diffusion $D_{\theta c}$ of scale-variance is negligibly small at all scales, showing that in the logarithmic layer the contributions directly associated with inhomogeneity play a minor role. The molecular diffusion in the space of scales $D_{\theta r}$, is relevant only at small scales to became negligible at increasing separations where the effective dissipation is mainly constituted by E_θ. The qualitative behavior described in the logarithmic region is the same independently of the boundary conditions or the Pr number considered.

We can suppose that this behavior, little affected by the inhomogeneity, could be analogous to the behavior of a passive temperature field sustained by a mean gradient, transported by a homogeneous shear flow, see paragraph 4.1.3. In fact in the logarithmic layer the inhomogeneous effects are negligibly small and the local mean gradients do not vary sharply in function of the wall normal distance. Consequently the large scale features which initialize the cascade are nearly the same for the scalar both in the logarithmic layer and in the homogeneous shear flow.

The similarity of the qualitative behaviors in the logarithmic layer, for different boundary conditions and different molecular Prandtl numbers, is also maintained in the detailed budget 6.35 shown in right panels of figure 6.13. Let us observe that in each case the comparison between the relative magnitude of the production and the cascade terms leads to the identification of two distinct ranges of scales. At large separations the production $\Pi_{\theta e} \simeq \Pi_\theta$ overwhelms the transfer through scales, i.e. $\Pi_{\theta e} > T_{\theta r}$ down to a crossover scale ℓ_g at which:

$$\Pi_\theta(\ell_g, Y_c) \simeq T_{\theta r}(\ell_g, Y_c)\,. \tag{6.36}$$

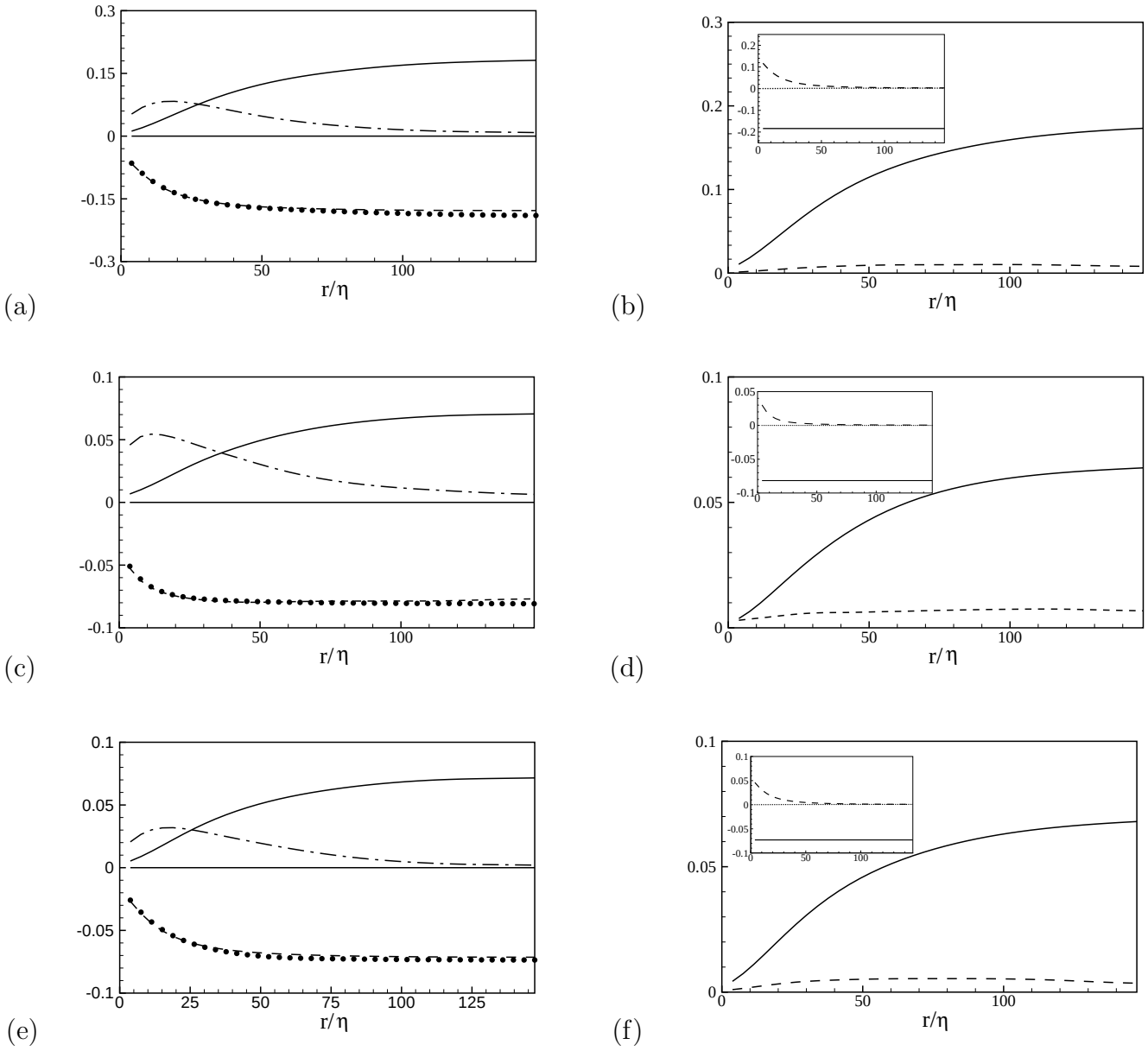

Figure 6.13: Left panels: Detailed balance 6.35 in the logarithmic layer at $(h-|Y_{\rm c}|)^+ = 100$, in the CT case (a), in the CF case at Pr = 2 (c) and in the CF case at Pr = .71 (e). -$\Pi_{\theta {\rm e}}$ solid line, -$E_{\theta {\rm e}}$ dashed line, -$T_{\theta {\rm r}}$ dashed-dotted line, $(T_{\theta {\rm r}} + \Pi_{\theta {\rm e}})$ filled symbols. Right panels: Different contributions to the effective production $-\Pi_{\rm e}$ (see equation 6.35) at $(h-|Y_{\rm c}|)^+ = 100$ in the CT case (b), in the CF case at Pr = 2 (d) and in the CF case at Pr = .71 (f). Π_θ solid line, $T_{\theta {\rm c}}$ dashed line, and $\Pi_{\rm S}$ dotted line (almost null). Insets: Different contributions to the effective dissipation $E_{\theta {\rm e}}$ (see equation 6.35), E_θ solid line, $D_{\theta {\rm c}}$ dotted line, $D_{\theta {\rm r}}$ dashed-dotted line.

below ℓ_g the cascade term $T_{\theta r}$ essentially balances the dissipation. The existence of this crossover scale is a characteristic feature of all the simulations performed and is due to the action of the mean gradients on the scalar fluctuations.

In paragraph 4.1.3 we observed that it is possible to propose two different estimates for the cross over scale ℓ_g between production dominated and convective dominated ranges of scales. The first estimate

$$L_{G_1} = \left(\frac{\langle \epsilon_\theta \rangle^3}{\langle \epsilon \rangle G^6} \right)^{\frac{1}{4}} . \tag{6.37}$$

is valid if $L_S > L_G$, where L_S is the shear scale for the velocity field, $\langle \epsilon \rangle$ is the mean dissipation of turbulent kinetic energy, and $G = G(h - |Y_c|)$ is the local value of the mean temperature gradient. If $L_S < L_G$ there is an intermediate range where the dynamics of the scalar is dominated by the convection term, while the velocity is still dominated by the production mechanism. In this case we proposed a different dimensional prediction for the scale associated with the mean gradient

$$L_{G_2} = \left(\frac{\langle \epsilon_\theta \rangle}{S G^2} \right)^{\frac{1}{2}} . \tag{6.38}$$

In panel figure 6.14 the values of the cross-over scales ℓ_G, between the effective production and the transport through scales term, are compared with the dimensional predictions L_{G_1} and L_{G_2}.

In panel (b) of figure 6.14 the full circles show the values of the cross-over scale ℓ_S (see par. 5.7.1) for the velocity field, obtained in the present simulations. It seems that for the CT case, shown in panel (a) of the same figure, the shear scale is smaller than ℓ_G in the lower logarithmic layer, say $(h - |Y_c|) < 90$, and larger above this location. As a consequence the estimate L_{G_2} for the scale associated with the mean scalar gradient should be more accurate in the low logarithmic layer, while in the upper part we should refer to the estimate L_{G_1}. This observation is partially confirmed by our data, as shown in the panel (a) of figure 6.14, where there is a good agreement between the circles, which represent the scale ℓ_G, and the estimate L_{G_2} (solid line) for the low logarithmic layer and with L_{G_1} (dashed-dotted line) above. Let us observe however that the two estimates give scales of the same order of magnitude.

Moreover these estimates can be further specialized according to the characteristic features of the logarithmic layer. In fact assuming that in the logarithmic layer the production and dissipation of the global scalar variance are locally in balance it is

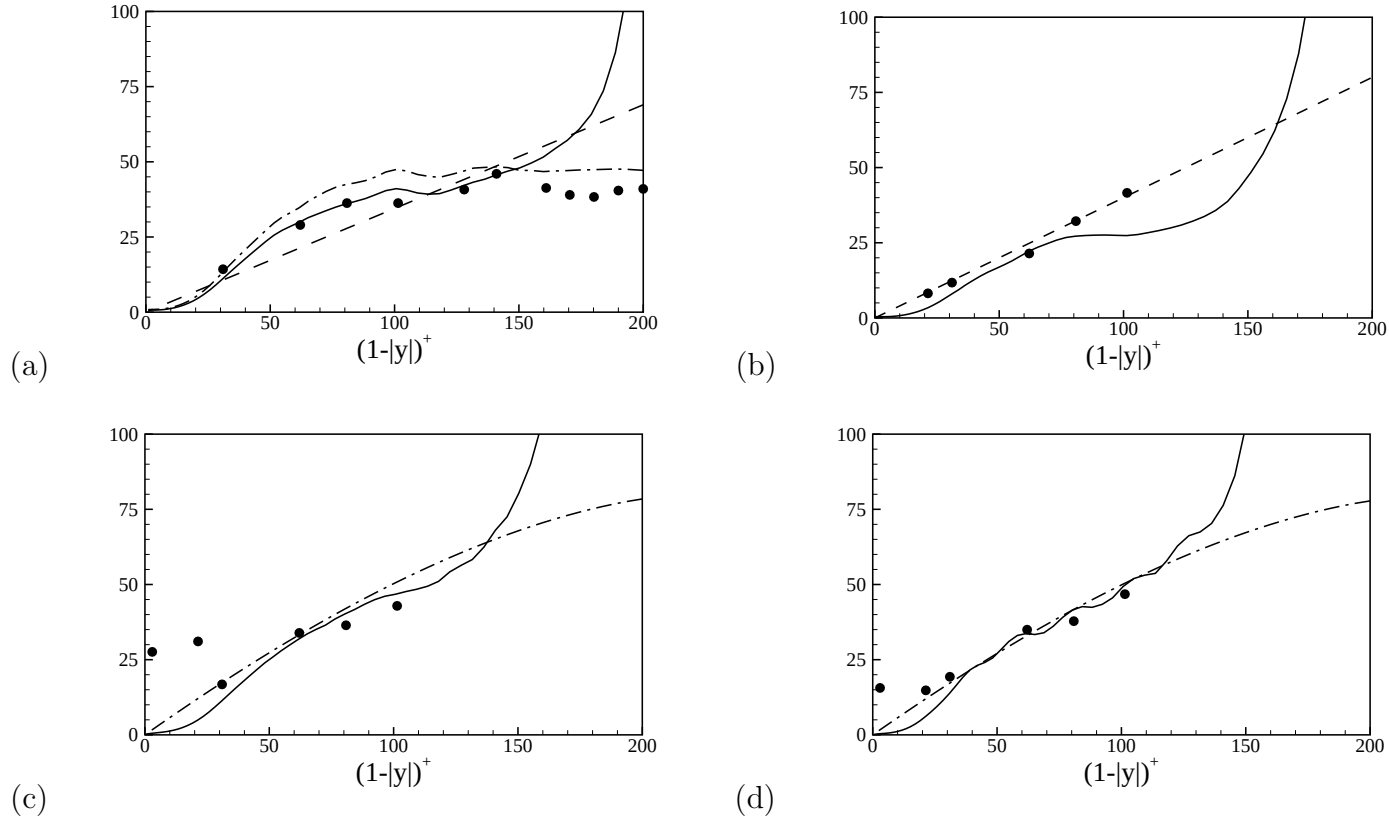

Figure 6.14: Panel (a) shows L_{G_2} solid line, $L_{\mathrm{g}} = \sqrt{\alpha k}\,(h - Y_{\mathrm{c}})^{+}$ dashed line, and L_{G_1} dashes-dotted line in the CT case. The filled circles correspond to the values of ℓ_{g} obtain in our simulation. Panel (b) shows the shear scale for the velocity field, $L_{\mathrm{s}} = \sqrt{\epsilon/S^3}$ solid line, $L_{\mathrm{s}} = \sqrt{k}(h - Y_{\mathrm{c}})^{+}$ dashed-dotted. The solid circles corresponds to the value of ℓ_{s} obtained in the present simulation. Panels (c) and (d) show the values of the cross-over scale in the CF case with Pr = .71 and Pr = 2, respectively. L_{G_2} solid line, $L_{\mathrm{g}} = \sqrt{(-\Theta_* u_* + a\int_0^{Y_{\mathrm{c}}} U dY_{\mathrm{c}})/(GS)}$ dashed-dotted line, full circles correspond to the values of ℓ_{g} obtained in the present simulations.

possible to estimate the dissipation as $\langle \epsilon_\theta \rangle \simeq \langle \theta v \rangle\, G$. The value of the turbulent flux of global variance θ_{rms} can be estimated as $\langle \theta v \rangle \simeq \Theta_* u_*$ leading to $\langle \epsilon_\theta \rangle \simeq \theta_* u_* G$.

However if the mean gradients of velocity and scalar field are estimated through the respective logarithmic laws we obtain the following prediction for $L_{\mathrm{G}_2} = \sqrt{\alpha k}\,(h - |Y_{\mathrm{c}}|)$, and for $L_{\mathrm{G}_1} = (\alpha k)^{(1/4)}\ (h - |Y_{\mathrm{c}}|)$, [7] the former of which is also shown in panel (a). In the bulk region, where G is present and the mean shear S is vanishing we should recur to the estimate L_{G_1}. In this region the dissipation of the turbulent kinetic energy, the dissipation of the temperature variance and the mean gradient G are almost constant,

[7] where k is the Kármán constant k = .41

and consequently L_{G_1} should be almost constant, as shown in panel (a).

In the CF cases, instead, the comparison between panel (c) for Pr = .71, panel (d) for Pr = 2, and panel (b), show that the shear scale L_S seems to be smaller than L_G every where, and consequently the estimate to use should be L_{G_2}. Also in these cases there is a good agreement between the values of the cross-over scales obtained in the present simulations and the dimensional predictions. If now we specialize the estimate according to the characteristic features of the logarithmic layer, we have to consider that the boundary conditions adopted cause a modification in the estimate of the turbulent flux, which results $\langle \theta\, v \rangle \simeq -\Theta_* u_* + a \int_0^{Y_c} U dY_c$, consequently a different expression for $L_{G1} = \sqrt{(-\Theta_* u_* + a \int_0^{Y_c} U dY_c)/(GS)}$ is obtained. As previously the gradient G and the shear S can be evaluated using the logarithmic laws for the scalar and the velocity fields, while the integral can be decomposed as $\int_0^h U D y_c - \int_{Y_c}^h U dY_c = Q/(2\Lambda_z) - \int_{h-Y_c}^h U dY_c$, where Q is the mass flux, Λ_z the spanwise extension of the computational domain and the last integral can be evaluated assuming that the logarithmic law for the velocity profile is valid from the log-layer up to the channel centerline. This last estimate is shown by the dashed-dotted line in panels (c) and (d). It appears that the values of the cross-over scales in the logarithmic layer are very close for both Pr numbers. In fact it is easy to show that, as a consequence of the boundary conditions applied, the estimate for the cross-over scale L_{G_1} follows a simple relation. Let us consider two different Pr numbers, namely Pr_a and Pr_b, and for the former let us refer using the subscript a to the terms appearing in the estimate L_{G_1} and the subscript b for the latter. If we impose the same heat flux at the wall for the two Prandtl numbers, and in addition to this the statistical characteristics of the velocity fields are the same, it is easy to that $\Theta_{*a} = \Theta_{*b}$, $a_a = a_b$ and $G_a = (\alpha_b/\alpha_a)\, G_b$, where α_a and α_b are the constants of the respective logarithmic profiles. As a consequence the ratio of the estimates of the cross-over scales reads $L_a/L_b = \sqrt{\alpha_b/\alpha_a}$, and is close to one if $\alpha_a \simeq \alpha_b$.

For the CF wall boundary conditions the mean gradient G is quite negligible in the outer region causing the absence of a gradient dominated range of scales.

Let us observe that panels (c) and (d) clearly show the existence of a cross-over scale also in the diffusive sub layer. This issue will be analyzed in full details in paragraph 6.11.3. Above the cross-over scale the scalar fluctuations are sustained by the mean gradient, i.e. by the local production term, while, below the cross-over scale, the scalar fluctuations are sustained by the flux of scale-variance term. The log-layer is traversed by an almost constant flux of scale-variance directed towards the bulk region of the flow, see par. 6.10.1. Hence the divergence $T_{\theta_c}$of the flux of scale variance should

be null, and effectively it is sufficiently small in comparison with the other terms of the budget - see the right panels of figures 6.13- but it is not exactly null. This may be due to a lack of asimptoticity.

6.11.2 The centerline

The right panels of figure 6.15 show for each simulation the different contributions to the effective production Π_{θ_e} at the channel center, namely at $(h-|Y_c|)^+ = 200$. Panel (b) of figure 6.15 shows that in the CT case, as found in the logarithmic region, the sustainment of turbulence is due to the local production Π_θ related to the presence of a mean scalar gradient G, since the inhomogeneous contribution T_{θ_c} is negligible.

In the CF cases, instead, as the bulk of the flow is approached the scalar gradient becomes smaller and smaller and approaches a zero value exactly at the centerline. As a consequence the local production Π_θ, see panels (d) and (f) of figure 6.15, is absent at all scales and the turbulence is sustained by the divergence of the spatial turbulent flux of scale-variance. Also here, as everywhere else, the contribution of the streamwise production term is essentially null. The insets show the different contributions of the effective dissipation E_{θ_e}. In all cases the inhomogeneous diffusion is negligible at all scales and the diffusion in the space of scales D_{θ_r} is active only at small scales.

The detailed balances at the symmetry line are shown in the left panels of figure 6.15. In the CT case the balance, shown in panel (a), shows a great correspondence to the balance in the logarithmic region, showing the existence of two distinct regions separated by the scale ℓ_g. Above ℓ_g the turbulence dynamics is dominated by the mean gradient G, while below the cascade of variance through scales is dominant. In fact, as we anticipated, in the case of constant temperature imposed at the walls the existence of a mean scalar gradient relevant in all the channel section causes the equilibrium layer to extend up to the channel center. The analyses of the temperature variance budget (see par. 6.8) reveals that from the logarithmic layer up to the channel center all the terms occurring in this balance remain almost constant. As a consequence the value of the large scale parameters, which initialize the cascade of scale-variance, are almost constant in the outer region, and in particular equal to the values assumed in the logarithmic layer. Our findings show that this behavior is also reproduced in a scale by scale context. In fact not only the shape, but also the numerical value of the different terms in the scale by scale budget 6.35 are almost constant from the logarithmic layer up to the channel center, as shown by a direct comparison between panels (a) of figure 6.13 and panel (a) of figure 6.15. Hence in this case there is an extended equilibrium region, where the dynamics of the scalar reproduces itself at each scales

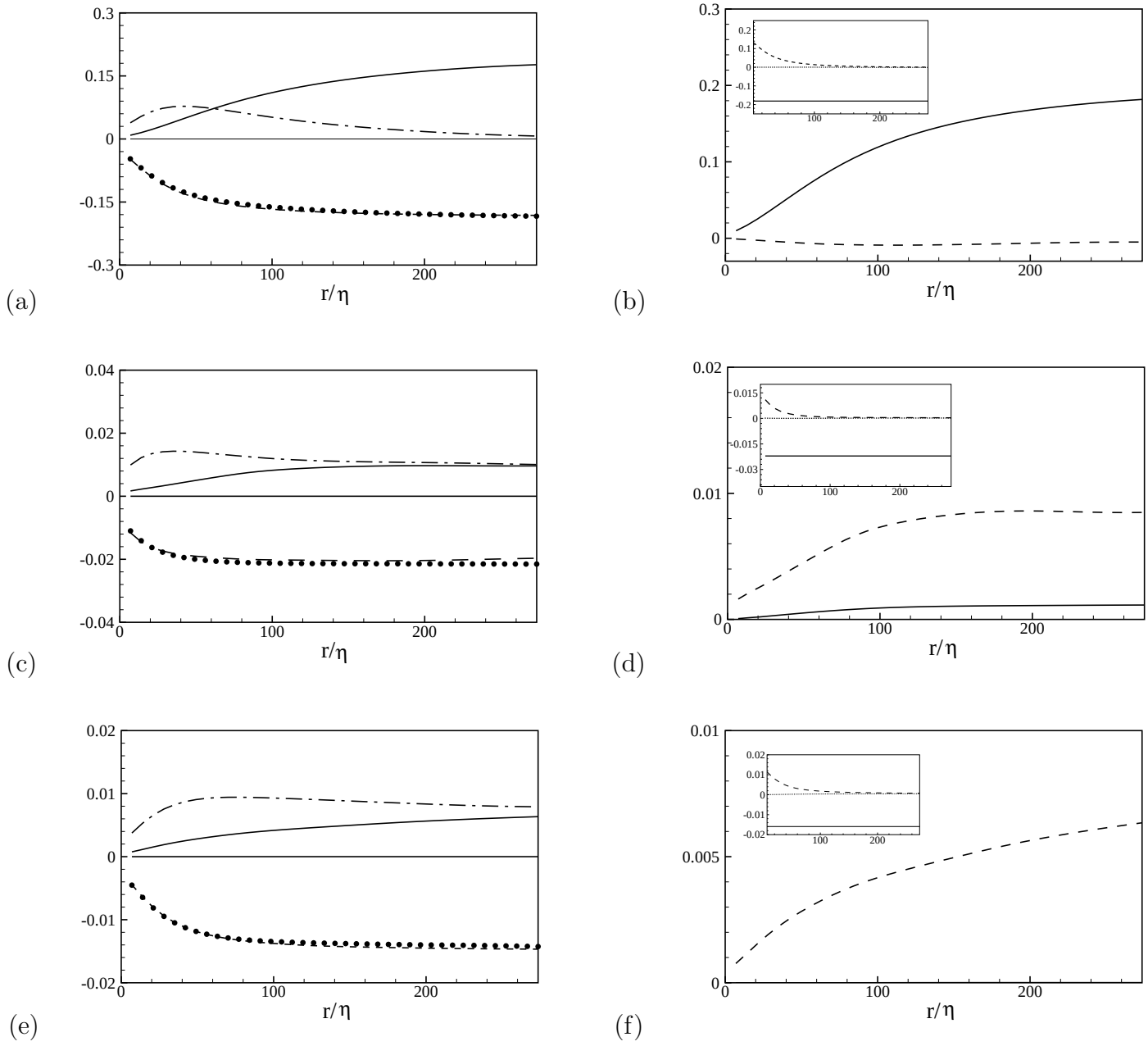

Figure 6.15: Detailed balance (5.25) in the bulk region, $(h - |Y_c|)^+ = 200$. See caption of figure 6.13 for definitions and symbols.

for different wall normal distances.

The behavior is substantially different in the CF cases, as shown in panels (d) and (f) of figure 6.15. The effective production $\Pi_{\theta e}$ is constituted only by the divergence $T_{\theta c}$ of the turbulent component of the inhomogeneous spatial flux $\Phi_{\theta c}$. In fact as the bulk of the flow is approached the mean gradient becomes smaller and smaller entailing

the drastic reduction of the local production term Π_θ. Hence the scalar fluctuations in the other region are maintained by the spatial flux originated in the buffer layer, see par. 6.10.1. The detailed balances 6.35 are shown in panels (c) and (e) of figure 6.15, for Pr = .71 and Pr = 2, respectively. The effective production, essentially given by the divergence $T_{\theta \mathrm{c}}$ of the turbulent component of the spatial flux, is less than the turbulent flux through scales $T_{\theta r}$ at all separations. However at large separations they present a common limit, since $\lim_{r\to\infty} T_{\theta \mathrm{r}} = \lim_{r\to\infty} T_{\theta \mathrm{c}} = \partial\langle\theta^2 v\rangle/\partial y$, which is represented by the turbulent transport of global scalar variance. This turbulent transport represents the mechanism through which the fluctuations are carried in the middle region of the channel. Let us observe that despite the analogy in the qualitative behavior the common limit is reached at smaller separations in the CF case for Pr = 2.

6.11.3 The diffusive sublayer

The insets in the right panels of figure 6.16 show for each simulation the different contributions to the effective production $\Pi_{\theta \mathrm{e}}$ at a location $(h - |Y_{\mathrm{c}}|)^+ \simeq 3$, that according to the estimates performed in par. 6.4 should belong to the diffusive sublayer for all the cases under consideration. In subsection 6.10.1 we saw that, in this sub layer, the most important component of the spatial flux of scale variance was the diffusive one. The derivative of this latter term with respect to Y_{c} is the diffusive inhomogeneous contribution $D_{\theta \mathrm{c}}$ of the scale by scale budget 6.35.

As shown in the insets $D_{\theta \mathrm{c}}$ contributes to the effective dissipation mostly at large scales, where it has the same limiting value of the diffusion through scales $D_{\theta \mathrm{r}}$. This latter term is relevant at small scales, where it balances the dissipation. The different contributions of the effective production are shown in the right panel of figure 6.16. For all the simulations the main contributions to $\Pi_{\theta e}$ is represented by the local production Π_θ, but the divergence of the turbulent transport $T_{\theta \mathrm{c}}$ is not vanishing and reaches quite half of the value of Π_θ at large scales. Clearly in this region, similarly to the viscous sub layer of the velocity field, the presence of the wall induces effects of inhomogeneity which are not negligible.

The detailed balances are shown in the left panels of the same figure. In the CT case, shown in panel (a) the behavior is analogous to the behavior of the scale by scale budget in the viscous sub layer (see par. 5.7.3). This correspondence stems directly from the similarity between the boundary conditions applied to the velocity and the temperature field. Opposite to the bulk region, the effective production is dominant at all scales, causing the absence of a range essentially dominated by the transfer of scale-variance through scales. The effective production and the effective dissipation

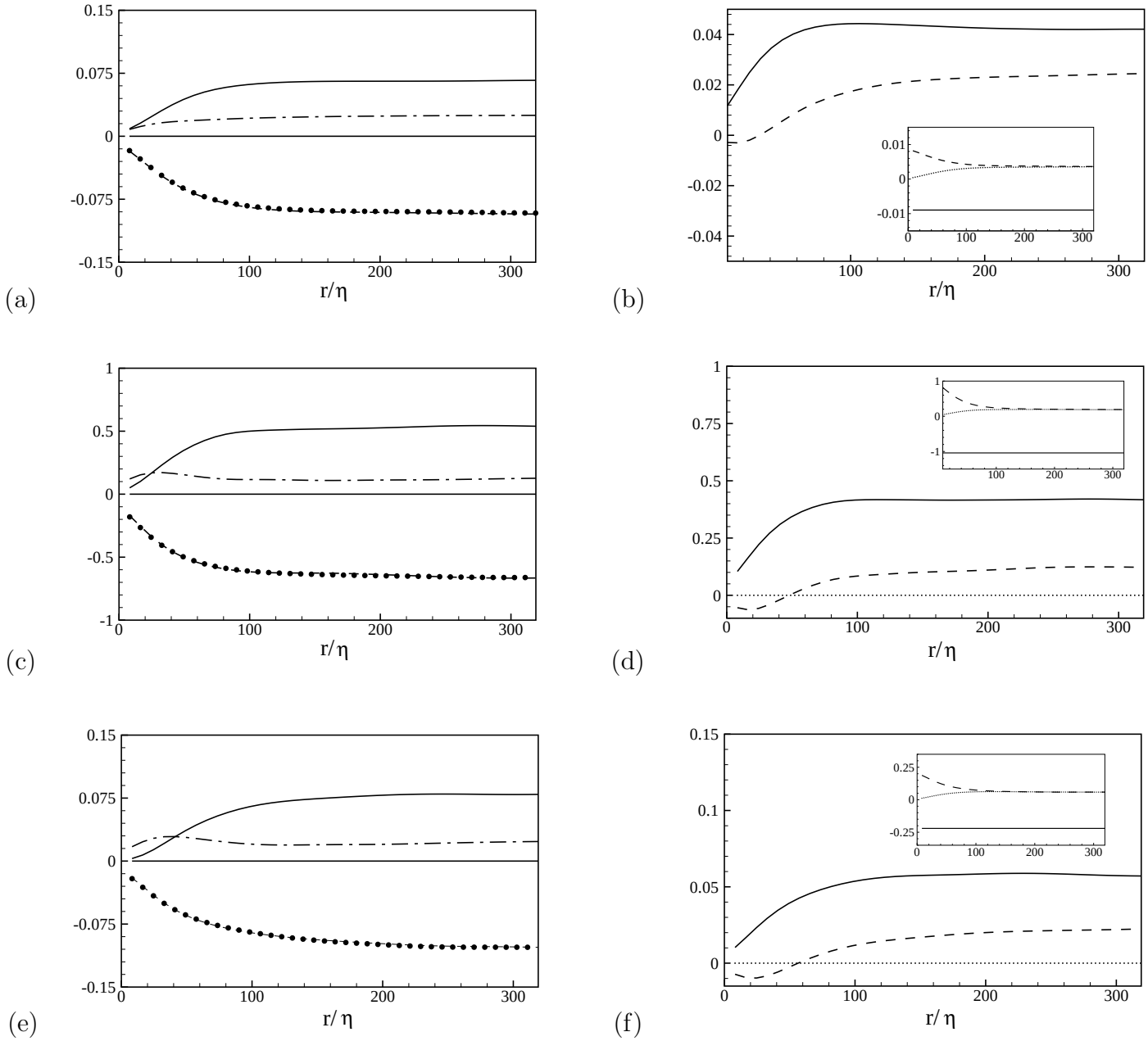

Figure 6.16: Detailed balance (5.25) in the diffusive sublayer, $(h - |Y_c|)^+ = 3$. See caption of figure 6.16 for definitions and symbols.

are almost locally in balance and there is not a separation between production and dissipative ranges, but the diffusivity is active at all scales.

This picture is profoundly modified for the case of constant heat flux applied at the walls, as shown in panels (c) and (e). A peculiar aspect is existence of two different ranges of scales, dominated by the production term or by the cascade term, respectively.

It means that there is a separation between dissipative and production ranges in a layer which is strongly affected by the action of the molecular diffusivity. Moreover in the same layer the detailed scale by scale budget for the velocity field, discussed in par. 5.7.3, does not show a separation between production and dissipative ranges, and consequently, under this respect, the dynamics of the scalar is not inherited from that of the velocity field.

The presence of a range where the convection term is the most important contribution in the scale by scale budget may be related to the non vanishing value of the scalar fluctuations at the wall, which are associated with a rise of the convective contribution at small scales.

This behavior seems to held independently on the molecular Pr number, nevertheless the cross-over scale is smaller in magnitude for $\mathrm{Pr} = 2$. Let us observe that this behavior is similar to that of the mean spanwise spacing of the thermal streaks, which diminishes at increasing Pr numbers.

6.11.4 The buffer layer

As analyzed in section 6 in the buffer layer the local production of global variance exceeds the dissipation and the excess of variance is drained from the buffer to sustain the fluctuations in the other regions of the flow. This picture effectively describes the behavior of the temperature variance budget in the CF cases, whereas in the CT case the sustainment of the fluctuations, in all the channel section, is due to the action of the local mean gradient. The same conclusions hold for the analyses of the scale by scale behavior as shown in section 6.10.1. In the CF cases the buffer represents a sort of *engine* for the turbulent fluctuations, from where the scale variance is extracted and drained to sustain the fluctuations in the other regions.

Let us now analyze the different components of the effective production, shown in the left panels of figure 6.17. The divergence T_{θ_c} of the inhomogeneous spatial flux at all scales results opposite in sign with respect to production Π_θ, meaning that it absorbs the scale-variance from the buffer and transfers it towards the other regions. In the CF cases the contribution due to the production term Π_S, associated with the mean streamwise temperature gradient, is negligible at all scales as in all the channel section.

The insets of the right panels show the different contributions of the effective dissipation E_{θ_e}. The contribution of the viscous diffusion in the space of scales D_{θ_r} is significant mostly at small scales, whereas the inhomogeneous diffusion in physical space D_{θ_c} plays a minor role here with respect to the viscous sub layer.

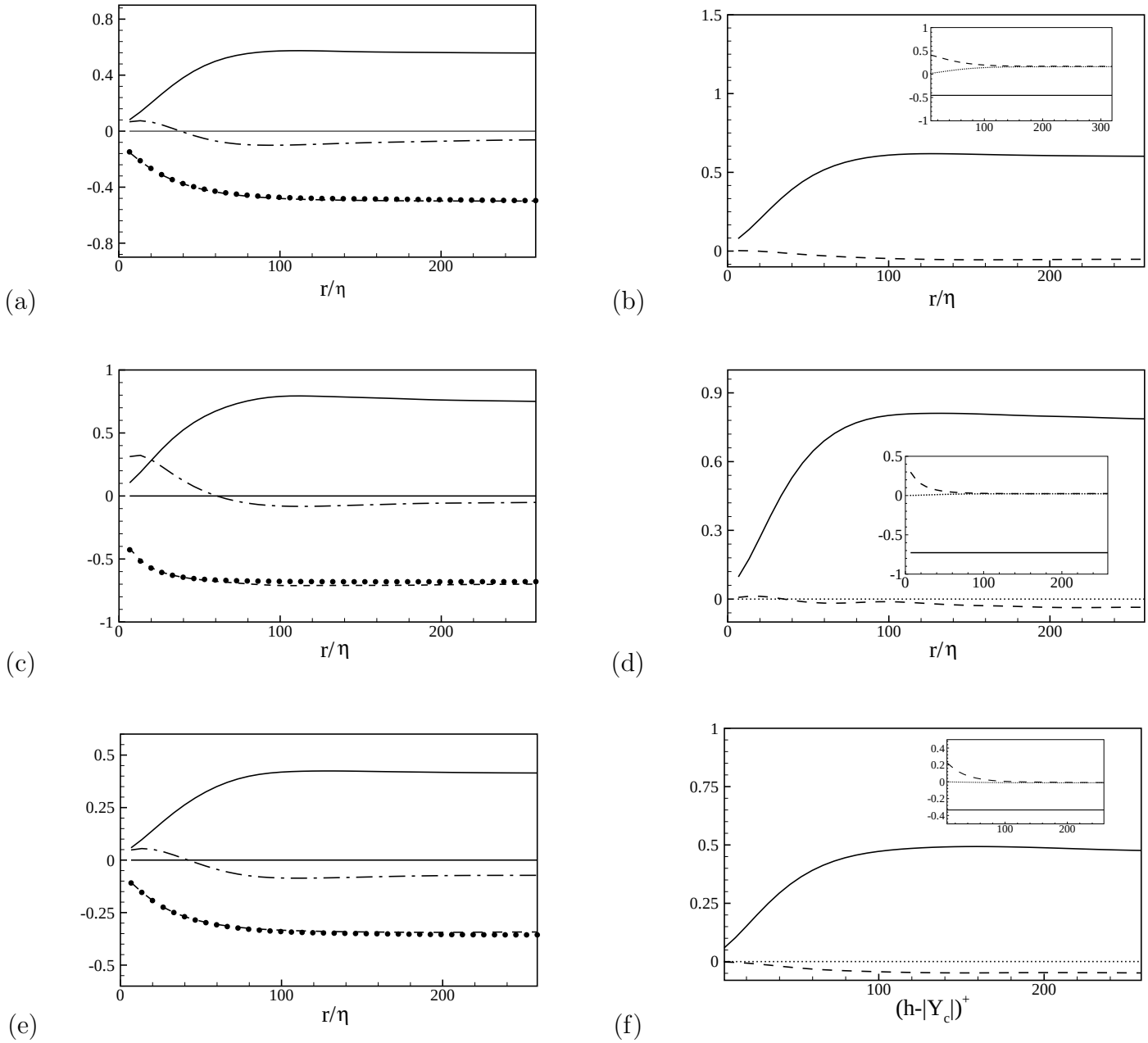

Figure 6.17: Detailed balance (5.25) in the buffer layer, $(h - |Y_c|)^+ = 20$. See caption of figure 6.16 for definitions and symbols.

Let us now analyze the detailed scale by scale budgets shown in the left panels of figure 6.17. A common feature of all the simulations performed is the change in sign of the term $T_{\theta r}$ related to the cascade of variance through scales. This term has a sign

opposite to the effective production at large scales and consequently reduces the amount of scale-variance available at a specific scale r through a transfer of scale-energy towards larger scales. At small scales, instead, T_r is positive and therefore is associated with a direct variance cascade (from larger to smaller scales) as everywhere else in the channel. This behavior is characteristic only of the buffer layer and may be related to the organization of the scalar field into coherent structures that resemble the velocity streaks (see section 6.7) and undergo a regeneration cycle constituted by a formation and instability of the structures and a following breakdown of the organized motions.

Chapter 7

Concluding Remarks

In homogeneous isotropic condition the cascade of energy is initialized by an external mechanism which could be an external forcing active only at large scales. For the homogeneous shear flow there is a local production of scale-energy due to the anisotropy induced by the shear. For a wall bounded flow the picture is more complex, since we have essentially two processes which initialize the scale-energy cascade.

Let us show a sketch of the phenomenology, which has been described in the previous paragraphs.

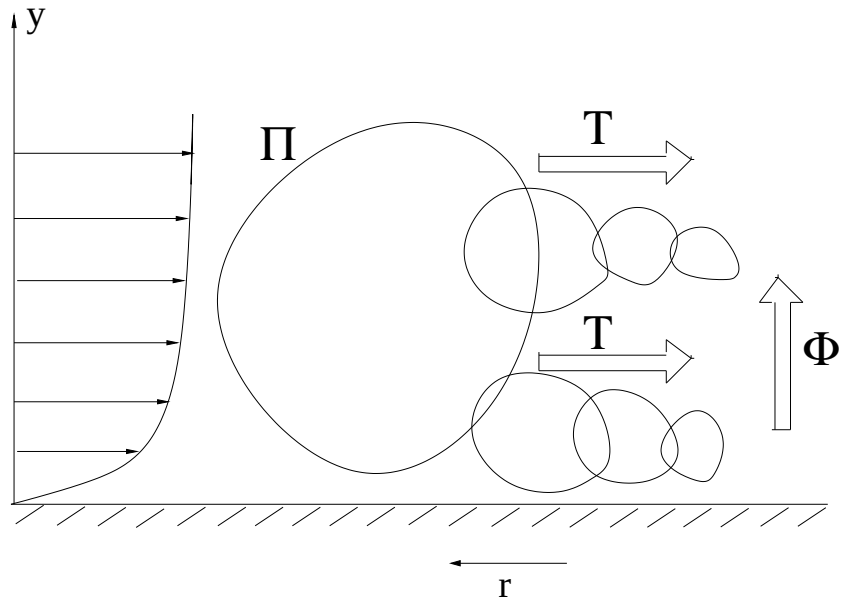

The existence of a coupled transfer of energy in physical space and in the space of scales, was already considered by other authors ([17], [30]). For instance Jiménez [30], following [76], discussed the role of the attached eddies [1], which should be responsible

[1] eddies whose size is of the order of the distance of their center from the wall

for the inverse energy cascade, i.e. a transfer of energy from small eddies, located near the wall, towards larger eddies away from the wall. In the sketch we can identify a flux of energy Φ in the wall normal direction from one hierarchy of eddies to an another hierarchy and a local energy transfer T from large eddies towards small ones.

At a given wall normal distance the interaction between the attached eddies and the mean shear gives a local production term Π but in addition to this we have to consider the scale-energy flux arriving from an another hierarchy of eddies. These two contributions initialize the cascade through scales towards the dissipation range where the scale-energy is dissipated.

In this context the generalized Kolmogorov equation, originally derived in [26], allows to simultaneously address the scale-energy cascade and the spatial fluxes, since it makes accessible the dynamics of a given scale as a function of the wall normal distance.

This equation represents the link between the classical approaches followed in the characterization of wall bounded flows. Two of the most important results in turbulence theory concern the idealization of the flow aimed, on the one hand, at the dynamics of the small scales and, on the other, at the description of the near-wall layer of wall bounded flows. The two theories are, in a sense, the dual one of the other. Both belong to the realm of singular perturbations, in the sense that viscous effects are confined to a vanishingly narrow range, and are fundamental in the definition of the large Reynolds number asymptotics of the Navier–Stokes equations. Even if the viscous effects are negligible at any finite scale for infinity Reynolds number, there should be finite limits of the dissipation ϵ in one case and of the wall shear stress τ_0 in the other.

The external conditions, namely the energy production at large scales in the first case, fixes the incoming flux of turbulent kinetic energy T_r, while for instance the pressure gradient in the second case, fixes the momentum flux τ_R (namely the Reynolds stress).

The dual nature arises from the fact that, in the first case, the description is given in the space of scales - the separation r or, equivalently, the wave-number - while in the other it is given in physical space. Clearly the appropriate tool to describe the scale dependent dynamics, i.e. to reconcile the description in the space of scales and in physical space is the generalized form of the Kolmogorov equation. This equation provides a realistic description of small scales turbulence, especially when asymptotic conditions are not fulfilled, since it accounts exactly for the inhomogeneity and anisotropy of the flow under consideration. In particular, the analysis of the role played by the various scales in the dynamics of turbulence (e.g. the characterization of the shear scale)

is of valuable interest in the refinements of turbulence models, such as Large Eddy Simulations.

Of particular interest - we believe - is that the classical decomposition of the channel into different regions maintains a well defined meaning also in the context of a scale by scale analysis. The buffer layer appears as the region where production of scale-energy is predominant and feeds the spatial flux towards adjacent zones. The log-layer is an equilibrium layer where local production and local dissipation balance, meaning that it is traversed by an almost constant flux of scale-energy, which does not interfere with the local dynamics. The spatial flux of scale-energy is instead crucial for the sustainment of the turbulence in the bulk region. In the space of scales, typically in the log-layer, the large-scale production range is followed by a nearly classical transfer range, closed by diffusion at the local dissipative scales. In the buffer layer the analysis reveals the existence of a double cascade regime. i.e. a direct scale-energy cascade at small scales and an inverse scale energy-cascade at large scales.

The methodology of analysis used to characterize the scale dynamics of the velocity field is sufficiently general to be easily extended to the characterization of other quantities, such as the passive scalar field. In this case the generalized Yaglom equation 4.2 allowed us to simultaneously address the scale-variance cascade and the spatial fluxes induced by the inhomogeneity of the flow. This analysis has been performed for a passive scalar field subjected to two different kind of wall boundary conditions. In the first case the value of the instantaneous temperature is prescribed at the walls, whereas in the second case the thermal heat flux is imposed, without enforcing any constraint on the fluctuating temperature. For this wall boundary conditions a second simulation at a different Prandtl number has been performed.

Our main findings concern the behavior of the scale by scale dynamics of the scalar field in a turbulent channel flow. Irrespective of the wall boundary conditions the buffer layer appears as the region where the local production of scale-variance is predominant with respect to the local dissipation and the consequent excess of scale-variance is transported away through the spatial flux. This spatial flux is almost constant in the logarithmic layer, where production and dissipation are almost locally in balance. The behavior in the core region of the flow, instead, is profoundly affected by the wall boundary conditions, in fact in the CT case the scale by scale budget is indistinguishable from that in the logarithmic layer. As a consequence there is an extended equilibrium layer, where the dynamics of the scalar reproduces itself at different wall normal distances, and the spatial flux of scale-variance is negligible. This flux, instead, is the source of scalar fluctuations in the bulk region for the CF wall boundary conditions.

A peculiar aspect emerges from the analysis of the scale by scale budgets in the diffusive sub layers. In the CT case the behavior is similar to that of the scale by scale energy budgets, showing a local balance between effective production and effective dissipation. Consequently a separation between production and inertial ranges does not appear. This picture is substantially modified for constant wall heat flux boundary conditions, since a separation between a production and a convective range appears clearly, even if it is absent in the scale by scale budget for the velocity field.

Appendix A

The generalized Kolmogorov equation

Here we summarize the procedure to obtain the generalized Kolmogorov equation starting from the Navier-Stokes equations (our derivation is based on the procedure described in Hill [25]). We consider an incompressible fluid described by the Navier-Stokes system of equations:

$$\begin{cases} \dfrac{\partial \tilde{u}_{\mathrm{i}}}{\partial t} + \tilde{u}_{\mathrm{j}} \dfrac{\partial \tilde{u}_{\mathrm{i}}}{\partial x_{\mathrm{j}}} = -\dfrac{1}{\rho} \dfrac{\partial \tilde{p}}{\partial x_{\mathrm{i}}} + \nu \dfrac{\partial^2 \tilde{u}_{\mathrm{i}}}{\partial x_{\mathrm{j}} \partial x_{\mathrm{j}}} \\ \\ \dfrac{\partial \tilde{u}_{\mathrm{i}}}{\partial x_{\mathrm{i}}} = 0 \,, \end{cases}$$

where $\tilde{u}_{\mathrm{i}}$ denotes the ith component of the velocity vector $\tilde{\boldsymbol{u}}(x_1, x_2, x_3, t)$ with respect to a Cartesian coordinate system $x_1 = x, \quad x_2 = y, \quad x_3 = z$, p is the pressure, ν the kinematic viscosity, ρ the density of the fluid, and the Einstein convention is used.

We follow the classical Reynolds decomposition for the fluid dynamic variables, for instance the velocity $\tilde{u}_{\mathrm{i}}$ is decomposed into a mean $\langle u_{\mathrm{i}} \rangle$ and a fluctuation component u_{i}, where the angular brackets denote an ensemble average. The equation for the fluctuation velocity field is easily obtained by subtracting the evolution equation for the mean flow from the Navier-Stokes system [A.1]:

$$\begin{cases} \dfrac{\partial u_{\mathrm{i}}}{\partial t} + \dfrac{\partial}{\partial x_{\mathrm{j}}} \left[u_{\mathrm{j}} u_{\mathrm{i}} + U_{\mathrm{j}} u_{\mathrm{i}} + u_{\mathrm{j}} U_{\mathrm{i}} - \langle u_{\mathrm{j}} u_{\mathrm{i}} \rangle \right] = -\dfrac{1}{\rho} \dfrac{\partial p}{\partial x_{\mathrm{i}}} + \nu \dfrac{\partial^2 u_{\mathrm{i}}}{\partial x_{\mathrm{j}} \partial x_{\mathrm{j}}} \\ \\ \dfrac{\partial u_{\mathrm{i}}}{\partial x_{\mathrm{i}}} = 0 \,, \end{cases}$$

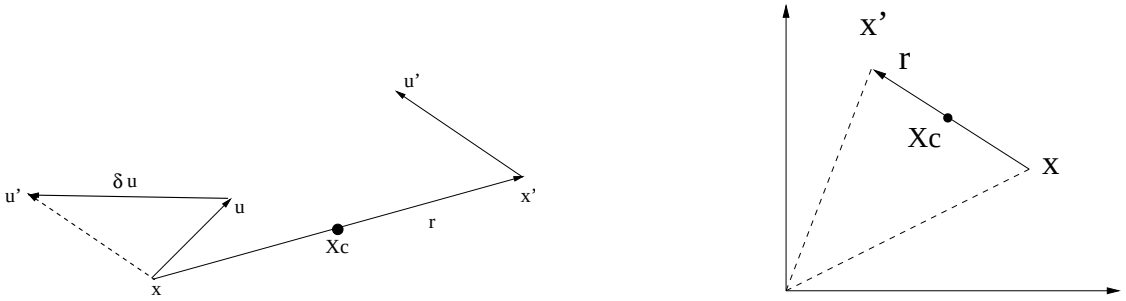

Figure A.1: Sketch of the arrangement for two-point correlations. The velocity evaluated at $\mathbf{x}'$ ($\mathbf{u}'$) and at $\mathbf{x}$ ($\mathbf{u}$) are used to construct the increment $\delta\mathbf{u}$. The separation vector is $\mathbf{r}$, while $\mathbf{X}_\mathrm{c}$ denotes the mid-point.

where for sake of simplicity we use an upper case letter U_i to denote the mean velocity. We are looking for an exact equation which relates quantities evaluated at two geometrical points $\boldsymbol{x}$ and $\boldsymbol{x'}$ which have no relative motion and thus are two independent variables. The quantity we want to analyze is the second order structure function $\delta u^2 = \delta u_\mathrm{i}\delta u_\mathrm{i}$, where $\delta u_\mathrm{i} = u_i(x_\mathrm{s}+r_\mathrm{s}) - u_i(x_\mathrm{s})$ [1], s=1,3 and i=1,3, denotes the difference of the fluctuating velocities evaluated at x_i and x'_i. The two panels of figure A.1 show a sketch which allows to identify the different terms appearing in the definition of the velocity increment. Clearly δu^2 depends on the distance between the measuring points, which defines the separation vector $r_\mathrm{i} = x'_\mathrm{i} - x_\mathrm{i}$ and for an inhomogeneous flow also depends on the geometrical location of the mid-point $X_{\mathrm{c_i}} = (x'_\mathrm{i} + x_\mathrm{i})/2$. This corresponds to a change of variables from $(x_\mathrm{i} - x'_\mathrm{i})$ to the variables $(r_\mathrm{i} - X_{\mathrm{c_i}})$. The rules for the transformation of the derivatives under the change of variables easily follow:

$$\partial x_\mathrm{i} = \partial r_\mathrm{i} + \partial X_{\mathrm{c_i}}/2 \quad \partial x'_\mathrm{i} = -\partial r_\mathrm{i} + \partial X_{\mathrm{c_i}}/2 \quad \partial X_{\mathrm{c_i}} = \partial x_\mathrm{i} + \partial x'_\mathrm{i} \quad \partial r_\mathrm{i} = (\partial x_\mathrm{i} - \partial x'_\mathrm{i})/2\,,$$

where it is essential to held fixed the correct variables for each of the partial derivatives. For instance the partial derivative $\partial X_{\mathrm{c_i}}$ is obtained with r_i held fixed.

Now if we subtract equation A.1 for u_i from the analogous equation for u'_i in order to obtain an evolution equation for δu_i, we obtain

[1] here and henceforth if not necessary for the algebra we will not show the temporal dependence

$$\frac{\partial \delta u_{\rm i}}{\partial t} + u'_{\rm j}\frac{\partial (u'_{\rm i} - u_{\rm i})}{\partial x'_{\rm j}} - u_{\rm j}\frac{\partial (u_i - u'_i)}{\partial x_{\rm j}} + U'_{\rm j}\frac{\partial (u'_{\rm i} - u_{\rm i})}{\partial x'_{\rm j}} - \tag{A.1}$$

$$U_{\rm j}\frac{\partial (u_{\rm i} - u'_{\rm i})}{\partial x_{\rm j}} + u'_{\rm j}\frac{\partial (U'_{\rm i} - U_{\rm i})}{\partial x'_{\rm j}} - u_{\rm j}\frac{\partial (U_{\rm i} - U'_{\rm i})}{\partial x_{\rm j}} = -\frac{1}{\rho}\frac{\partial (p' - p)}{\partial x'_{\rm i}}$$

$$+\frac{1}{\rho}\frac{\partial (p - p')}{\partial x_{\rm i}} + \nu\frac{\partial^2 (u'_{\rm i} - u_{\rm i})}{\partial x'_{\rm j}\partial x'_{\rm j}} - \nu\frac{\partial^2 (u_{\rm i} - u'_{\rm i})}{\partial x_{\rm j}\partial x_{\rm j}} + \frac{\partial \langle u'_{\rm i}u'_{\rm j}\rangle}{\partial x'_{\rm j}} - \frac{\partial \langle u_{\rm i}u_{\rm j}\rangle}{\partial x_{\rm j}}\,,$$

where we used the properties $\partial u_{\rm i}/\partial x'_{\rm j} = \partial u'_{\rm i}/\partial x_{\rm j} = \partial p/\partial x'_{\rm i} = \partial p'/\partial x_{\rm i} = 0$, since a generic quantity evaluated at point $x_{\rm i}$ ($x'_{\rm i}$) does not depend on $x'_{\rm i}$ ($x_{\rm i}$). Using the rules for the transformation of the first derivatives and observing that for the second derivatives we have

$$\partial^2 x'_{\rm i} = \partial^2 r_{\rm j} + \partial r_{\rm j}\,\partial x_{\rm j} + 1/4\partial^2 x_{\rm j} \qquad \partial^2 x_{\rm i} = \partial^2 r_{\rm j} - \partial r_{\rm j}\,\partial x_{\rm j} + 1/4\partial^2 x_{\rm j}\,, \tag{A.2}$$

equation A.1 reads:

$$\frac{\partial \delta u_{\rm i}}{\partial t} + (u'_{\rm j} - u_{\rm j})\,\frac{\partial \delta u_{\rm i}}{\partial r_{\rm j}} + \frac{1}{2}(u'_{\rm j} + u_{\rm j})\frac{\partial \delta u_{\rm i}}{\partial X_{\rm c_j}} + \delta U_{\rm j}\frac{\partial \delta u_{\rm i}}{\partial r_{\rm j}} + \tag{A.3}$$

$$\frac{1}{2}(U'_{\rm j} + U_{\rm j})\frac{\partial \delta u_{\rm i}}{\partial X_{\rm c_j}} + \delta u_{\rm j}\frac{\partial \delta U_{\rm i}}{\partial r_{\rm j}} + \frac{1}{2}(u'_{\rm j} + u_{\rm j})\frac{\partial \delta U_{\rm i}}{\partial X_{\rm c_j}} =$$

$$-\frac{1}{\rho}\frac{\partial \delta p}{\partial X_{\rm c_i}} + 2\nu\frac{\partial^2 \delta u_{\rm i}}{\partial r_{\rm j}\partial r_{\rm j}} + \frac{\nu}{2}\frac{\partial^2 \delta u_{\rm i}}{\partial X_{\rm c_j}\partial X_{\rm c_j}} + \frac{\partial \langle u_{\rm i}u_{\rm j}\rangle}{\partial x_{\rm j}} - \frac{\partial \langle u'_{\rm i}u'_{\rm j}\rangle}{\partial x'_{\rm j}}$$

where for simplicity of the algebra the terms involving the Reynolds stresses are expressed in the old system of coordinate. If now we multiply equation A.3 by $\delta u_{\rm k}$ and the analogous equation for $\delta u_{\rm k}$ by $\delta u_{\rm i}$ and add the two resulting expressions, we find an equation for the evolution of the tensor $\delta u_{\rm i}\delta u_{\rm k}$. In order to obtain this equation, we observe that

$$\text{I)}\quad \delta u_{\rm k}\frac{\partial \delta u_{\rm i}}{\partial t} + \delta u_{\rm i}\frac{\partial \delta u_{\rm k}}{\partial t} = \frac{\partial(\delta u_{\rm i}\delta u_{\rm k})}{\partial t}$$

$$\text{II)}\quad \delta u_{\rm k}\delta u_{\rm j}\frac{\partial \delta u_{\rm i}}{\partial r_{\rm j}} + \delta u_{\rm i}\delta u_{\rm j}\frac{\partial \delta u_{\rm k}}{\partial r_{\rm j}} = \frac{\partial(\delta u_{\rm k}\delta u_{\rm i}\delta u_{\rm j})}{\partial r_{\rm j}}$$

$$\text{III)}\quad u^*_{\rm j}\delta u_{\rm i}\frac{\partial \delta u_{\rm k}}{\partial X_{\rm cj}} + u^*_{\rm j}\delta u_{\rm k}\frac{\partial \delta u_{\rm i}}{\partial X_{\rm cj}} = \frac{\partial(\delta u_{\rm i}\delta u_{\rm k}u^*_{\rm j})}{\partial X_{\rm cj}}$$

$$\text{IV)}\quad -\frac{1}{\rho}\left[\delta u_{\rm k}\frac{\partial \delta p}{\partial X_{\rm ci}} + \delta u_{\rm i}\frac{\partial \delta p}{\partial X_{\rm ck}}\right] = -\frac{1}{\rho}\left[\frac{\partial(\delta u_{\rm k}\delta p)}{\partial X_{\rm ci}} + \frac{\partial(\delta u_{\rm i}\delta p)}{\partial X_{\rm ck}}\right] + \frac{\delta p}{\rho}\left[\frac{\partial \delta u_{\rm k}}{\partial X_{\rm ci}} + \frac{\partial \delta u_{\rm i}}{\partial X_{\rm ck}}\right]$$

$$\text{V)}\quad 2\,\nu\left[\delta u_{\rm k}\frac{\partial^2 \delta u_{\rm i}}{\partial r_{\rm j}\partial r_{\rm j}} + \delta u_{\rm i}\frac{\partial^2 \delta u_{\rm k}}{\partial r_{\rm j}\partial r_{\rm j}}\right] = 2\,\nu\left[\frac{\partial^2(\delta u_{\rm i}\delta u_{\rm k})}{\partial r_{\rm j}\partial r_{\rm j}} - 2\,\frac{\partial \delta u_{\rm k}}{\partial r_{\rm j}}\,\frac{\partial \delta u_{\rm i}}{\partial r_{\rm j}}\right]$$

$$\text{VI)}\quad \frac{\nu}{2}\left[\delta u_{\rm k}\frac{\partial^2 \delta u_{\rm i}}{\partial X_{\rm cj}\partial X_{\rm cj}} + \delta u_{\rm i}\frac{\partial^2 \delta u_{\rm k}}{\partial X_{\rm cj}\partial X_{\rm cj}}\right] = \frac{\nu}{2}\left[\frac{\partial^2(\delta u_{\rm i}\delta u_{\rm k})}{\partial X_{\rm cj}\partial X_{\rm cj}} - 2\,\frac{\partial \delta u_{\rm k}}{\partial X_{\rm cj}}\,\frac{\partial \delta u_{\rm i}}{\partial X_{\rm cj}}\right]$$

where an asterisk denotes an average with respect to the mid-point $u^*_{\rm j} = (u_{\rm j} + u'_{\rm j})/2$ and the evolution equation for the tensor $\delta u_{\rm i}\delta u_{\rm k}$ easy follows,

$$\begin{aligned}\frac{\partial(\delta u_{\rm i}\delta u_{\rm k})}{\partial t} &+ \frac{\partial(\delta u_{\rm i}\delta u_{\rm k}\delta u_{\rm j})}{\partial r_{\rm j}} + u^*_{\rm j}\frac{\partial(\delta u_{\rm i}\delta u_{\rm k})}{\partial X_{\rm cj}} + \frac{\partial(\delta u_{\rm i}\delta u_{\rm k}\delta U_{\rm j})}{\partial r_{\rm j}} \\ &+ \frac{\partial(\delta u_{\rm i}\delta u_{\rm k}\,V^*_{\rm j})}{\partial X_{\rm cj}} + \delta u_{\rm j}\delta u_{\rm k}\,\frac{\partial \delta U_{\rm i}}{\partial r_{\rm j}} + \delta u_{\rm j}\delta u_{\rm i}\frac{\partial \delta U_{\rm k}}{\partial r_{\rm j}} + u^*_{\rm j}\delta u_{\rm k}\frac{\partial \delta U_{\rm i}}{\partial X_{\rm cj}} \\ &+ u^*_{\rm j}\delta u_{\rm i}\frac{\partial \delta U_{\rm k}}{\partial X_{\rm cj}} = -\frac{1}{\rho}\left[\frac{\partial(\delta u_{\rm k}\delta p)}{\partial X_{\rm ci}} + \frac{\partial(\delta u_{\rm i}\delta p)}{\partial X_{\rm ck}}\right] + \frac{\delta p}{\rho}\left[\frac{\partial \delta u_{\rm k}}{\partial X_{\rm ci}} + \frac{\partial \delta u_{\rm i}}{\partial X_{\rm ck}}\right]\end{aligned} \tag{A.4}$$

$$+\,2\,\nu\,\left[\frac{\partial^2(\delta u_{\rm i}\delta u_{\rm k})}{\partial r_{\rm j}\partial r_{\rm j}}\,-\,2\,\frac{\partial\delta u_{\rm k}}{\partial r_{\rm j}}\,\frac{\partial\delta u_{\rm i}}{\partial r_{\rm j}}\right]\;+\;\frac{\nu}{2}\left[\frac{\partial^2(\delta u_{\rm i}\delta u_{\rm k})}{\partial X_{\rm cj}\partial X_{\rm cj}}\,-\,2\,\frac{\partial\delta u_{\rm k}}{\partial X_{\rm cj}}\,\frac{\partial\delta u_{\rm i}}{\partial X_{\rm cj}}\right]$$
$$-\,\delta u_{\rm k}\frac{\partial\langle u'_{\rm i}u'_{\rm j}\rangle}{\partial x'_{\rm j}}\,+\,\delta u_{\rm k}\frac{\partial\langle u_{\rm i}u_{\rm j}\rangle}{\partial x_{\rm j}}\,-\,\delta u_{\rm i}\frac{\partial\langle u'_{\rm k}u'_{\rm j}\rangle}{\partial x'_{\rm j}}\,+\,\delta u_{\rm i}\frac{\partial\langle u_{\rm i}u_{\rm j}\rangle}{\partial x_{\rm j}}.$$

Hence, since we are interested in the equation for δu^2, we consider the trace of the tensor by putting $i = k$, and observing that $\partial\delta u_{\rm i}/\partial X_{\rm ci}$ is zero for incompressibility, and that after averaging the viscous term can be expressed as

$$-\,4\,\nu\langle\frac{\partial\delta u_{\rm i}}{\partial r_{\rm j}}\frac{\partial\delta u_{\rm i}}{\partial r_{\rm j}}\rangle\,-\,\langle\nu\frac{\partial\delta u_{\rm i}}{\partial X_{\rm cj}}\,\frac{\partial\delta u_{\rm i}}{\partial X_{\rm cj}}\rangle\,=\,-2\,\nu\langle\left[\left(\frac{\partial u'_{\rm i}}{\partial x'_{\rm j}}\right)^2\,+\,\left(\frac{\partial u_{\rm i}}{\partial x_{\rm j}}\right)^2\right]\rangle\,=\,-\,4\,\nu\langle\left(\frac{\partial u_{\rm i}}{\partial x_{\rm j}}\right)^2\rangle\,,$$

the final averaged form for the generalized Kolmogorov equation reads

$$\frac{\partial\langle\delta u^2\rangle}{\partial t}+\quad\frac{\partial\langle\delta u^2\delta u_{\rm j}\rangle}{\partial r_{\rm j}}\,+\,\frac{\partial\langle\delta u^2u^*_{\rm j}\rangle}{\partial X_{\rm c_j}}\,+\,\frac{\partial\langle\delta u^2\rangle\delta U_{\rm j}}{\partial r_{\rm j}}+\qquad\qquad(A.5)$$
$$\frac{\partial\langle\delta u^2\rangle U^*_{\rm j}}{\partial X_{\rm c_j}}\,+\,2\langle\delta u_{\rm j}\delta u_{\rm i}\rangle\frac{\partial\delta U_{\rm i}}{\partial r_{\rm j}}\,+\,2\langle\delta u_{\rm i}u^*_{\rm j}\rangle\frac{\partial\delta U_{\rm i}}{\partial X_{\rm c_j}}\,=$$
$$-\frac{2}{\rho}\frac{\partial\langle\delta p\delta u_{\rm i}\rangle}{\partial X_{\rm c_i}}\,+\,2\nu\frac{\partial^2\langle\delta u^2\rangle}{\partial r_{\rm j}\partial r_{\rm j}}\,+\,\frac{\nu}{2}\frac{\partial^2\langle\delta u^2\rangle}{\partial X_{\rm c_j}X_{\rm c_j}}\,-\,4\,\langle\epsilon\rangle$$

where an asterisk denotes an average with respect to the mid-point $u^*_{\rm i} = (u'_{\rm i} + u_{\rm i})/2$. Let us observe that $\langle\epsilon\rangle$ is the one-point mean pseudo dissipation defined as $\langle\epsilon\rangle = \nu\langle\partial u_{\rm i}/\partial x_{\rm j}\,\partial u_{\rm i}/\partial x_{\rm j}\rangle$, which is different from the thermodynamical definition of the dissipation $\langle\tilde{\epsilon}\rangle = 2\nu\langle e_{ij}e_{ij}\rangle$, where $e_{ij} = (\partial u_{\rm i}/\partial x_{\rm j} + \partial u_{\rm j}/\partial x_{\rm i})/2$ is the rate of strain tensor. The dissipation and the pseudo dissipation are exactly the same only in homogeneous conditions, and the general relationship between them is:

$$\langle\tilde{\epsilon}\rangle = \langle\epsilon\rangle\,+\,\nu\,\frac{\partial^2\langle u_{\rm i}u_{\rm j}\rangle}{\partial x_{\rm i}\partial x_{\rm j}}\qquad\qquad(A.6)$$

As reported in Pope [61], the last term in equation A.6 is small (a few percent of $\langle\epsilon\rangle$) in virtually all applications, and the distinction between the two expressions is seldom important, especially for a channel flow where it is usual to refer to $\langle\epsilon\rangle$ as the dissipation.

Let us observe that the change of variables $((x_{\mathrm{i}} - x'_{\mathrm{i}}) \Rightarrow (X_{\mathrm{c_i}}, r_{\mathrm{i}}))$ allow us to show that the $X_{\mathrm{c_i}}$ dependence is associated with inhomogeneity, since the terms containing derivatives with respect to the mid-point vanish as homogeneous isotropic condition are approached, and the generalized Kolmogorov equation A.5 approaches the Kolmogorov equation 2.21. Before analyzing in more details the general feature of the generalized equation A.5 we want to recall some results characterizing homogeneous isotropic turbulence and homogeneous shear flows.

Bibliography

[1] Abe, K., Suga, K. 2001, Towards the development of a Reynolds-averaged algebraic turbulent scalar flux model, *Int. J. Heat and Fluid Flow* **22**, 19-29.

[2] Astarita, T., Marati, N. 2003, Visualization of coherent thermal structure in a turbulent channel flow, *Proceedings of AAIDA*, Roma.

[3] Bounoua, S., Ould-Rouis, M., Le Gal, P., Anselmet, F. 1997, Modeling low order statistics of temperature increments in fully developed turbulence, *Int. J. Heat Mass Trans.*, **41** (13), 2049-2057.

[4] Batchelor R. 1953, The theory of homogeneous turbulence, *Cambridge university press.*

[5] Benzi, R., Amati, G., Casciola, C.M., Toschi, F., Piva, R., 1999, Intermittency and scaling laws for wall bounded turbulence, *Phys. Fluids* **11** (6), 1-3.

[6] Calmet, I., Magnaudet, J., 1997 Large eddy simulation of high-Schmidt number mass transfer in a turbulent channel flow, *Phys. Fluids* **9** (2), 438-455.

[7] Casciola, C.M., Benzi, R., Gualtieri, P., Jacob, B., Piva,R., 2002, Double scaling in shear dominated flow, *Phys. Rev. E* **65**.

[8] del Àlamo, J., Jiménez, J. 2003, Spectra of the very large anisotropic scales in turbulent channels, *Phys. Fluids* **15** (6) 41-44.

[9] Casciola, C.M., Gualtieri, P., Benzi, R. and Piva, R. 2003, Scale by scale budget and similarity laws for shear turbulence, *J. Fluid. Mech.* **476**, 105-114.

[10] Celani, A., Lanotte, A., Mazzino, A., Vergassola, M., 2001, Fronts in passive scalar turbulence, *Phys. Fluids* **13** (6), 1768-1783.

[11] Danaila, L., Anselmet, F., Zhou, T., Antonia, R.A. 2000, Turbulent energy scale budget equation in a fully developed channel flow, *J. Fluid. Mech.* **430**, 87-109.

[12] Danaila, L., Anselmet, F., Antonia, R.A. 2002, An overview of the effect of large-scale inhomogeneities on small-scale turbulence, *Phys. Fluids* **14** (7), 2457-2484.

[13] Danaila, L., Antonia, R. A., Burattini, P. 2004, Progress in studying small-scale turbulence using 'exact' two-point equations, *New J. Phys.* **6** (128).

[14] Darek, B., Domaradzki, J. A., Yeung, P. K., 1997, Direct numerical simulations of passive scalars with $\mathrm{Pr} > 1$ advected by turbulent flow, *J. Fluid. Mech.* **343**, 111-130.

[15] Debusschere, B., Rutland, C. J., 2004 Turbulent scalar transport mechanisms in plane channel and Couette flows, *Int. J. Heat Mass Trans.* **47**, 1771-1781.

[16] Dol, H. S., Hanjalič, K., Vesteegh, T. A. M. , 1999 A DNS-based thermal second-moment closure for buoyant convection at vertical walls , *J. Fluid Mech.* **391**, 211-247.

[17] Domaradzki, J.A., Liu, W., Härtel,C., Kleiser, L., 1993, Energy transfer in numerically simulated wall-bounded turbulent flows, *Phys. Fluids* **13** (6), 1768-1783.

[18] Eckelmann, U. 1974, The structure of the viscous sublayer and the adjacent wall region in a turbulent channel flow *J. Fluid. Mech.* **65**, 439-459.

[19] Frisch, U. 1995, *Turbulence*, Cambridge University Press, 1995.

[20] Gad-el-Hak M., Bandyopadhyay P. R., Reynolds number effects in wall-bounded turbulent flows, *Appl. Mech. Rev.* **47** (8), 307-365.

[21] Gualtieri, P., Casciola, C.M., Benzi, R., Amati G. and Piva, R., 2002a, Scaling laws and intermittency in homogeneous shear flow, *Phys. Fluids* **14** (2), 583-596.

[22] Hamilton, J.M., Kim, J., Waleffe, F. 1995, Regeneration mechanisms of near-wall turbulence structures, *J. Fluid. Mech.* **287**, 317-348.

[23] Handler, R. A., Saylor, J. R., Leighton, R. I., Rpvelstad, A. L., Transport of a passive scalar at the shear-free boundary in fully developed open channel flow, *Phys. Fluids* **9** (11), 2607-2625.

[24] Hill, R. J. 1997, Applicability of Kolmogorov's and Monin's equations of turbulence, *J. Fluid. Mech.* **353**, 67-81.

[25] Hill, R. J., Borotav, N. 2001, Next order structure function equations, *Phys. Fluids* **13** (1), 276-283.

[26] Hill, R. J. 2002, Exact second-order structure-function relationships, *J. Fluid. Mech.* **468**, 317-326.

[27] Hill, R. J. 2002, Structure-function equations for scalars, *Phys. Fluids* **14** (5), 1745-1756.

[28] Jacob, B., Olivieri, A., Casciola, C.M. 2002, Experimental assessment of a new form of scaling law for near wall turbulence, *Phys. Fluids* **14** (2), 481-491.

[29] Jiménez, J., Moin, P. 1991, The minimal flow unit in near wall turbulence, *J. Fluid Mech.* **225**, 213-240.

[30] Jiménez, J. 1999, The physics of wall turbulence, *Physica A.* **263**, 252-262.

[31] Jiménez, J., Pinelli, A. 1999, The autonomous cycle of near wall turbulence, *J. Fluid Mech.* **389**, 335-359.

[32] Kader, B. A. 1979, Temperature and concentration profiles in fully turbulent boundary layers, *Int. J. Heat Mass Trans.* **9** (24), 1541-1544.

[33] Kasagi, N. Tomita, Y., Kuroda, A. 1992, Direct Numerical Simulation of Passive Scalar Field in a Turbulent Channel Flow, *Transactions of the ASME* **114**, 598-606.

[34] Kawamura, H., Abe, H., Shingai, K. , DNS of turbulence and heat transfer in a channel flow with different Reynolds and Prandtl numbers and boundary conditions, 3^{th} *Int. Symp. Turbulence, Heat and Mass Transfer.*

[35] Kawamura, H., Kouichi, O., Abe, H., Kiyoshi, Y. 1998, DNS of turbulent heat transfer in channel flow with low to medium-high Prandtl number fluid, *Heat and Fluid Flow* **19**, 482-491.

[36] Kim, J., Moin, P., 1987, Transport of passive scalars in a turbulent channel flow, *Turb. shear Flows* **6**, Springer-Verlag, Berlin, 85-96.

[37] Kim, J., Moin, P., Moser, R.D. 1987, Turbulence statistics in fully developed channel flow at low Reynolds number, *J. Fluid. Mech.* **177**, 133-166.

[38] Klebanoff, P.S. 1954, Characteristics of turbulence in a boundary layer with zero pressure gradient, TN 3178, NACA.

[39] Kline, S.J., Reynolds, W.C., Schraub, F.A., Runstadler, P.W. 1967, The structure of the turbulent boundary layers, *J. Fluid. Mech.* **134**, 741-773.

[40] Kolmogorov, A. N. 1941, The local structure of turbulence in incompressible viscous fluid for very large Reynolds number, Dolk. Akad. SSSR **30**, 301, 1941, reprinted in Proc. R. Soc. Lond. A **434**, 15-19, 1991.

[41] Kong, H., Choi, H., Lee, J. 2000, Direct numerical simulation of turbulent thermal boundary laters, *Phys. Fluids* **12** (10), 2555-2568.

[42] Kurien, S., Sreenivasan, R. 2001, Dynamical equations for high-order structure functions, and a comparison of a mean-field theory with experiments in three dimensional turbulence, *Phys. Rev. E.* **64**, 056302.

[43] Lesieur, M. 1997, Turbulence in Fluids , *Kluwer academic publishers.*

[44] Lindborg, E. 1996, A note on Kolmogorov's third order structure-function law. The local isotropy hypothesis and the pressure-velocity correlation, *J. Fluid. Mech.* **326**, 343-356.

[45] Lindborg, E. 1999, Correction to the four-fifths law due to variations of the dissipation, *Phys. Fluids* **11** (3), 510-512.

[46] Lu, D. M., Hetsroni, G., 1995, Direct numerical simulation of a turbulent open channel flow with passive heat transfer, *Int. J. Heat Mass Trans.* **38** (17), 3241-3251.

[47] Lundbladh A., Henningson D. S. & Johansson A. V. 1992 An efficient spectral integration method for the solution of the time-dependent Navier–Stokes equations, FFA-TN-28, Aeronautical Research Institute of Sweden.

[48] Lyons, S. L., Hanratty, T. J., McLaughlin, J. B. 1991, Direct numerical simulation of passive heat transfer in a turbulent channel flow, *Int. J. Heat Mass Trans.*, **4** (34), 1149-1161.

[49] Mansour, N.N., Kim, J., Moser, R.D. 1987, Reynolds-stress and dissipation-rate budgets in a turbulent channel flow, *J. Fluid Mech.* **194**, 15-44.

[50] Marati, N., Casciola, C.M., Piva, R. 2004, Energy cascade and spatial fluxes in wall turbulence, *J. Fluid Mech.* **521**, 191-215.

[51] Mc Comb, W. D. 1990, The Physics of Fluid turbulence, *Oxford science publication.*

[52] Moisy, F., Tabeling, P.,Willaime, H. 1999, Kolmogorov Equation in a fully developed turbulence experiment , *Phys. Rev. Lett.* **82** (20), 3994-3997.

[53] Monin, A.S., Yaglom, A.N. 1975, *Statistical Fluid Mechanics*, MIT Press.

[54] Moser, R.D., Kim, J., Mansour, N.N. 1999, Direct numerical simulation of turbulent channel flow up to $\mathrm{Re}_\tau = 590$, *Phys. Fluids.* **11** (4), 943-945.

[55] Mydlarski, L., Warhaft, Z. 1998, Three-point statistics and anisotropy of a turbulent passive scalar, *Phys. Fluids* **10** (11), 2885-2894.

[56] Nie, Q., Tanveer ,S. 1998, A note on third order-structure functions in turbulence, *Proc. r. Soc. Lond. A* 1999.

[57] Na, Y., Hanratty, T. J. 2000, Limiting behaviour of turbulent scalar transport close to a wall, *Int. J. Heat Mass Trans.* **43** , 1749-1758.

[58] Nikora, V. 1999, Origin of the "-1" spectral law in wall bounded turbulence, *Phys. Rev. Lett.* **83**, 734, 1999.

[59] Oberlack, M. 2001 A unified approach for symmetries in plane parallel turbulent shear flows *J. Fluid Mech.* **427**, 299–328.

[60] Perry, A.E., Henbest S., Chong M.S. 1986, A theoretical and experimental study of wall turbulence, *J. Fluid Mech.* **165**, 163-199, 1986.

[61] Pope, S.B. 2000, *Turbulent Flows*, Cambridge University Press.

[62] Pumir, A 1994, Small-scale properties of scalar and velocity differences in three-dimensional turbulence, *Phys. Fluids.* **6**, 3974-3984.

[63] Qian, J. 1999, Slow decay of the finite Reynolds number effect of turbulence, *Phys. Rev. E.* **60**, 337-342.

[64] Robinson, S.K. 1991, Coherent motions in the turbulent boundary layer, *Ann. Rev. Fluid. Mech.* **23**, 601.

[65] Ruiz-Chavarria, G., Ciliberto, S., Baudet, C., Lévêque, E. 2000, Scaling properties of the streamwise component of velocity in a turbulent boundary layer, *Physica D* **141**, 183-198.

[66] Ruiz-Chavarria, G., Baudet, C., Ciliberto, S. 1996, Scaling laws and dissipation scales of a passive scalar in fully developed turbulence , *Physica D* **99**, 369-380 .

[67] Saddoughi, S.V., Veeravalli, S.G. 1994, Local isotropy in turbulent boundary layer at high Reynolds number, *J. Fluid Mech.* **268**, 333-372.

[68] Shraiman, B.I., Siggia, E.D. 2000, Scalar turbulence, *Nature* (London) **405**, 639-646.

[69] Sreenivasan, K.R. 1991, On local isotropy of passive scalars in turbulent shear flows, *Proc. R. Soc. Lond. A* **434**, 165-182.

[70] Sreenivasan, K.R., Antonia, R.A. 1997, The phenomenology of small scale turbulence, *Annu. Rev. Fluid Mech.* **29**, 435-472.

[71] Sreenivasan, K.R. 1984, On the scaling of turbulent energy dissipation rate, *Phys. fluids* **27**, 1048-1051.

[72] Tiselj, I., Pogrebnyak , C., Mosyak, A., Hetsroni, G. 2001, Effect of wall boundary conditions on scalar transfer in a fully developed turbulent flume, *Phys. Fluids* **13** (4), 1028-1039.

[73] Tiselj, I., Bergant, R., Mavko, B., Baisić, I., Hetsroni, G. 2001, DNS of Turbulent Heat Transfer in Channel Flow With Heat conduction in the Solid Wall, *J. Heat Trans.* **123**, 849-857.

[74] Toschi, F., Amati, G., Succi, S., Benzi, R., Piva, R. 1999, Intermittency and structure functions in channel flow turbulence *Phys. Rev. Lett* **82** (25), 5044-5049.

[75] Tennekes, H. Lumley, J. L., 1972, *A First Course in Turbulence*, The MIT Press.

[76] Townsend, A. A. 1956, *The structure of turbulent shear flow*, Cambridge University Press.

[77] Warhaft, Z. 2000, Passive scalars in turbulent flows, *Annu. Rev. Fluid Mech.* **32**, 203-240.

[78] Wikström, P. M. 1998, Measurement, Direct Numerical Simulation and Modeling of Passive Scalar Transport in Turbulent Flows, *Doctoral Thesis*, Royal institute of Technology, Stockholm.

[79] Yakhot, V. 2001, Mean-field approximation and small parameter in turbulence theory, *Phys. Rev. E.* **63**, 026307.

[80] Zagarola, M.V. & Smits, A.J. 1997, Scaling of the mean velocity profile for turbulent pipe flow, *Phys. Rev. Lett.* **78**, 239-242.

[81] Zhou, T., Antonia, R. A., Danaila, L., Anselmet, F. 2000, Approach to the forth-fifths law for grid turbulence, *J. Turbulence* **1**, 5.